Österreichische Beiträge zu Meteorologie und Geophysik

ISSN 1016-6254

Heft 38

BASIC METEOROLOGICAL CONCEPTS AND RECOMMENDATIONS FOR THE EXPLOITATION OF WIND ENERGY IN THE ATMOSPHERIC BOUNDARY LAYER

Hartwig Dobesch and Georg Kury

Wien 2006

Österreichische Beiträge zu
Meteorologie und Geophysik

Heft 38

Basic meteorological concepts and recommendations for the exploitation of wind energy in the atmospheric boundary layer

Wien 2006

Zentralanstalt für Meteorologie und Geodynamik, Wien

Publ.Nr. 419

ISSN 1016-6254

IMPRESSUM

Herausgeber: Zentralanstalt für Meteorologie und Geodynamik (ZAMG), Wien

Leitende Redakteure: Sophie Debit, Fritz Neuwirth, ZAMG, Wien

für den Inhalt verantwortlich:
Hartwig Dobesch, Georg Kury

Druck: Grafisches Zentrum HTU GmbH
1040 Wien, Wiedener Hauptstraße 8-10
www.grafischeszentrum.at

Verlag: Zentralanstalt für Meteorologie und Geodynamik
Hohe Warte 38, A-1190 Wien
Austria (Österreich)

BASIC METEOROLOGICAL CONCEPTS AND RECOMMENDATIONS FOR THE EXPLOITATION OF WIND ENERGY IN THE ATMOSPHERIC BOUNDARY LAYER

by

Hartwig Dobesch

Central Institute for Meteorology and Geodynamics (ZAMG)
Vienna, Austria

and

Georg Kury

ENAIRGY
Vienna, Austria

TABLE OF CONTENTS

FOREWORD

In 1981 the secretariat of the World Meteorological Organisation edited the Technical Note No. 175, (WMO – No. 575) "Meteorological Aspects of the Utilisation of Wind as an Energy Resource". This document focused mainly on the description of wind as a renewable energy resource from a meteorological point of view and on the role of the boundary layer and atmospheric turbulence for wind fields. Compiled around 1980, this Technical Note was edited at the beginning of the stormy development of wind power exploitation taking place in Europe. Therefore little can be found find on wind energy technology, the assessment of wind energy potentials and the estimation of energy yield at given sites. This is not surprising given the remarkable development of methods and technology over the last twenty years. A recently edited WMO report ("Meteorological Aspects and recommendations for Assessing and Using the Wind as an energy source in the Tropics", WMO/TD-No. 826, June 1997) contains guidelines for prospecting wind energy in the tropics, particularly for the numerous islands in this region. Based on experiences made in Hawaii, this report can be seen as a complimentary document to the above mentioned WMO report No. 575 for those who plan to conduct wind energy surveys in tropical areas. It contains many details and hints under consideration of the unique tropical weather conditions, compiled and presented for direct practical use but lacking the physical background in hydrodynamics necessary for example to asses wind energy yield.

This new report will therefore try to fill the gaps in the contents of the above mentioned reports, from the knowledge base now available at the beginning of the third millennium. It will reflect the scope of modern wind technology and its close connection with meteorology, to provide a coherent presentation of the fundamental aspects of wind energy exploitation and the technical and physical background. It will emphasise the technical solutions available in the existing area of knowledge and the part of meteorology, in particular the mathematical-physical bases for the assessment of wind energy potentials, the optimal siting together with the evaluation of the energy yield of **W**ind **T**urbine **G**enerating **S**ystems (abbreviated in the following text as **WTGSs**) - beside all practical and theoretical aspects reflected in many textbooks and reports (e.g. in Petersen et al., 1998) that already contain a realm of wisdom.

Acknowledgement

The authors thank herewith Dr. Jean Palutikof, University of East Anglia, Norwich, and Prof. Dr. Georg Skoda, Institute for Meteorology and Geophysics, University Vienna, for their engagement in reading carefully this report and for their valuable comments to the text.

1 INTRODUCTION

A range of environmental impacts and resource problems have always emerged from the use of energy technology. For modern societies the supply and sources of energy in their many forms have been an essential source of economic and political tensions but also a challenge for science and technology. Together with environmental problems arising from energy consumption (increase of carbon dioxide and greenhouse effect, acid rain, radioactive waste, oil pollution of the sea, etc.), the problems of sustainability and potential social conflict which may result from unevenly distributed resources, vulnerability due to centralisation and dangers from nuclear proliferation, make it imperative for mankind to devise a set of energy technologies, which can meet human needs without producing irreversible environmental effects on a global scale (Elliott, 1997). This implies beside the requirement to use energy more efficiently, the promotion of technologies that use renewable energy resources extensively needs to be encouraged.

1.1 Facts about world energy consumption

In the seventies of the 20th century people worried about a coming shortage of energy resources and the direct consequences for the environment e.g. acid rain. From the 1980's, the indirect consequences of high energy consumption e.g. global warming and the ozone hole, became a greater concern.

The outlook for future energy demand is that it is predicted to rise quite dramatically. It is supposed (Greenpeace, 2005) that until 2020 the world-wide yearly electricity demand will rise according to Table 1.1, with an average annual growth rate of about 2 percent. Until 2025, the consumption of the developing countries is estimated to rise on the basis of population growth and increasing industrialisation by more than 100 percent, followed by the former Soviet Union and Eastern Europe with an increase of about 80 percent. Although the share of fossil fuels used in the production sector will shrink remarkably, the CO_2 emissions will increase by about 50 percent due to overall rising consumption. The G8 Governments intend to establish national renewable portfolio standards to generate at least 25% of electricity from renewable energy sources by 2025.

Table 1.1: Forecast of annual energy consumption (basis 2000)

until	increase	energy consumption	CO2 emissions
2010	30%	20 852 TWh	27 715 Mio tons
2020	ca. 50%	27 326 TWh	37 124 Mio tons
2025	ca. 2%	yearly increase	

The aforementioned risk to the biosphere and the limit on fossil fuel energy resources will force new solutions. One of the best solutions on the basis of today's technologies, consists of a combination of saving energy by different measures and the exploitation of additional sustainable resources of energy such as solar energy (photovoltaic, heat collectors) and wind energy.

1.2 The global situation in the use of wind energy - overview

Wind energy is the kinetic energy content of a moving air mass. The kinetic energy content of the global atmosphere equals on average a turnover time of about seven days of kinetic energy production or dissipation, also assuming average rates (Sørensen, 2000). The annual streaming energy of the atmosphere lies between 8.2 and 13.6 x10^{22} J. The entire electricity demand of the earth in 2000 could have been covered by the use of only 0.045 percent of this energy. The world's total onshore wind resources (without

Antarctica, Greenland) are estimated to be about 53000 TWh with the following distribution (M. Grubb and N. I. Meyer, 1993): Western Europe 4800 TWh (UK has here the largest share with 986 TWh/a), Eastern Europe and former Soviet Union 10600 TWh, Asia (without former USSR) 4600 TWh, Latin America 5400 TWh, North America 14000 TWh, Australia 3000 TWh and Africa 10500 TWh.

There is also an enormous wind resource to be found in the coastal areas of oceans around many coastlines of the continents. The *"Study of Offshore Wind Energy in the EC"* (by Hassan, 1995) performed under the EU's JOULE programme, estimates an **offshore wind potential** of 3028 TWh in the EU (without Norway and Sweden) under the assumptions of a water depth of up to 40 meters and up to 30 km offshore. Here the large (3 MW and up) turbines can be used which has already given the wind industry in Europe new impetus. Additionally, because of environmental constraints, public concerns and minimizing visual impact, suitable sites for wind turbines in heavily-populated regions such as western Europe are becoming in short supply. Offshore location of wind turbines offer resource benefits, namely:

- Low vertical wind shear, due to relatively low roughness lengths over the sea. The vertical profile of wind speeds is such, therefore, that wind speed changes little with hub height. Under these circumstance, it may be more economic to use lower towers than would be optimal on land (perhaps 0.75 rotor diameter, compared to the more typical 1.0 times rotor diameter on land).
- Low turbulence intensity, because the temperature contrast between the sea surface and the overlying air will generally be less than the contrast between land and air. Lower stresses on turbines should lead to a longer life span offshore (perhaps 25 years compared to 20 years for onshore machines).
- Generally higher wind speeds due to lower drag coefficients. This is a particular advantage for countries with low-lying terrain, such as Denmark and the Netherlands. However, the offshore resource will generally not exceed the onshore resource from hilltop sites where speed-up effects can produce wind speeds greater than are experienced offshore. Hence, for countries with undulating terrain, such as the UK, Italy and Greece, the offshore resource offers fewer advantages.

However, costs of turbine construction, grid connection and maintenance in the often hostile offshore environment are such that electricity from offshore turbines is likely to be more expensive than from land-based turbines for the foreseeable future.

1.3 Historical background of wind power usage up to the second oil crisis in 1980

The exploitation of the wind as an energy resource by man began with the transition of nomadic tribes to settlement and agriculture. It was one of the first non-animal sources of energy to be exploited by early civilisations. The wind was harnessed to propel ships by means of sails as early as the fourth millennium B.C. It is thought that the static exploitation of wind energy by means of windmills had been going on for about 4000 years. Evidence that Greeks or Romans had some other applications of wind power is given by Hero (in his *Pneumatics*) of the 1st century A.D. in describing an air pump for a water organ. Later, wind was used in the symbiosis of sail and whim-gin mills, which were driven by draught animals, for grinding grain and irrigation. In the Middle Ages a shift to wind wheels with horizontal axis to achieve higher efficiency occurred, though mainly in areas where hydraulic power was unavailable. With increasing industrialisation at the beginning of the 18th century more and more fossil energy was used thus replacing slowly regenerative energy, until finally at the end of the 19th century the fossil fuels overtook regenerative energy use (the trade statistics of the German empire 1895 provide the following figures: 18,362 wind machines, 21,350 combustion engines, 54,529 water machines and 58,530 steam engines (Gasch, 1991). The 20th century cared little for wind energy until a renaissance in the 70's and 80's as a consequence of oil crisis and ecology movements.

1.3.1 Wind wheels with vertical axis

Wind wheels with vertical axis are based usually on the resistance principle, which was already known by early civilisations as power sources. Early evidence of a simple windmill was found in Egypt and Mesopotamia 1000 B.C. where they were used for irrigation. Another early occurrence is reported from Afghanistan in the 7th century. All these early power plants were constructed around the following mechanism: In a half open tower a turntable with resistance surfaces from round timbers or woven mats was established, which was rotated by one-sided upwind. The disadvantage of this arrangement was its directional dependence. This was initially overcome by the Chinese around 1000 A.D. by turning the sail-mats out of the wind on their return travel against the wind. Another solution Veranzio discovered in Italy around 1600 by generating a torque in asymmetric wind flow: He used resistance bodies, which had, according to the direction of flow, larger or smaller drag-coefficients – which employs the same principle as the cup anemometer (Gasch,1991).

Through the striking success of the horizontal axis rotors the vertical axis principle experienced no improvement until 1924 when the SAVONIUS rotor, named after its Finnish inventor, was introduced. By the use of the buoyancy principle, a higher efficiency is attainable with this WTGS. A further design step in competition to the horizontal axis is the DARRIEUS rotor. Developed by the French inventor Darrieus in 1929, this rotor can reach an efficiency of 38 percent after steered start up to the rated-speed range (Molly,1990).

1.3.2 Wind wheels with horizontal axis

The vertical axis turbines that exploit an effect sailors had discovered early on, i.e. sail ships travel faster if the wind comes from the side instead of behind, spread slowly. The physical explanation for this lay in the use of dynamic buoyancy where much greater power can be generated than with the aerodynamic resistance principle. The first windmills using this principle consisted of up to ten wooden booms, rigged with jib sails. Such primitive types of windmills are still found today in the eastern Mediterranean regions (sail windmills in Greece). The concept of this 'propeller' windmills arrived in England and France with returning crusaders, where it appeared in the 12th century in the form of the buck-windmill, spreading from there to Holland and Germany in the 13th century, and thence Poland and Russia in the 14th century. During the subsequent Middle Ages most manorial rights included the right to refuse permission to build windmills, thus compelling tenants to have their grain ground at the mill of the lord of the manor. Additionally, planting of trees near windmills was banned to ensure free wind (DeRenzo, 1979). The oldest construction was the so-called "post-mill" in which the whole body of the mill was moved around a large upright post when the wind direction changed. This mill had to be brought into the wind by the miller or a donkey. The disadvantage of the post-mill was that heavy loads like millstones and grain sacks had to be carried into the mill house and that it could not be used for the drainage of the countryside for which a high demand had long existed in Holland. A further development of this type of mill took place 300 years later in the form of the Wippmill which could be used for water pumping. The disadvantage remained that the entire mill needed turning manually into the wind (Gasch 1991).

An essential improvement was the Dutchman windmill or tower windmill of the 17th century. Here the rotor and cap, as the only moving parts, were supported by a relatively tall tower. The wings turned fairly slowly to provide mechanical power. To turn the mill into the wind direction at a slanting flow, a small wing rosette was installed that stood crosswise to the main rotor. Another innovation was the development of the mill wing as an adjustable Venetian blind, which enabled an easy-to-handle power reduction at any time. Between 1608 and 1612, Beemster Polder, in the Netherlands, which laid 19 feet below the sea level, was drained by 26 windmills of up to 50 hp each. Here the first oil mill was built in 1682 and the first paper mill in 1686. At their zenith, before the industrial revolution, it is estimated that in Great Britain for example some 10,000 tower mills were operated (Boyle, 1996), forming a familiar feature of the countryside.

The third innovation came in 1759 by J. Smeaton and was the distortion of the rotor foils, which led to a higher power output. By the middle of the 19th century, some 9000 windmills were in use in the Netherlands but with the industrialisation the use of wind power started to decline. By the turn of the 20th century only 2500 windmills were in operation and by 1969 only 1000 were still in working condition (DeRenzo 1979).

In the 19th century a quite new wind wheel type, the *Western Mill*, came widely into use. Industrially mass produced and completely made of metal it could be operated fully automatically without supervision for the first time, which was a crucial advantage on the vast pastures of the North American great plains. The large number of blades at slanting flow allowed a high staring torque and a low speed with high wind velocities, the directional control given by a wind-vane. The performance of this wind wheel with a diameter of approximately four meters amounted to about 100 to 200 watt with a wind speed of 7 m/sec. In the middle of the 19th century approximately 6 million Western Mills were in use (Hau 1996; Molly 1990; Gasch 1991).

With electrification the wish emerged to produce electricity from wind energy. To reduce price and keep the weight of generator and its gear small, a high rotor speed is necessary which means that the number as well the real surface of rotor blades should be as low as possible. A first attempt into this direction was made 1939 with the 2-blade MW Smith-Putnam plant in Vermont, USA. The plant had a hub-height of 36 m, a rotor diameter of 53 meters and a performance of 1.25 MW at rated wind speed. This machine was a landmark in technological development. Only 800 hours were completed successfully before the machine failed by loosing a blade due to a sub-standard site weld repair. This failure and the low petroleum price led to a shut down of these activities concerning wind energy until the petroleum crisis of the 1970's. The next milestone in turbine development was the Danish GEDSER plant, installed 1956-1957 on the island of Gedser in the south east of Denmark. With a 24 meters rotor diameter and 200 KW nominal power it operated from 1958 until 1967. It was a simple rugged design of a tubular tower, 3 blades and tip brakes and had all the ingredients of the later mainstream Danish wind turbines. The next in the early 1960's was the a 100 KW plant of Prof. Huetter (Stuttgart, Germany) with 34 meters rotor diameter – a two bladed, teetered rotor with high tip speed. These machines could be considered as the prototypes of modern WTGSs.

1.4 Development in wind energy technologies and markets since 1973

The first oil crisis led 1973 to a resumption of research and development activities in the field of wind energy: Since then modern grid connected wind turbines have been installed in more than 50 countries around the world. Early installations were predominantly in industrialised countries. Large plants with more than 50 meter rotor diameter and 1 Megawatt nominal performance were designed for electricity companies and for the private operators smaller WTGSs with 10 to 15 meter rotor diameter. In the USA 1975 the MOD-0 wind power plant with 38 meters rotor diameter and 100 KW nominal performance was erected by NASA, followed in 1979 by the MOD-1 with 61 meter diameter and 2000 KW. These two prototypes were the basis for the 1987 construction of the biggest wind power plant of the USA, the Boeing MOD-5b with 97 meter rotor diameter and 3.2 MW power output. This plant had two metal rotor blades that were provided on the perimeter with flaps for the power regulation, similar to these used in the aeroplane construction. As a result of the flaps a contortion of the entire rotor could be avoided, allowing the two rotor blades to be manufactured in one piece and installed on a commuting hub. Due to technical problems non of these three prototypes reached series maturity (Hau, 1996; Thomas, 1976; Gasch 1991).

The construction of vertical-axis turbines was further developed in Canada: 1988 a DARRIEUS rotor with 4.2 MW power was installed that holds the world record in generator performance since then and, additionally, reached a high technical availability (95 percent) in the first two years of operation. Because of the high cost this development was not followed up until now . Also in Sweden megawatt generators with a relatively high technical availability were installed. The first Swedish prototype was the MAGLARP WTS 3 with 78 meter rotor diameter and 3 MW performance, followed by the two AEOLUS plants, AEOLUS I

with 2 MW and a rotor diameter of 75 meters and AEOLUS II with 3 MW and 80 meter rotor diameter (Molly, 1990). In Germany of the 1980's, starting from the 100 KW HUETTER machine with a rocking suspension of a two-bladed rotor in the lee of the tower, a 3 MW turbine with 100 meter rotor diameter and 100 meters hub height was erected. This generator was named GROWIAN (= "Große Wind Anlage") and completed only 420 hours in operation due to material fatigue of some components of the rotor teetering hub and was demolished in spring 1988. In 1989 with the MONOPTEROS 50 the first larger single blade turbine with a rotor diameter of 56 meters and a nominal power of 640 KW was erected. The goal of this development was to lower the costs by reducing material expenditure for the rotor blade and by decreasing the translation of the gear (single- bladed rotors can reach essentially higher speeds as two- or three-blade rotors). However, with increasing speed of the blade tips the noise emission increases to the 5^{th} power of speed, single-bladed rotors could not succeed. Another megawatt plant followed in 1990 with the WKA60 of 60 meters diameter and 1200 KW power, however none of these had any effects on the current WTGS market (Hau, 1996; Molly, 1990; Gasch, 1991).

In Nordjütland, Denmark, two medium-sized installations „NIBE A "and „NIBE B" were constructed in 1979 and 1980. Their design was based on the GEDSER turbine, erected in 1957. They both had 40 meter rotor diameters and 630 KW power, but differed in the control mechanism: one unit could change the angle of attack of the entire rotor blade, the other unit could only vary the angle of attack of the blade tips in two positions. This blade tip regulation is in fact cheaper, but produced less energy yield. However, a comparison of both systems did not lead to a preference to one of either construction principle (Molly, 1990).

As early as 1977 on a private initiative of students in Denmark a 2 MW plant, the TVIND mill, with a 54 meter rotor diameter was built. It provided a pronounced impetus for the Danish anti-nuclear movement. But only considerably later, in 1988, was another 2 MW plant, the ELSAM-2000 with 61 meter rotor diameter installed, funded by the Danish government. At the end of the 1970's from small - and medium sized enterprises smaller units with up to 15 meter rotor diameter were developed for private operators, all based on the principle of the GEDSER design: This principle known under the name „Danish concept" marks WTGSs with horizontal axis, wind-ward side rotor with three GFK-blades on a stiff hub and with constant rotational speed propelling a network-connected asynchronous generator. The drive train consists of standard components (gear, brake, clutch, generator) in linear order on a machine bearer. The windward orientation takes place with a yaw motor, the power restriction by flow separation at the rotor blades and the protection against high winds by mechanical and aerodynamic brakes (Gasch, 1991). A more extended overview of the above outlined development is given for example in Quarton et al. (1998).

In the past and presently different market regulation, market stimulation and development incentives are offered by governments as political initiatives to promote wind energy usage. Thus the Federal Public Utility Regulatory Policies Act (PURPA) of the U.S. Carter-Administration, passed in 1978, led especially in California to the development of a market, where a guarantee was given for independently produced electricity, providing favourable regulation for feeding into the grid and fiscal relief for the operating of WTGSs. From 1982 Danish companies, like VESTAS, could install thousands of VESTAS-V15s with 15 meter rotor diameter and 55 KW performance in the Tehachapi Mountains and on the Altamont Pass, the locations of the largest Californian wind farms. The large turbines from the aeronautics industry (Boeing, MBB, DORNIER) mostly failed due to technical or financial problems, but the Danish WTGS manufacturers had recognised the demands of the market and took on the leading role in the world market: From 18,000 erected WTGSs in California that were erected until 1990 (total-performance 1500 MW), 45 percent came from Denmark (Hau, 1996; Gasch, 1991). But after this boom the growth of wind energy in California was not sustained neither was any development elsewhere in the USA and only in 1997 the US market was starting to re-emerge. In contrast, there has been striking developments in Europe markets as in Germany in the early 1990's where around 200 MW of wind power were installed per annum. Since shown in a study by the EC of 1988 that the advantages of a promotion of the operator instead of the manufacturer and additionally, that more effective plants should get bigger market odds, a support of EU 0.03 per

generated KWh was guaranteed by the 250 MW-Programme (started in 1991) By this buyback policy and other measures the use of wind energy in Germany boomed, and the annual installation had reached 150 MW in 1993, 309 MW in 1994 and 509 MW in 1995 (Energiewerkstatt, 1993). This increase was due to the enlargement of the generator performance from 250 to 500/600 KW, but in the following years this generator performance was quickly raised up to 5 MW and even larger are planned.

Global wind power capacity installed by the end of 2003 was in total Americas 6905 MW, in total Europe 29301 MW, total South on East Asia 2707 MW, total OECD Pacific 1083 MW, total Africa 211 MW and the rest of the world 95 MW (Renew Energy World, Rev. Issue Aug.2004). India has a capacity of about 46 GW from which 2,125 GW are already used in 2003 (BTM report 2003) being the 5th largest wind power producer. In China the total potential of wind energy is estimated with 3226 GW from which about 253 GW can be used not including offshore potentials. The highest wind energy resources can be found in Inner Mongolia.

Great progress was made in the last years in the offshore installations where Europe leads the way in offshore wind farm development. Until the end of 2004 there exist in Europe 326 offshore installations with 604,46 MW installed capacity. The first wind farm in European waters under operation was Vindeby in Denmark with a rated capacity of 4,95 MW from 11 turbines; the largest is build in Horns Rev, Denmark, with 160 MW rated capacity from 80 turbines. The situation is changing very rapidly, with new installations being commissioned all the time. The goals are ambitious. Denmark plans for 4000 MW of offshore-based power by 2030, which should meet some 40% of national demand. The UK plans for 2600 MW offshore capacity by 2010. In Spain around Cape Trafalgar 6 large off-shore wind farms are planned with an overall capacity of 2563 MW.

The future prospects for wind energy exploitation are described in a Greenpeace study (Windforce 12, 2005). The aim of this study has been to assess the technical, economic and resource implications for a penetration of wind power into the global electricity systems equal to 12 percent of total future demand and whether such a 12 percent penetration might be possible within two decades. In this 12 percent scenario a carbon dioxide reduction due to the use of wind power will amount from 13.3 million tonnes/year in 1998 to 1.780 million tonnes/year in 2020 which gives a cumulative reduction of 10.650 million tonnes/year until 2020.

Wind power utilisation continues to grow further rapidly and it is assumed that this rapid increase will go on so that in 2035 (after BTM Consult, ApS, Denmark, 2005) 10% of total electricity consumption (= 1.9 TW) will be covered by wind energy. After a press release from 17 August 2005 issued by the Global Wind Energy Council (GWEC) the global wind energy marked will double to a $25 billion per year by 2010. The total capacity of global wind power grew to almost 48 GW during 2004. Europe maintained its role as the largest wind power continent in 2004 with 73 % of all new installation. Asia registered strong development mainly driven by the markets in China, India and Japan and accounted for 20.2 %. Most of the capacity in Europe has been installed in countries which have set up legally secured conditions for renewable energies (Germany, Spain, Denmark, Austria). In the 1990 and the first years of 2000 many projects which fulfilled some lowest limit for economic operation (for Central European conditions these are 400 hours/year with full load and 220 W/m^2 of swept rotor area) have been sponsored by many European governments. However, these measures have been revoked now in most countries arguing that this kind of green energy can already compete in the common market for energy. Industry statistics released for the EU wind energy market show that cumulative wind power capacity increased by 20% to 34205 MW at the end of 2004, up from 28568 MW at the end of 2003 and the wind power market increased by 4% in this years. The two largest producers, namely Germany and Spain, have here a share of cumulative wind energy capacity of 16629 MW and 8 263 MW respectively. China has by the end of 2004 1292 WTGSs with accumulative installed capacity of 764 MW. These WTGSs are distributed in 43 wind farms in 14 provinces, autonomous regions and cities. In the years 2000-2004 the average annual rate of growth for installed WTGSs was 22 % and the rate for accumulated installed capacity was 36 % (based on the data of the end of 1999). According to the information from the State Development and the Reform Commission of China the average annual growth rate of installed WTGSs will be 30% and accumulated installed capacity will reach 4000 MW until 2010. From 2010 to 2020 the rate of increase will be 20% and the capacity will reach 20 000 MW until 2020.

But the penetration of wind power of the world's electricity supply is still very low, so at the end of 2004 it reached 0.54% (AWEA, 2005) and the end of 2005 0.57 % (BTM Consult ApS, 2005). The main barriers to large scale implementation of wind power are the perceived intermittency of wind and the difficulty in identifying good wind locations, especially in developing countries. In the first case a solution may be a linking of multiple wind farms together over a wide area to reduce spatial and temporal correlation of wind speeds and in the second case a high resolution global assessment of wind energy potentials still has to be carried out.

2 SOME TECHNICAL ASPECTS OF WIND ENERGY UTILISATION

Utilising wind energy entails installing a device that converts part of the kinetic energy in the atmosphere to, say, mechanically useful energy. This kind of conversion of wind energy into the motion of a body has been in use for a long time. Almost any physical construction that produces an asymmetric force in a wind flow can be made to rotate, translate or oscillate thereby generating power. How this works is shown in the next sections.

2.1 The power of a moving air mass

If a body of mass m moves with speed v it has the energy

(2.1) $$E = \frac{1}{2} m v^2$$

The mass of air for a given volume with known air density ρ (the height dependency of ρ is treated in paragraph 3.1) is:

(2.2) $$m = \rho \cdot V$$

The volume streaming through the rotor circle F is per time-unit

(2.3) $$V = F.v$$

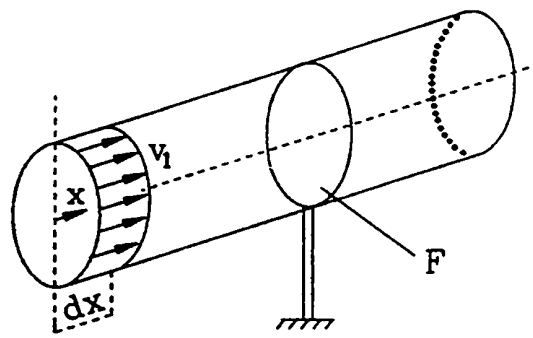

Figure 2.1: Mass flow through a surface F (Gasch, 1991)

From Eq.(2.1) to Eq.(2.3) the power of the air per unit time results in

(2.4) $$P = \frac{1}{2} \rho v^3 F$$

2.2 The power of an ideal WTGS

If the overall power of a given wind vector is known, the question arises how much power can really be extracted from it. It is clear that if a WTGS achieves no deceleration of the air flow the extracted power is zero. If the air flow were to stop at the rotor level a following air parcel can not blow through the converter but only flow around it. This results again in a performance of zero. Between these two extremes there is a range within which the extracted power reaches a maximum. For the estimation of this maximum the following should be valid: Firstly, the air should be regarded as incompressible, which is approximately true for wind speeds below 100 m/sec. Secondly, the converter should not have any aerodynamic or mechanical losses, a so-called ideal WTGS (Hau, 1996; Molly; 1990, Gasch, 1991).

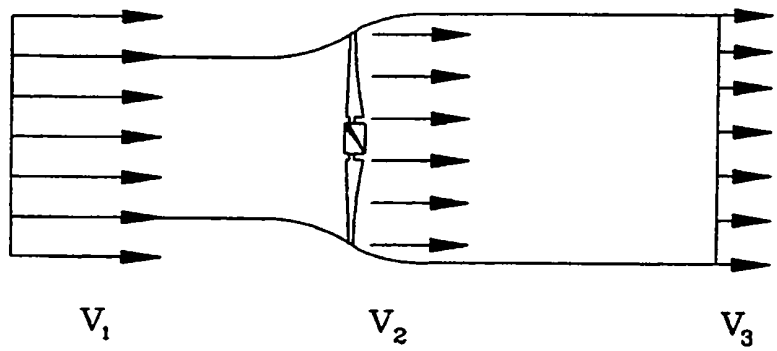

Figure 2.2: Flow through an idealised wind turbine (Gasch, 1991)

Marking the properties with the index 1 on the windward side of the WTGS, with the index 2 those in the converter level and with the index 3 those on the leeward side, the extractable energy flux or power is given by

$$P_{extr} = P_1 - P_3 = \frac{1}{2}\rho(F_1 v_1^3 - F_3 v_3^3) \tag{2.5}$$

In consideration of the continuity equation for an incompressible medium

$$F_1 v_1 = F_2 v_2 = F_3 v_3 \tag{2.6}$$

one can express F_3 by substitution:

$$P_{extr} = \frac{1}{2}\rho F_1 v_1 (v_1^2 - v_3^2) \tag{2.7}$$

In this equation F_1 is unknown, because only the surface facing against the wind is known. For the modification of Eq.(2.7) the fact that the force acting on the converter being the same as that which the converter exerts on the moving air mass can be used (Molly, 1990). The extractable power is then

$$P_{extr} = S v_2 \tag{2.8}$$

with

$$S = \dot{m}(v_1 - v_3) = \rho F_1 v_1 (v_1 - v_3) \tag{2.9}$$

Setting Eq.(2.7) equal to Eq.(2.9) it follows

$$v_2 = \frac{1}{2}(v_1 + v_3), \tag{2.10}$$

which is known as the *Froude-Rankine' theorem* (Gasch, 1991). Considering Eq.(2.6) the extractable power results as:

$$P_{extr} = \frac{1}{4}\rho F_2 (v_1 + v_3)(v_1^{\,2} - v_3^{\,2}) \tag{2.11}$$

Dividing Eq.(2.11) by the power

$$P = \frac{1}{2}\rho F_2 v_1^{\,3} \tag{2.12}$$

the rate of effective extractable power of the WTGS, called the ***power-coefficient,*** yields

$$c_p = \frac{P_{extr}}{P} = \frac{1}{2}(1 - x^2)(1 + x), \tag{2.13}$$

with $x = v_3/v_1$. In order to determine the maximum of c_p, the first derivation of c_p with respect to x must be set to zero and then x determined from this, introducing this result into Eq.(2.13) we get the so-called *maximum power-coefficient:*

$$c_{p\,\mathbf{max}} = \frac{16}{27} = 0.5926 \tag{2.14 a}$$

$$v_{3opt} = \frac{1}{3}v_1 \tag{2.14 b}$$

$$v_{2opt} = \frac{2}{3}v_1 \tag{2.14 c}$$

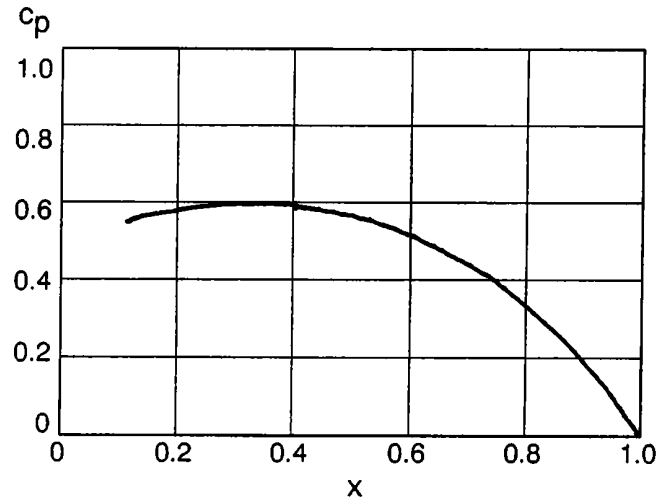

Figure 2.3: The course of the power-coefficient with respect to the ratio of the velocities in front and behind a rotor, $x = v_3/v_1$ (Hau, 1996)

The maximum power density that can be extracted by a WTGS from the wind flow will be consequently at a maximum at 59.26 percent (Figure 2.3) of the actual given wind power. For comparison caloric power plants have only an efficiency of about 30 to 40 percent.

2.3 Aerodynamic concepts for power extraction

2.3.1 The aerodynamic drag

The utilisation of the aerodynamic drag represents the oldest form of extracting power from the wind. Each surface F, standing vertically in the flow, experiences a force which is equal to the drag of the surface opposite to that flow and which acts in the flow direction (Molly, 1990; Gasch, 1991). This force is proportional to F, to the air density and to the square of the wind speed:

$$W = c_w \frac{\rho}{2} F v^2 \tag{2.15}$$

The factor c_w is called the ***drag-coefficient*** and quantifies the effects from the form of the resistance surface. In Table 2.1 the drag-coefficients of different bodies are listed:

Table 2.1: The drag-coefficients of different bodies (Boeswirth, 1993)

Body	c_w
Hemispheric cup, open opposite to the current	1.33
Hemispheric cup, with surface, opposite to the current	1.17
Hemispheric cup, with surface	0.40
Circular disk	1.11
Rectangular strip, w : h = 4	1.19

For a rotating system of resistance surfaces, which is affected only half-sided by the flow an upwind speed results with

$$v_r = v_w - u = v_w - \omega r \tag{2.16}$$

where v_w is the wind speed and u the rotation speed of the outer parts of the resistance surface rotating with the angular velocity ω and an average radius r. For the drag force W it can be written therefore as

$$W = c_w \frac{\rho}{2}(v_w - u)^2 F \tag{2.17}$$

The averaged - in reality slightly pulsating – propulsion power is then

$$P = uW = \frac{\rho}{2} F v_w^{\,3} \left[c_w (1 - \frac{u}{v_w})^2 \frac{u}{v_w} \right] \tag{2.18}$$

and c_p

$$c_p = c_w (1 - \frac{u}{v_w})^2 \frac{u}{v_w} \tag{2.19}$$

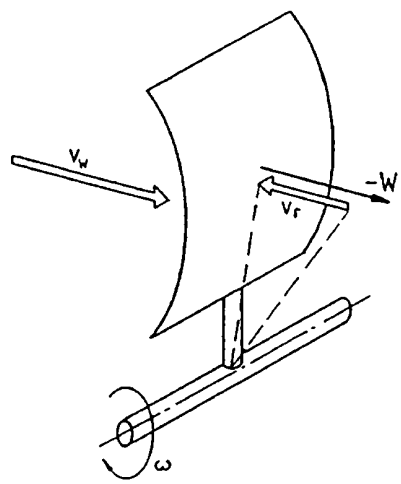

Figure 2.4: Flow conditions and air forces for aerodynamic drag (Hau, 1996)

The ratio $u/v_w = \lambda$ is generally called ***tip-speed-ratio*** of the WTGS. It is obvious that with converters based on the aerodynamic drag principle this tip-speed-ratio must lie between zero and one. The optimal power-coefficient is given with $\lambda = 1/3$, hence

$$c_{p\,\mathrm{max}} = \frac{4}{27} c_w \tag{2.20}$$

Assuming a maximum $c_w = 1.33$ (open hemisphere in flow direction), the maximum possible power-coefficient amounts to $c_{pmax} = 0.197$. But when considering real machines the surfaces of the covered half-side experience a drag force proportional to the rotation speed, the power-coefficient is further reduced and it becomes clearly evident, why this principle plays no current role in the exploitation of wind energy.

2.3.2 The aerodynamic buoyancy

Already by the 18th century power-coefficients from the Dutch Windmills reached 0.28 and present-day plants have power-coefficients up to $c_p = 0.5$. The principle by which such high efficiencies are reached is aerodynamic buoyancy. Similar to flow drag it is proportional to the air density, the surface and the square of the flow velocity. The buoyancy A acts perpendicular to the flow direction (Boeswirth, 1993; Schlichting, 1967)

$$A = c_a \frac{\rho}{2} F v^2 \tag{2.21}$$

c_a is named the ***lift-coefficient*** and is dependent on the angle of attack α (the angle between the surface of the rotor plane and the flow direction). For a flat plate thus it is valid:

$$c_a(\alpha) = 2\pi \sin\alpha \tag{2.22}$$

Most aerodynamically formed profiles from aeroplane design reach higher c_a values because they possess a curvature that reinforces the buoyancy. The drag-coefficients of these profiles compared with the lift-coefficient are very small: good profiles reach a ***lift-drag ratio*** ε (= ratio of c_a to c_w) of over 150. The point of attack of the force lies for small angles approximately within one third upto a quarter of the blade depth. The lift-coefficient with larger angles of attack deviates more and more from the theoretical one as given by Eq.(2.22). If the angle of attack is larger than a profile-specific threshold that usually lies approximately around 15 degrees, it decreases with larger angles. The drag increases in this range greatly: By the strong slanted position of the surface, the flow over the rear can not maintain a regular form, bigger whirls are formed, leading to a separation of the regular flow from the surface. This condition (see paragraph.5.1.4) is called *flow-separation* or *stall* (Boeswirth, 1993; Schlichting, 1967).

To show the function for the most important group of WTGSs, (the buoyancy using turbines with horizontal axis) in the following the distribution of forces on a rotating rotor blade with radius R is discussed. Firstly, we consider a cross-section of the rotor blade at a distance r from the rotation axis (Gasch, 1991). Because the blade rotates the wind speed is supplemented by the circumference speed to the resulting upwind speed. How this takes place is shown in Figure 2.5 where the angle of attack β (with respect to the axial direction) can be estimated very simply from the tip-speed-ratio:

$$\tan\beta = \frac{3}{2}\lambda\frac{\mathrm{r}}{\mathrm{R}} \tag{2.23}$$

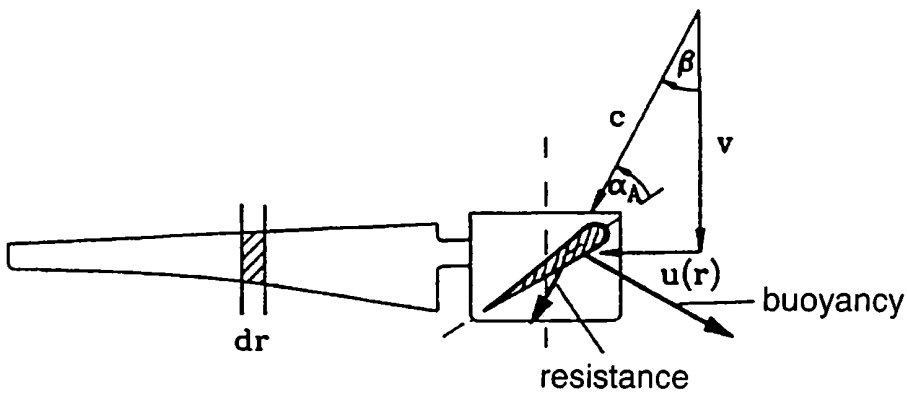

Figure 2.5: Air forces in the wing path plane (Gasch, 1991)

For this angle the forces can be determined in axis - and in rotation direction. The force in axis direction is the shear stress dS on the surface, the force dU in the rotation direction causes a power reduction:

(2.24a) $$dU = \frac{\rho}{2} c^2 (c_a \cos\beta - c_w \sin\beta) dr$$

(2.24b) $$dS = \frac{\rho}{2} c^2 (c_a \sin\beta - c_w \cos\beta) dr$$

Two important results can be derived from this: Firstly, wind turbines based on the buoyancy principle can reach tip-speed ratios $\lambda > 1$. Presently, rotors with high tip-speed ratio reach a λ between 5 and 10. Because the force of the air depends on the square of the flow speed it is clear why buoyancy using wind turbines reach essentially higher power-coefficients than aerodynamic drag using types. Secondly, the faster the rotor blades rotate, the larger the angle β becomes. Because the lift-coefficient is multiplied by the cosine and the drag-coefficient by the sine it follows that rotor blades for high rotation speeds must have profiles with a favourable relationship of c_a and c_w (Hau, 1996; Molly, 1990).

To reach the optimal range of attenuation of the air in the rotor circle plane (and with it optimal power extraction), each wing section must have an exactly defined blade shape and angle. Accordingly, if the spin of the air flowing away is taken into account, or not, one speaks of Schmitz's or Betz's design of the rotor blades. After Schmitz the cord length of a turbine with n rotor blades is

(2.25) $$t_{schmitz} = \frac{16\pi r}{c_a} \sin^2\left(\frac{1}{3}\alpha_1\right) \frac{1}{n}; \qquad \text{with} \quad \alpha_1 = \tan^{-1}\left(\frac{R}{r\lambda}\right)$$

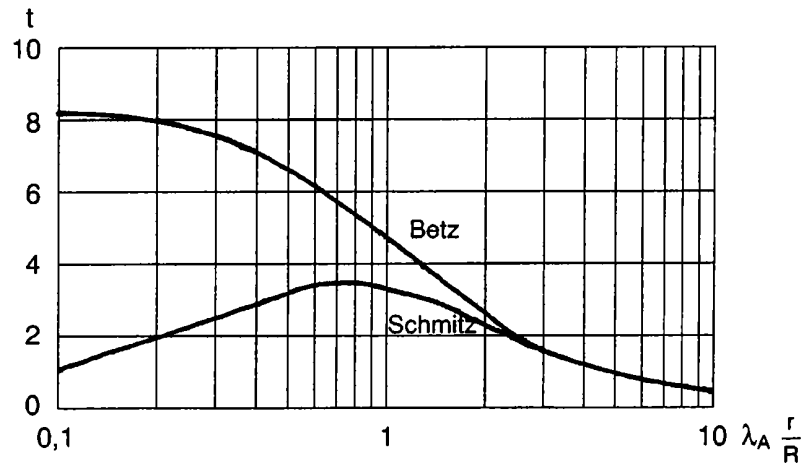

Figure 2.6: Comparison of the dimensionless rotor blade depth (t)after Betz and Schmitz, with reference to the local tip-speed ratio (Gasch, 1991)

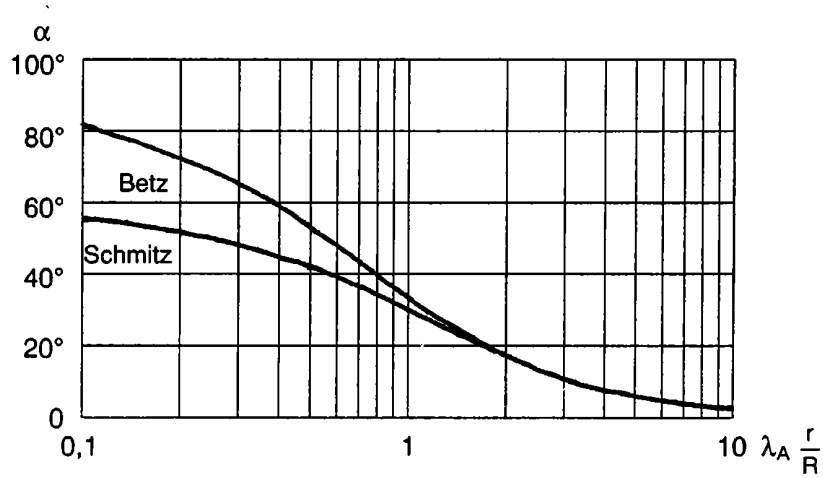

Figure 2.7: Angle of attack α in the rotor plain with and without regard to the spin with reference to the local tip-speed ratio (Gasch, 1991)

That WTGSs can not reach the Betz's efficiency has three aerodynamic causes (beside the electrical and mechanical ones): The losses due to the profile resistance, the edge whirls at the blade tips and the spin that is induced by the rotation in the air flowing away. The profile losses are directly proportional to the tip-speed-ratio and indirectly proportional to the lift-drag-ratio ε of the profile.

$$\zeta_{\text{profil}} = \frac{\lambda}{\varepsilon} \tag{2.26}$$

The losses at the blade tips decrease with increasing number of blades and tip-speed-ratio.

(2.27) $$\zeta_{tip} = 1 - (1 - \frac{0.92}{z\sqrt{\lambda^2 + \frac{4}{9}}})^2$$

For high tip-speed-ratios, and as they are usually two - and three-blade rotors, this can be simplified to:

(2.28) $$\zeta_{tip} \approx \frac{1.84}{z\lambda}$$

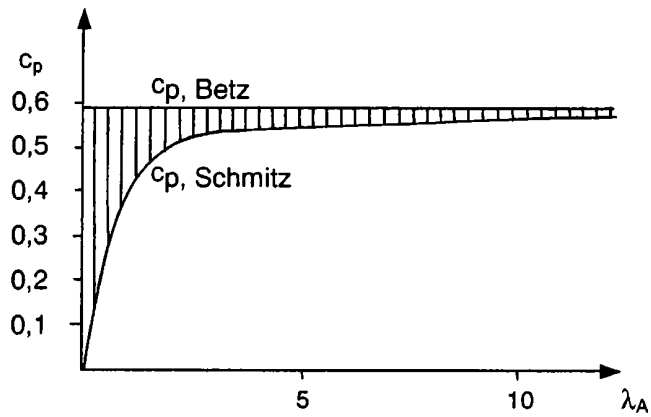

Figure 2.8: The power-coefficient after Betz (without) and Schmitz (with wake spin). The hatched area represents the spin losses (Gasch, 1991).

The spin losses become more inferior with increasing tip-speed ratio and for $\lambda > 5$ they lie under 10 percent. Generally in high-speed WTGSs the power-coefficient is almost only reduced by the profile drag, in low-speed turbines only by the wake spin (Molly, 1990; Gasch, 1991).

A WTGS has however, as already mentioned, not only aerodynamic losses. The rotor gives its power to a working machine, for example a pump or a generator, which also causes a loss in performance. Beside this further losses originate from the bearings of the axis (Franquesta, 1989).

To illustrate all this information about blade depth, angle of attack and efficiency, the data of a rotor with 4 blades with a Clark Y-profile and plain underside are given here:

Table 2.2: Design and geometrical data of a small wind wheel

ROTOR 4.4	
Diameter	3 m
Number of the blades	4
Tip-speed-ratio	4
Profile	Clark Y
Profile thickness	11.7% of the wing depth
Cord length, outside radius (r=R)	0.149 m
Angle of attack, outside radius	9.4°
Cord length inside radius (r=0.1*R)	0.389 m
Angle of attack inside radius	42.4°

A quintessential point is the calculation of the power-coefficient in relation to the actual tip- speed-ratio. In the case of coupling a rotor with a generator the rotational speed, which corresponds to the design-tip-speed-ratio, is usually reached only at a certain wind speed. Above and below this speed the rotor blades are not in the optimal direction of air flow, resulting in a lower power-coefficient. Such a $c_{p\lambda}$ curve for the Rotor 4.4 is represented in Table 2.3.

Table 2.3: The power-coefficient and the tip-speed ratio dependent on the angle of attack of the flow

Angle of attack	0°	2°	4°	6°	8°	10°	12°	14°
Tip-speed ratio λ	7.19	5.41	4.57	4.00	3.54	3.21	2.96	2.51
Power-coefficient c_p	.295	.352	.370	.375	.364	.349	.329	.292

The rotor has a maximum power-coefficient of 37.5 percent at the design-tip-speed ratio and for a wide range in angle of attack (between 2° and 10°) a power-coefficient over 35 percent is reached. These values can indeed not be reached by large WTGSs, since the rotor works with much lower Reynolds numbers.

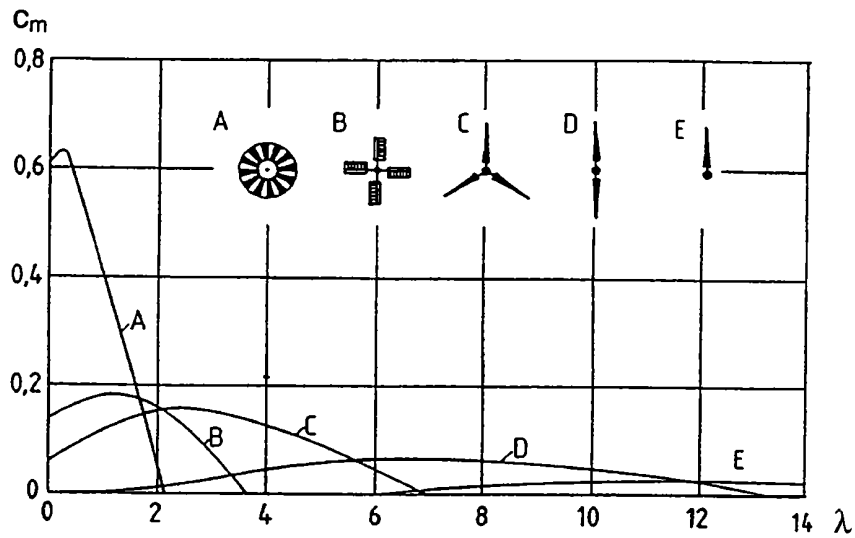

Figure 2.9: The torque-coefficients for rotors of different construction (Hau, 1996)

From the $c_{p\lambda}$ curve for each wind speed the power and torque at a rotation speed of the rotor can be determined. From the torque characteristics another difference between low-speed and high-speed WTGSs becomes evident: Low-speed ones have only a very small torque-coefficient in the start-up phase ($\lambda = 0$), which is inversely proportional to the square of the tip-speed ratio (Franquesta, 1989):

$$c_{m0} \approx \frac{1}{2\lambda^2} \tag{2.29}$$

Low-speed WTGSs with many blades (high area coverage) are therefore used mostly to drive a piston pump for water pumping, because in this case a high torque in the start phase is required. Rotors with a high tip-speed ratio are used in the generation of electricity because these generators show very high nominal rotational speeds with a low gear translation, resulting in a low weight of the nacelle. For the torque required in the start phase, either the angle of attack is changed or the rotor is brought firstly into a high rotational speed and then by means of a flyball coupling connected to the generator (Franquesta, 1989).

The aerodynamic principle for power output is not only restricted to the group of the horizontal axis WTGSs. The rotors with vertical axis have several different designs which can reach a higher tip-speed-ratio than 1 and consequently use the buoyancy principle. For example the Savonius rotor consists of two curved surfaces, which are installed displaced against each in opposition between two plates. The advantages of this rotor type are the easy start-up, operation at low wind speeds and independence from the wind direction. The disadvantages are the high material expenditure and the low efficiency. So an in-series manufactured Savonius rotor with 500 KW reaches only an efficiency of 9 percent. A higher efficiency is reached by the Darrieus rotor which is build like a "whisk" - or in H-form, the latter with straight blades developed by Musgrove in the UK (later adopted in a direct drive design of Heidelberg Machine). The disadvantage of this rotor is that it is not self-starting and only delivers an usable torque at high rotation speed. Nevertheless the simple design of Darrieus-type rotors led to several countries experimenting with them. Problems with resonance effects and the inferior energy yield due to the position of the rotor in low wind speed zones near the earth surface resulted in these vertical axis rotors rarely being built (Molly, 1990).

Another vertical axis rotor using the buoyancy principle is the Giromill, a H-shaped rotor with cyclic angle-of-attack steered rotor blades. In fact this design reaches even higher power-coefficients than the Darrieus rotor, but the advantage of independence from wind direction is traded for the special kind of angle steering required.

2.4 Conversion of kinetic energy into other energy forms

Since the mechanical energy of the rotor has only limited possibilities in direct applications (e.g. for grinding grain, water pumping) it is changed mostly into another energy form such as heat, potential and electrical energy.

2.4.1 Heat

Wind energy is converted into heat by means of an eddy-stream-brake in a liquid medium. Because this process is a fluid-mechanical one, the power characteristic of the working machine is identical to that of the rotor, which enables a virtually loss-free conversion. Disadvantages of this kind of heat production result from the situation of the medium to be warmed: Firstly, it must be located on the ground due to its weight, which makes it necessary for the horizontal axis rotors to have a power turn-round gear and a long shaft in the mast. Secondly, with heat conduction big losses are inherent, so proximity to the consumers must be given. This leads to optimal locations with wind energy potential often not being utilised. For these reasons and also on the basis of the advantages of alternatives (bio-mass, sun-collectors) this kind of energy conversion is hardly in use.

2.4.2 Potential energy

Increasingly important, especially in the developing countries, is the conversion from wind energy into potential energy for pumping water. Several types of application can be distinguished: Drinking water supply (for animals too), irrigation and drainage. Another differentiation can be made on the basis of the

location of the water to be pumped. The hydraulic performance is proportionally to the output M and the height H (e.g. for pumping) namely:

$$P_{hydr} = gHM\rho_w \tag{2.30}$$

ρ_w denotes the density of the water and g the acceleration due to gravity. This means that with the same power, either small outputs from deep locations (groundwater) or big outputs from near-surface locations can be achieved.

Which wind generator in which application is used depends on the working machine, in this case the pump. While piston-pumping using slow up - and downward movement of the plunger can pump water from up to 300 meters (typical example is the *Western Mill*), quickly turning gyroscope pumps can work only over a height of 10 m.

A disadvantage of the conversion into potential energy is again the linking of the WTGS site to the water occurrences, which is the reason why some wind pump systems use an electrical energy conversion unit (Gasch, 1991).

2.4.3 Electric energy

The conversion of rotational movement into electricity usually takes place with generators of various designs. The electrical energy is fed either into the existing electric grid (*network-parallel-solution*) or, independently from the grid, is directly used or accumulated in some kind of storage (*island-solution*).

In the latter case the supply security of the system is of great importance. Because of the strongly fluctuating wind energy potential large storage capacities must be established to attain a supply security of 100 percent. These storage capacities, in most cases batteries, in rare cases flywheels, are not completely ecologically harmless in production and raise the costs per generated KWh considerably. Therefore WTGSs in island solutions are usually linked with photovoltaic (PV) units, or diesel generators. Island solutions often work as a wind/diesel combination with constant frequency and with varying generators to a PV/wind compound system.

In the network-parallel-solution, one distinguishes *direct and indirect feeding* into the grid: Direct feeding is allowed if the current of the generator is delivered directly into the grid at constant frequency of 50 Hz (*Europe*). Indirect feeding is possible if a direct-current converter exists between generator and grid, i.e. the generator current is rectified and then reshaped into an alternating current with constant frequency. In this case a constant frequency at the generator is not necessary and operation with variable rotational speeds is possible (Molly, 1990).

Advantages of indirect feeding into the grid are the higher aerodynamic efficiency of the rotor, which can operate over a wide range of design tip-speed-ratios, disadvantages are the additional expenses and losses due to the frequency conversion technique. Although the number of WTGSs with indirect feeding into the grid is increasing recently, still most installations are feeding directly into the grid. Because of the necessity of an approximately constant rotation speed, which is only reached at a certain wind speed (where the design-tip-speed-ratio is reached), the unit works in all other speed ranges with poorer efficiency. To widen the optimal performance range most directly feeding turbines operate as either a high – or a low-wind speed generator or a pole-changing generator (Hau, 1996).

A variety of designs are used for electrical generators. In smaller WTGSs mainly for the loading of accumulators generators with permanent magnets are in use since these can generate electricity even if the accumulators are completely depleted. Beside the synchronous machines in rarer cases direct-current generators are used, these require no rectifier but have a higher maintenance expenditure (the voltage must be taken from the collector with slip rings). An important characteristic of generators is the number and

order of the poles. When the spool is within the magnet field, one speaks of an external pole generator, which has the disadvantage that current is collected over wearable slip rings. For internal pole generators with permanent magnets, or in generators with electromagnets only a low power transfer by slip rings is necessary. The larger the number of poles the more often the current changes its sign in one revolution. To attain the grid frequency of 50 Hz with a great number of poles a lower generator speed is required, which enables the rotor to drive the generator directly without gearing. This gear-less concept is used mostly in smaller units but can be found in large single plants too. The disadvantages are the high weight and cost of the generator, the advantages are the loss-free transfer of power from the rotor to the generator as well as the lack of noise pollution and lack of maintenance-intensive rotating parts.

Units with direct grid-feeding have either synchronous or more often asynchronous generators, while in the indirect grid-feeding units both variants are approximately equally often applied. This can be justified by the fact that synchronous generators with direct feeding can be disrupted by strong gusts due to the exact grid synchronisation required, and leads to infringement of the tilting moment which can result in stalling. In contrast, the asynchronous generator can stand small rotational speed fluctuations, that results in a simpler grid synchronisation. Furthermore, this kind of generator is simple and inexpensive but its disadvantage is the need for power to induce the magnetic field that must be taken from the grid or reactance-output condensers.

2.5 Power curves of real wind turbines

To forecast the energy yield from a WTGS the power curve is used as the technical characteristic for evaluation of the available power dependent on the wind speed and other relevant meteorological parameters. Since the working machine, including gears and bearings has a certain resistance against rotation and as units with high tip-speed-ratio show a low moment-coefficient when still, WTGSs begin to operate initially from a certain minimum wind speed, the so-called cut-in wind speed. This speed is defined by the technical design and is between 3 and 5 m/sec. With increasing wind speed the power output of grid-feeding WTGSs show their strongest increase at 1.4 to 2 times the average annual wind speed (Hau, 1996; Franquesta, 1989). The power increase slows up to the rated wind speed (V_{rated}) at which the rated power is reached. Typical values of V_{rated} are for low-wind units 10 to 13 m/sec and for strong-wind units 14 to 17 m/sec. If the rated power is reached the output of the unit is limited by a number of control systems to prevent overload of the generator and damage to the gearing. With further increasing wind speed the rated power output is maintained approximately until the so-called *cut-out wind speed* is reached and the rotation of the rotor is strongly braked or even stopped to avoid too higher thrust loading on the rotor blades and the tower. This cut-out speed for almost all grid-feeding units is at 25 m/sec. Low-speed WTGSs, e.g. a very small accumulator charger in the 100 W range often have no cut-out speed. As these units have lower blade-tip-speeds halting the unit will hardly cause a reduction in the thrust forces on the many rotor blades.

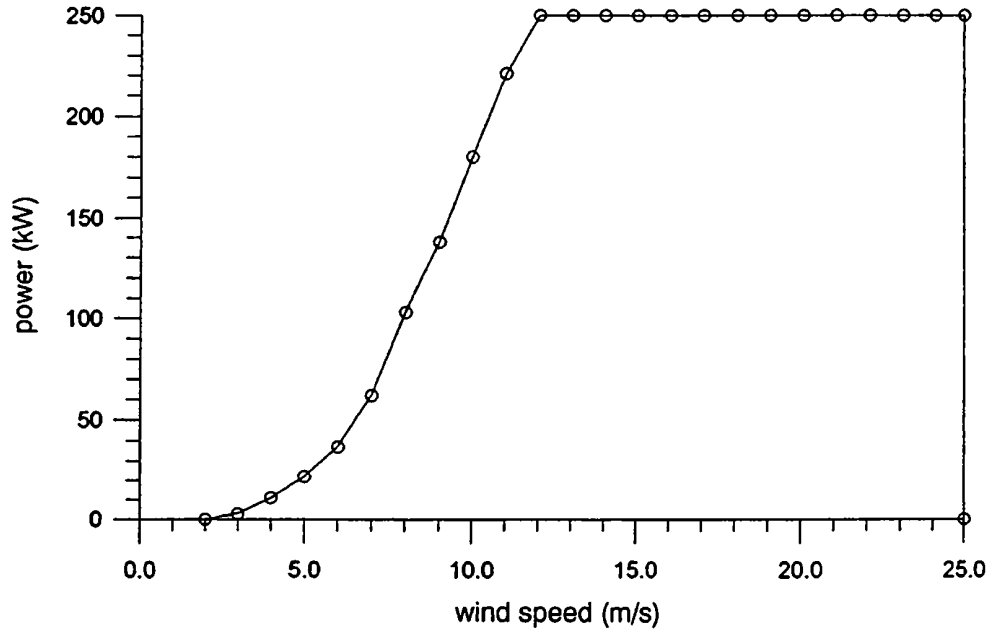

Figure 2.10: Power curve of a WTGS with pitch control (Lagerwey 250 KW)

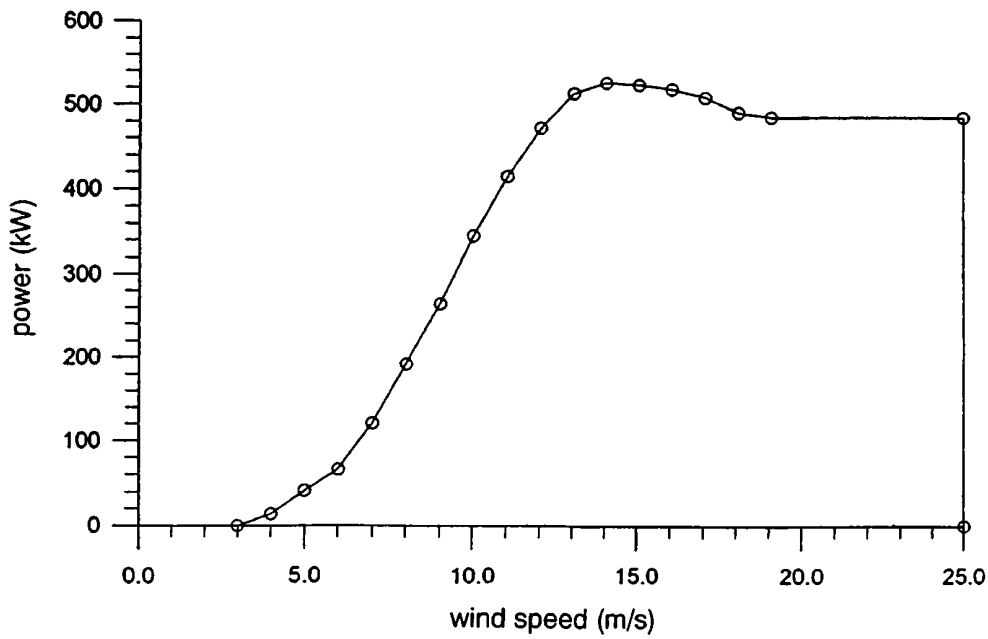

Figure 2.11: Power curve of a WTGS with stall control (Micon 500 KW)

Switching-off brings losses in the energy yield, but wind speeds above 25 m/sec are rare events, so that additional expense for the reinforcement of tower and rotor to stand higher wind speeds exceed the financial profit by the possible surplus yield at usual sites.

2.6 Control systems and yaw drives of WTGSs

For the necessary limitation of power output from WTGSs beyond their rated performance there are different control systems available but the choice of pitch or stall control is still a matter of discussion. In small units the tower head is often installed eccentrically before the mast axis and held in the wind in the partial-load range by means of a spring. Above the rated wind speed, the wind thrust presses the rotor out of the wind and reduces the effective surface area for power production. Turning from the perpendicular into the so-called „helicopter-position" allows power reduction. Bigger units with direct feeding into the grid often use the effect of stalling at the rotor blade. Because the rotor is strictly bound to the grid frequency with constant rotation speed for increasing wind speed the angle of attack of the rotor blade profile in upwind direction (see paragraph 2.3.2) is increased. If an angle of above 15-20 degrees is reached flow separation occurs from the profile upper side together with strong eddy development. From this the resistance is increased strongly and the power is reduced. The great advantage of this control system is that a simple connection of the rotor blade on the hub is possible. For very big units and units with indirect feeding into the grid usually a blade-angle adjustment (pitch) is applied for power limitation. Through the variation of the angle of attack and the resulting tip-speed ratio the power and rotational speed is regulated. The disadvantage of costlier technical regulation should be compared with the advantages of increased efficiency in the partial-load range and no additional cut-out mechanism during storms. With stall-regulated units the cut-out during storms is by means of aerodynamic brakes like adjustable blade tips or movable spoilers. Almost all WTGSs with stall - and pitch control, have a secondary mechanical brake for emergencies

The yaw drive of a WTGS with horizontal axis either takes place passively or actively. A passive yaw drive is effected by the attachment of the rotor in the lee of the tower, but for generators with high tip-speed-ratio and low area coverage of the rotor-circle surface this principle only works for a moving rotor. In the case of stall either the nacelle side wall must be used or an additional surface must be installed in the lee of the tower. With the positioning of the rotor on the windward side of the tower a passive yaw drive is possible if a wind vane with a sufficiently long lever arm is placed in the lee. This possibility is only used at smaller units, because the required material expenditure is too high for larger WTGSs. Active yaw drive was achieved previously by a slower running wind wheel with high torque attached to the side of the nacelle, that started to spin when crosswind components occurred and transferred this movement by a worm gear to the mounting ring of the tower connection. Nowadays the application of an electric support motor is commonly used, that is triggered by a small wind vane appropriately mounted at the nacelle. The disadvantage of this system lies in the wind vane, which can for example be disturbed in its function by icing (Hau, 1996, Franquesta, 1989).

2.7 Technical availability and life span of WTGSs

Under the technical availability of a WTGS one understands the ratio of the actual output from the converter to the extractable annual energy yield. This ratio reached in early installations of the Californian wind farms was often only 0.6 but nowadays the value reaches up to 0.98. The causes for the two percent loss in "mass-produced" WTGSs are manifold. To gain a better overview they are divided into internal and external causes. Whereas the internal faults causes (for example faulty management software or faulty component material) are specific for certain WTGS-types, the external ones show strong site dependence. From the Institute for Solar Energy Supply Technology (ISET) at the University of Kassel (Germany) the following table was compiled.

Table 2.5: Frequency (%) of external damage causes for different site categories (Energiewerkstatt, 1995)

Region	Grid-disconnection	Lightening	Icing	Storm
Coastal area (43%)	69	22	16	24
North-German Plains (36%)	8	21	19	29
Sub-alpine mountains (21%)	23	57	65	47

Of the four main causes for external faults as grid-disconnection, lightning strikes, icing and storm, in the coastal area of Northern Germany up to two thirds of grid-disconnection was responsible and icing rarely occurred, whereas in the German sub-alpine mountains the main causes were lightning and icing (c.f. paragraph 3.4. and 3.5).

The life span can be dramatically influenced by lightning. Therefore at present the following lightening protection concepts are observed: The use of a non-conducting rotor blade material without an additional lightning protection, application of an aluminium cap at the blade top and an aluminium band along the blade edge or application of a steel cap at the blade tips and lightning-conducting copper tissues at the other blade surfaces.

The first concept is technically the simplest and cheapest but has the disadvantage that by surface contamination and condensation of water conductivity on the blade surface can be established and then no lightning protection exists. The second concept provides sufficient protection for the part most at risk, the blade tip, however the rest of the blade remains unprotected. The third concept provides the highest protection for the whole blade but is the most expensive (Dwenger, 1995).

In order to reach a life span of 20 years or more a high standard of durability of the components is required. While for standard parts like the gearing or generators the longevity could readily be proven from reliable information of numerous tests but for the rotor blades this is rare. To reach higher durability, instead of glass fibre a carbon-fibre reinforced plastic can be chosen which requires enhanced lightning protection. It is presently assumed, on the basis of the economic insecurity, that the maximum life span for a unit is 15 years.

3 METEOROLOGICAL PARAMETERS IMPORTANT FOR THE SITING PROCEDURE AND THE LIFE SPAN OF WTGSS

The main factors influencing the wind field in the boundary layer of the atmosphere are the large-scale gradients of pressure and temperature, the earth rotation, the roughness of the earth surface, the daily course of stability, the depth of the boundary layer, horizontal advection (of heat and momentum), certain meteorological conditions such as clouds and rainfall and topographic properties (influencing the local and meso-scale circulation as mountain wind systems and sea breezes).

Whereas large-scale differences in wind climatologies allow identification of regions with propitious wind resources, the small scale phenomenon of the atmosphere in space and time e.g. turbulence and rare events such as hail, icing and lightning, are important for the construction and operation of wind turbines and for the selection of the optimal site for a given technology. This requires exact knowledge of the local spatial variation of the wind vector in the lowest 100 meters of the atmospheric boundary layer.

The basis of yield estimate from wind energy for certain sites is comprised of topics from meteorology, topography, technical construction of WTGSs, economy, local infrastructure, people's perception, natural and landscape protection, land use, noise emission, safety areas for airports and military facilities and others. Additional measurements of hourly or 10-min averages of wind speed and wind direction must be available as well as the 2-dimensional probability distribution of these properties and the gustiness and/or standard deviation (cf. paragraph 7.1.2). Additionally some climatological fingerprints must be known as the annual course of wind speed, its absolute maximum, the long-term average of air density, the 2-dimensional frequency distribution of air temperature and air humidity, the number of hours with heavy rain or hail and the number of days with storms and/or lightning strikes.

The necessary meteorological parameters can be subdivided into three groups: The first group determines the amount of the momentary power output and comprises air density and wind speed, the second group determines the energy yield during the entire time of operation and comprises the frequency-distribution of the wind speed, seasonal variability, the number of the days with icing of the rotor blades, and finally the third group with parameters important for the live span of the WTGS as there are lightning strikes, icing, hail and maximum wind gusts. Sound emission and shadow casting are treated in chapter 8 because these strongly influence the choice of the site due to certain legislative restrictions rather than meteorological conditions. Problems of corrosion and high turbulence are more an issue in tropical areas and are addressed extensively in WMO/TD-No.826 ("Meteorological Aspects and Recommendations for Assessing and Using the Wind as an Energy Source in the Tropics").

3.1 The air density

3.1.1 Definition

The air density is defined as the mass of an air-package standardised with unit volume. The air density is a function of space and time, where especially the vertical height dependence is essential for questions concerning wind energy. The air, showing a variable density, is considered as a compressible medium. For dry air at sea level with an atmospheric pressure of p = 1013.25 hPa and a temperature of 288 K the pressure amounts to

(3.1) $$\rho_0 = 1.225 \quad kg/m^2$$

3.1.2 The height dependency of the air density

Because there are only very slight differences in air density during a season at a certain height, for reasons of simplicity the height dependency is taken into account only for the hydrostatic fundamental equation

(3.2) $$dp = -\rho(z)gdz$$

For air with good approximation the equation of state for ideal gases is valid

(3.3) $$p = RT\rho$$

with T the absolute temperature in Kelvin (K) and R the gas constant, which for air amounts to

(3.4) $$R = 287 \quad \frac{m^2}{s^2 \cdot K}$$

To calculate the function $p(z)$ and $\rho(z)$ the temperature gradient $T(z)$ must be known. By appropriate assumptions about $T(z)$ corresponding models for the description of the atmosphere can be derived. Linear temperature gradients (isentropic and polytropic atmosphere) play the most important role. Isentropy means that there is no heat exchange with the surroundings (adiabatic) and no friction-losses (reversible) if a movement of the air mass to other heights occurs due to external disturbances. For the adiabatic reversible change in state for ideal gases it is valid:

(3.5) $$\frac{p}{p_0} = \frac{\rho^{\kappa'}}{\rho_0^{\kappa'}} = konst.$$

The parameter κ' is called the isentropic exponent and is for air $\kappa' = 1.4$. From Eq.(3.5) it follows after the integration of Eq.(3.2) the density course in the isentropic atmosphere (H_o = height of the homogenous atmosphere) is:

(3.6) $$\rho(z) = \rho_0 (1 - \frac{\kappa'-1}{\kappa'} \frac{z}{H_0})^{\frac{1}{\kappa'-1}}$$

For the polytropic atmosphere the general (empirical) formulation is:

(3.7) $$\frac{p}{p_0} = \frac{\rho^{n'}}{\rho_0^{n'}} = konst.$$

with n' the polytropic exponent. For the polytropic atmosphere the same density course as for the isentropic atmosphere is valid where κ' is replaced by n'. For $n' = 1{,}235$ and $H_0 = 8434$ meters it follows from Eq.(3.6)

(3.8) $$\rho(z) = \rho_0 (1 - 0.0000226z)^{4.25532}$$

Another approach is the following frequently used formula:

(3.9) $$\rho(z) = 1.2255 - 1.1743 \cdot 10^{-4} z + 4.0267 \cdot 10^{-9} z^2$$

An example for $\rho(z)$ and $\rho(z)/\rho_0$ is given in Table 3.1 for the first 3000 meters of the standard atmosphere

Table 3.1: Density and relative density of air dependent on height

Height *(m)*	ρ (kg/m^3)	ρ/ρ_0	Height *(m)*	ρ (kg/m^3)	ρ/ρ_0
0	1.225	1.000	1200	1.090	0.890
100	1.213	0.990	1400	1.069	0.872
200	1.202	0.981	1600	1.048	0.855
300	1.190	0.972	1800	1.027	0.838
400	1.179	0.962	2000	1.006	0.822
500	1.167	0.953	2200	0.986	0.805
600	1.156	0.944	2400	0.967	0.789
700	1.145	0.935	2600	0.947	0.773
800	1.134	0.925	2800	0.928	0.758
900	1.123	0.916	3000	0.909	0.742
1000	1.112	0.907			

3.1.3 The effects of air density on the energy yield of WTGSs

A reduction in air density causes a reduction in the power of wind. From Table 3.1 it can be seen, that at 1000 meters only 90.7 percent, at 2000 meters only 82.2 percent and at 3000 meters only 72.2 percent of the power at sea level is available. This means that (apart from other power reducing effects) the wind speed at 3000 meters must be about 10.5 percent above that at sea level in order to balance the power reduction with the decrease in density. As an example the power curve of a VestasV63 dependent on ρ and wind speed is given in Table 3.2. Additionally, with a lower air density differences in the aerodynamic behaviour of the rotor blades occur, that cause changes in the control behaviour of the WTGS.

Table 3.2: Changes of the power-curve (KW) of the Vestas V63 with 1.5 MW with respect to air density ρ (kg/m^3) and wind speed u_{10} (m/s)

	stand.Atm.									
u_{10}	1.225	1.06	1.09	1.12	1.15	1.18	1.21	1.24	1.27	ρ
4.5	19.4	12	13.3	14.7	16.0	17.4	18.8	20.1	21.5	**KW**
6	145	121	125	130	134	139	143	148	152	
8	421	358	369	381	392	404	415	426	438	
10	836	716	738	760	781	803	825	847	865	
12	1267	1107	1139	1169	1199	1226	1253	1278	1301	
14	1474	1396	1419	1434	1451	1459	1468	1476	1481	
16	1500	1491	1494	1496	1497	1498	1500	1500	1500	

3.2 The spatial distribution of the wind vector

Much information can be found in the appropriate literature about global and regional wind meteorologies and climatologies (e.g. WMO No.175, Mortensen et al., 1993; Dobesch et al., 1997). But because this is an important aspect in assessing wind power potential, the main features of the global and local wind system will be outlined here.

Usually one distinguishes when investigating wind climates, the large- and small-scale flows. Whereas the large-scale flows are governed by the global distribution of the air pressure systems (*Großwetterlagen*), the small-scale flows are additionally influenced by the atmospheric properties due to the change of day and night and to the local orographic conditions. As a consequence quite different approaches for describing the resulting wind fields have to be followed.

3.2.1 Large-scale wind flows

The driving force for global circulation is the sun giving an average flux of solar energy at the earth's surface equal to 350 W/m^{-2} (Goody et al., 1989). Of this energy approximately 31 percent is scattered back into space, 43 percent is absorbed at the earth's surface and 26 percent is absorbed by the atmosphere. Considering the back scattered portion, the albedo (ratio of outward to incoming flux of solar radiation) allows an average of 225 W/m^{-2} available for heating, directly and indirectly the earth and its atmosphere. From the curvature of the earth's surface and the seasonal variation of the position of the axis of the earth to the sun, the irradiation is spatially and temporally very different in its distribution across the earth's surface. In consideration of these differences in the irradiance as well as the regional differences in the albedo and the black-body radiation, that is proportional to the fourth power of the temperature of the radiating surface, the spatial distribution of the annual total radiation balance of the earth's surface is established causing large-scale temperature gradients resulting in the global circulation system.

It is now shown briefly how the global circulation results from this temperature pattern starting with the equation of motion. In an inertia system the forces of pressure, gravity and friction have to be considered. For the pressure force acting on a mass m can be written (Holton, 1992):

$$\frac{\vec{K}}{m} = -\frac{1}{\rho}\vec{\nabla} p \tag{3.10}$$

The friction force results from molecular forces of two flow layers moving with different velocities and is proportional to the curvature of the velocity profile in the co-ordinate axes:

$$\frac{\vec{K}_{r,i}}{m} = \sum_j \nu \frac{\partial^2 v_i}{\partial x_j^{\,2}} \tag{3.11}$$

Because the rotating earth is used as the reference system the centrifugal and Coriolis forces have to be considered. The centrifugal force acts vertically to the axis of rotation and is proportional to the square of the angular velocity of the earth (Holton, 1992):

$$\frac{\vec{K}_z}{m} = -\omega^2 \vec{r} \tag{3.12}$$

The angular velocity ω results from the rotation of the earth around her own axis in 23h 56min 4s (= 1 siderial day), its value amounts therefore to $\omega = 7.3\text{x}10^{-5}$ rad/s. Because the centrifugal force depends additionally on the distance to the axis of rotation its amount is greatest at the equator and at the poles equally zero.

The Coriolis force can be written with the vector of the earth's rotation $\vec{\Omega}$ ($\omega = |\vec{\Omega}|$) as

$$\frac{\vec{K_c}}{m} = -2\vec{\Omega}\times v, \qquad \vec{u}[u,v,w] \tag{3.13}$$

Now the momentum equations of the atmosphere can be summarised in vector notation

$$\frac{d\vec{v}}{dt} = -2\vec{\Omega}\times\vec{v} - \frac{1}{\rho}\vec{\nabla}p + \vec{g} + \frac{\vec{K_r}}{m}, \qquad \vec{g} = [0,0,-g] \tag{3.14}$$

In large-scale flows, the friction can be neglected so that for horizontal stationary flows the following approximations yields:

$$\frac{du}{dt} = 0 = 2\omega \sin\varphi\, v - \frac{1}{\rho}\frac{\partial p}{\partial x} \tag{3.15}$$

$$\frac{dv}{dt} = 0 = -2\omega \sin\varphi\, u - \frac{1}{\rho}\frac{\partial p}{\partial y} \tag{3.16}$$

These equations are called geostrophic approximations. By means of these relations it is possible to define a wind vector, the so-called *geostrophic wind*:

$$\vec{v}_g \equiv \vec{k}\times\frac{1}{f_c\rho}\vec{\nabla}p \tag{3.17}$$

$\vec{k}$ being the unit vector in the vertical and f_c the Coriolis parameter ($=2\omega \sin\varphi = 1.45.10^{-4}\ \text{s}^{-1} \sin\varphi$). The geostrophic wind after Eq.(3.19) however is only valid in uncurved flow. To account for an existing curvature of the isobars the amount of v_g has to be modified by the given centrifugal force whereas the direction is maintained. Therefore with the curvature 1/r it can be written for cyclonal curvature

$$\frac{1}{\rho}\frac{\partial p}{\partial n} = f_c v + \frac{v^2}{r} \tag{3.18}$$

and for anticyclonal curvature

$$\frac{1}{\rho}\frac{\partial p}{\partial n} = f_c v - \frac{v^2}{r} \tag{3.19}$$

The wind resulting from this pressure distribution is usually called *gradient-wind* which is smaller in cyclonal flow and greater for anticyclonal curvature than the geostrophic wind with the same pressure gradient.

3.2.2 Small-scale wind systems

Small-scale wind systems usually result from pressure differences caused by the different conditions of the atmosphere during day and night. These pressure differences have their origin in the different speeds and amount of the transformation of radiation energy into heat (and vice versa), which emerges from the properties and condition of the earth's surface. A typical example for this is the land-sea breeze or the mountain valley circulation (see paragraph 5.2.2). Mathematically a circulation can be formulated as

$$Z = \oint \vec{v}.d\vec{s} \tag{3.20}$$

with $\vec{v}$ the velocity vector and $d\vec{s}$ the path element along the closed curve. By expressing the acceleration $d\vec{v}/dt$ in the pressure gradient form, it follows

$$\frac{dZ}{dt} = \oint \alpha dp \tag{3.21}$$

with α the specific volume, the inverse of the density. A more descriptive form is obtained, if the specific volume is substituted by the equation of state for ideal gases:

$$\frac{dZ}{dt} = R_L \oint T \, d\ln p \tag{3.22}$$

with R_L the gas constant of the air and T the absolute temperature. An estimation of the circulation acceleration when investigating of sea-breezes in coastal regions or large lakes for example can be made by the simple formula

$$\frac{dZ}{dt} = \frac{(T_L - T_W)}{R_L} \cdot \ln \Delta p \tag{3.23}$$

with T_L and T_W the temperature of the land and water surface and Δp the pressure difference. In general a sea-breeze circulation can reach horizontally up to 80 km with a vertical extend of approximately one kilometre with wind speeds of 5 to 8 m/s. In Djakarta (Indonesia) close to the equator sea-breezes were observed with a speed of 10 m/s and a vertical extend of 4 km. In contrast to sea breeze the land wind circulation at night is much less developed and reaches only an extent from 300 – 500 meters (Haeckl, 1990, WMO 175).

In more complex mountain regions orographical induced wind systems develop, being generally weaker than the land- and sea-breeze systems but considerably stronger where additionally channelling effects occur. A typical example of such a superimposition represents the wind system of Lake Garda, Italy. Another possibility for high and continuous wind speeds in valleys occur if the main wind direction lies parallel to the valley axis. A further discussion about orographic induced flows is given in chapter 5.2.

3.3 The temporal variation of the wind vector

The motions in the atmosphere can have scales in time and space varying from 1 second to month and 1 mm to thousands of kilometres. In describing certain atmospheric processes temporal and spatial variations need to be considered together as can be seen clearly in Figure 3.1, where small-scale phenomenon appear only short-termed and large-scale ones only long-termed (Oke, 1987). The change of high- and low pressure systems in the mid-latitudes takes place approximately within five days on a wavelength of about 5000 km. The land-sea breeze circulation only lasts for 12 hours with a spatial extent of 50 - 100 km. Cumulonimbus clouds reach an extent of approximately 10 km and have a life span of approximately 4 - 6 hours. Small-scale thermal effects reach diameters of 100 – 200 meters and last up to 10 minutes. An impressive representation in which some of these different phenomenon participate in the prevailing wind climate at a location is given in Stull (1988) as a the frequency-spectrum of the wind measured with high time resolution.

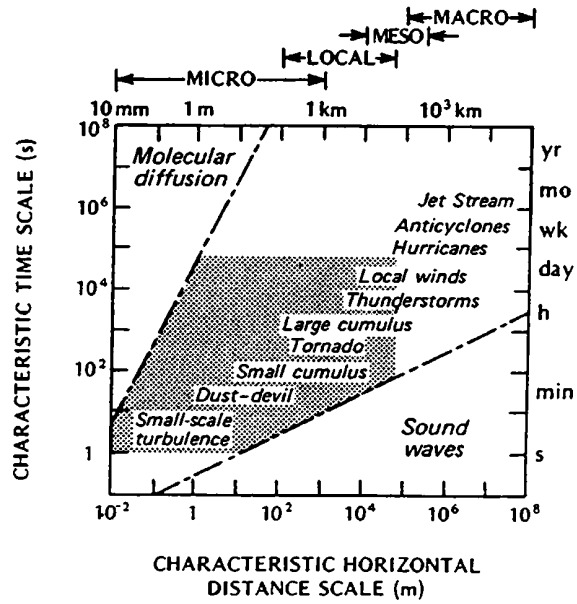

Figure 3.1: Time and spatial scales of atmospheric phenomenon (processes in the boundary layer in the hatched area); after Oke (1987)

It was shown by Van der Hoven (1956) that there exists a considerable lack of wind speed variation (spectral gap) in the time scale between about 20 and 120 minutes that is called the *energy gap*. The existence of this gap is described by the instantaneous wind speed u_i as a mean flow component $\overline{u}$ and a short term fluctuating component u' (Reynolds averaging) in the form:

$$u = \overline{u} + u' \tag{3.24}$$

The averaging period ($\bar{}$) T_o is chosen so that $\overline{u'} = 0$ and $\overline{u}$ is calculated, ideally, by

$$\overline{u} = \frac{1}{T_0}\int_0^{T_0} u(t)dt \tag{3.25}$$

or simply from N numbers of measurement by

$$\bar{u} = \frac{1}{N}\sum_{i=1}^{N} u_i \tag{3.26}$$

In order to simplify the calculation this average value is usually assumed as ergodic that means the spatial, temporal and the ensemble average are identical.

To characterise the short-term fluctuations within the averaging period the variance and the standard deviation of the wind speed is taken as

$$\sigma_u{}^2 = \frac{1}{N}\sum_{i=1}^{N}(u_i - \bar{u})^2 \tag{3.27}$$

and

$$\sigma_u \equiv (\overline{u'^2})^{1/2} \tag{3.28}$$

Furthermore, in horizontal homogenous terrain the turbulence intensity can be written as

$$I = \sigma_u / \bar{u} \tag{3.29}$$

The actual turbulence depends on the complexity of the terrain, the roughness of the land surface including single-standing obstacles on the windward side of the site, the existing vertical wind profile and the density stratification of the atmosphere. Typical values of the turbulence intensity lie between 0.08 for a smooth, even surface with stable density stratification and 0.5 for strongly inhomogeneous terrain with unstable density stratification. Because increasingly fluctuating aerodynamic forces originate with increasing turbulence intensity at the rotor blade, the knowledge of this parameter is for a certain site very important for WTGS installation (Molly, 1990; Wieringa, 1973). The turbulence intensity can be simplified for homogenous surface roughness z_o and neutral conditions to $I \approx 1/\ln(z/z_o)$.

Through different investigations it has been shown that the frequency spectrum of the turbulence derived from a point measurement on a mast differs quintessentially from that at a point on the rotor blade: In fact for the low-frequency turbulence range the assumption is valid that the eddy includes the entire rotor radius, consequently in this region the spectra are approximately the same. In the medium-frequency range the entire rotor is no longer involved and as a consequence the rotor blade enters the eddy only for a short time. Because of this the medium-frequency range is shifted into the high-frequency range where at each integral multiple of the rotor revolution a deflection occurs. This difference between the turbulence spectrum of an anemometer and that of a point on the rotor blade is illustrated in Figure 3.2.

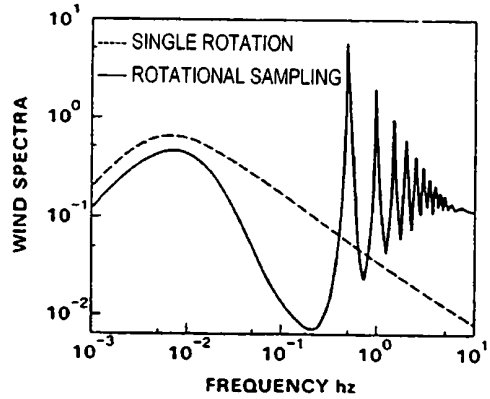

Figure 3.2: Comparison of the theoretical spectra of the wind speed at the rotor blade (straight line) and from a point measurement (broken line); after Aspliden et al. (1986)

Another parameter, that is necessary to describe the temporal development of turbulence is the average turbulent kinetic energy (*TKE*). It results, analogously to the kinetic energy of the average flow, as:

$$TKE = \frac{m}{2}(\overline{u'^2} + \overline{v'^2} + \overline{w'^2}) \tag{3.30}$$

A simple element to calculate is the so-called *gustfactor*:

$$G = u_{max} / \bar{u} \tag{3.31}$$

where u_{max} is the maximum gust during the averaging period of $\bar{u}$ (cf. Eq.(3.25)).

In order to get a three-dimensional picture of the parameters of a wind field measurements need to be made at numerous points, resulting in a high technical and financial expenditure. To reduce these efforts the Taylor-Hypothesis is often used, which states that for some special cases (where the turbulent eddies evolve with a time scale longer then the time it takes the eddy to be advected past a measurement device) turbulence might be considered to be frozen (*frozen field hypothesis*) as it moves past a sensor (Stull, 1988; Garratt, 1992). If the parameter X doesn't change in time ($dX/dt = 0$), then:

$$\frac{\partial X}{\partial t} = -u\frac{\partial X}{\partial x} - v\frac{\partial X}{\partial y} - w\frac{\partial X}{\partial z} \tag{3.32}$$

Having only one co-ordinate (for example the x-direction) and setting the air temperature as a turbulence element, gives

$$\frac{\partial T}{\partial t} = -u\frac{\partial T}{\partial x} \tag{3.33}$$

With a wind speed of 10 m/s and a temporal temperature fluctuation of -0.5 K/s a spatial temperature gradient of 0.05 K/m is obtained.

However the validity of the Taylor-Hypothesis is restricted for:

(3.34) $I \leq 0.5$

where the turbulence intensity is a measure of stationarity.

For WTGSs with active windward orientation the variation of the wind in the minute range is of great importance because greater changes in wind direction can not be compensated for over a very short time, as the gyroscopic forces developed evoke extreme structural loads. A consequence of such conditions is that the plant experiences some cross wind and does not reach the intended performance. Further performance reduction originates from fluctuations in the speed close to the cut-in and cut-out wind speed distributing the continuous operation in these velocity ranges.

Frequent strong fluctuations in the wind can occur within 24 hours. While during the night the air is mostly stable, stratified in the lowermost 50 meters, unstable conditions can develop during the day. This has the consequence that the vertical momentum transport is arrested almost completely in the second half of the night, while in unstable air in the early afternoon hours this is reinforced strongly. Because air packages are brought by momentum transport from higher levels with greater wind speeds into lower layers and vice versa, the highest speed can be observed at heights up to 50 meters at approximately 2:00 p.m. with the lowest during the second night-half (= daily course of the ground-type wind). The horizontal impulse is taken from the overlying layers, consequently these show exactly the opposite behaviour (= daily course of the height-type wind). In Figure 3.3 these two variants in the daily courses of wind speed are shown.

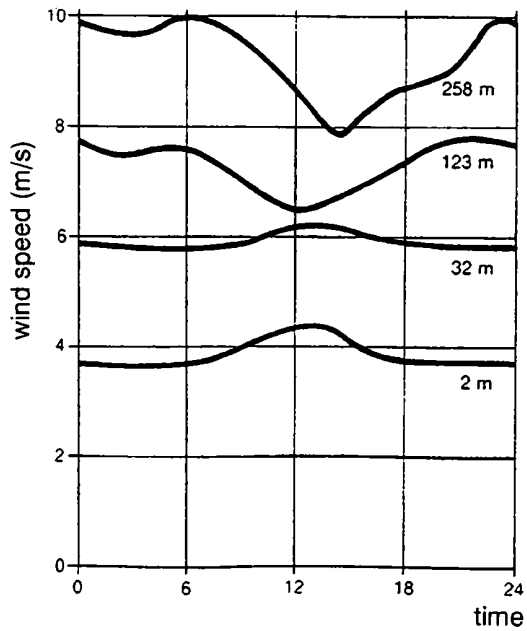

Figure 3.3: Daily course of wind speed at different heights for the radio-tower in Nauen (Haeckel, 1990)

If the demand for energy is subject to seasonal fluctuations, e.g. in the mid and high latitudes due to space heating in the winter, the seasonal distribution of wind energy is of interest for certain sites. This distribution is a function of the geographical latitude as well as the location of the site with respect to land surfaces properties and specific orographic features.

In general high wind speeds at mid-latitudes increase in the winter and at the beginning of spring. The relation of the wind energy density between winter and summer half year (without considering the air density fluctuations and possible icing) is for example at a typical location in the east of Austria respectively 0,62 and 0,38, and is positively correlated with demand.

In the tropics the yearly course is determined by the movement of the inner tropical convergence zone (ITK): While to the north and to the south of this zone powerful trade winds prevail, only low wind speeds can be observed within the regions. Due to the elevation of the sun these regions are shifted in July northward and in January southward, thus causing a low wind energy potential on the northern fringe areas of the tropics around July, in the southern fringe areas around January and at the equator twice a year around March and September (Aspliden et al., 1986).

Another important factor for the energy yield estimate of a WTGS is the deviation of annual average wind speed (measured over a short time period) from the long-time average value as the forecast should hold for the life span (15-20 years) of the WTGS. As a rule of thumb, the uncertainty introduced by a one-year-measurement of wind speed in comparison with the long-time average for a confidence level of 90 percent is 10 percent, which causes an uncertainty in the energy yield forecast of approximately 30 percent. In Austria a 114 year time series for a location in Vienna is available, the relative standard deviation of the annual average compared with the average of the long-time series amounts to 8.1 percent, thus being within the range determined by the aforementioned rule.

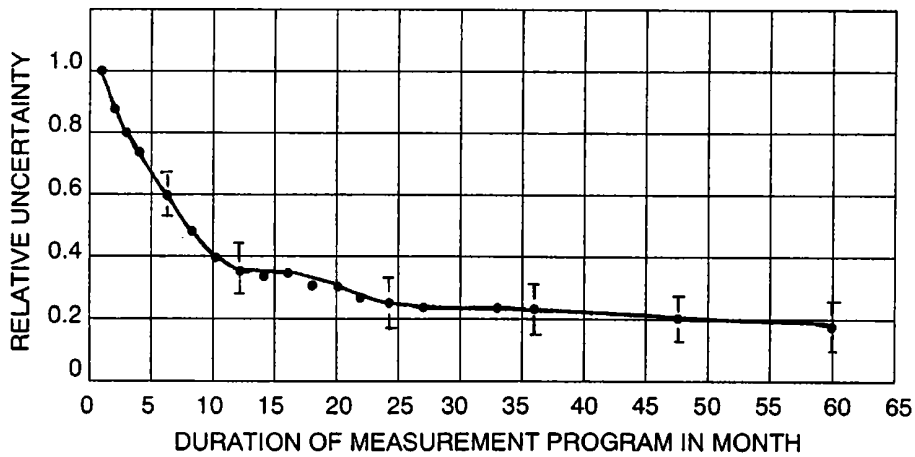

Figure 3.4: Relative error in the calculation of the wind power density with respect to the measurement period (Aspliden et al., 1986)

In Denmark the inter-annual variation of the energy yield estimated from a 22 year time series corresponded to an average relative standard deviation of 13 percent. Because of the seasonal fluctuations the extension of the measurement period leads to an increase in the forecast accuracy (Figure 3.4). Indeed, even for extreme cases with a 10-year measurement the differences in wind energy density can amount to 30 percent (Troen et al., 1989).

When in the siting procedure the problem arises that only a limited amount of measured wind data (typically one year) are available a straightforward technique must be applied to provide long term predictions of the wind characteristics at the site in question. For this analysis three sets of data are required:

- Time series data from the site containing wind speed and direction (u_s)

- Time series data from a meteorological station concurrent with the site data containing wind speed and direction (u_m)

- Historical data from the same meteorological station in the form of a time series or a frequency distribution table for wind speed and direction.

The site and meteorological station data are analysed to determine the correlation between the two sets of data in each of a number of directional sectors on the base of hourly values. This correlation is then used with the historical data to predict the wind climate that would have existed at the wind farm site during that historical period. The wind speeds are binned into directional sectors, and within each sector a linear best fit is applied which relates the wind speed at the meteorological station to that at the site, i.e. for an arbitrary direction

(3.35) $$u_s = c_1 u_m + c_2$$

The linear best fit can be made e.g. by standard least squares techniques or the York method (Press et al.,1992). This York method fits a strait line through the N data points (u_{s1}, u_{m1}), ..., (u_{sn}, u_{mn}) so that the sum of the squares of the distances of those points from the straight line is a minimum, where the distance is measured in the direction calculated by taking the relative errors of both data sets into account. Hence the chi-squared merit function

(3.36) $$\chi^2(c_1,c_2) = \sum_{i=1}^{N} \frac{(u_{mi} - c_2 - c_1 u_{si})^2}{\sigma_m^2 + c_1 \sigma_s^2}$$

is minimised which is the approach behind the York method.

A further improvement for the data from the site is that the frequency table, generated from the correlation process, can also be corrected for wind direction. The basis of the veer correction is to bin the hourly data from the meteorological station and site direction data into a square matrix (with the same dimensions as the historical direction sectors). This matrix is then normalised and used to redistribute the frequency data generated from the meteorological historical data to the final site frequency table.

3.4 The influence of precipitation events

3.4.1 Heavy rain

Slight or moderate rain does not influence the performance of a WTGS. During heavy rain however massive drop impacts occur at the rotor blades through which the flow around the profile is disturbed considerably. From measurements power losses up to 30 percent could be found according to the intensity of rain. The comparison of power curves with and without rain is illustrated in Figure 3.5. How far heavy rain influences the yearly energy yield can be made evident from the two-dimensional frequency distribution of precipitation and wind speed. However, it is to be expected that strong rain events will affect the operation of the WTGS during partial load, as this range delivers the greatest share of the energy yield.

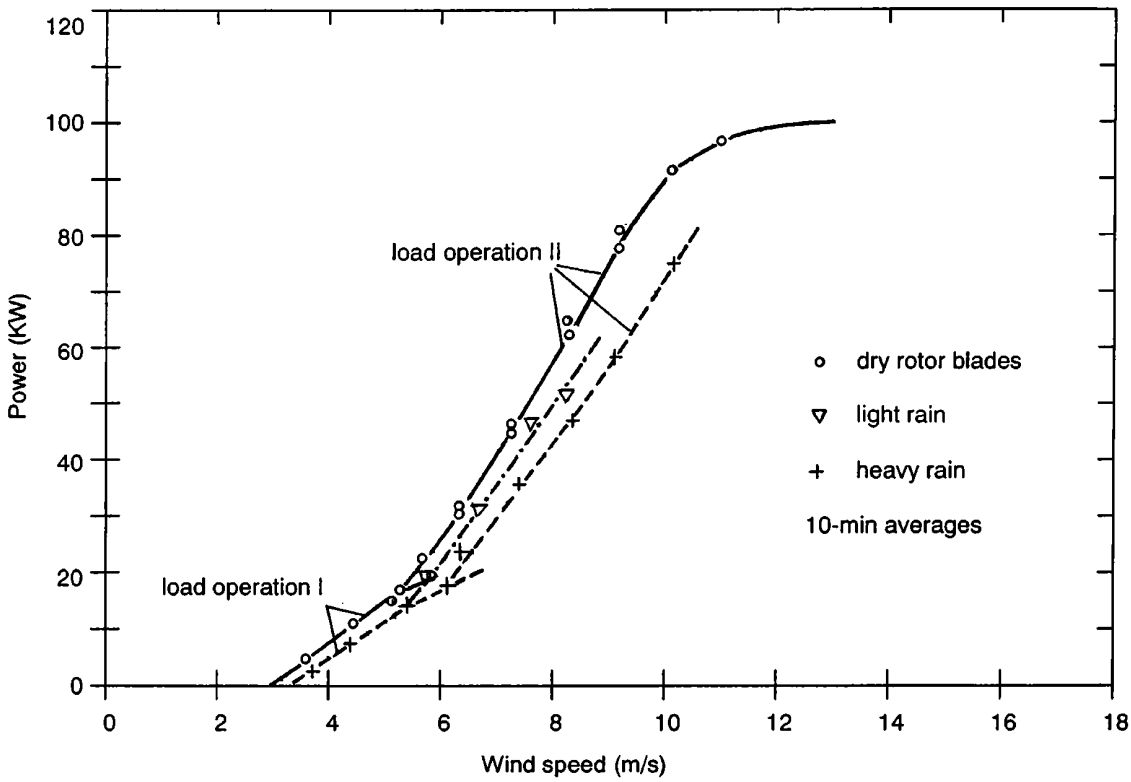

Figure 3.5: example of the influence of rain on the performance curve of a turbine (Energiewerkstatt, 1995)

3.4.2 Hail

The occurrence of hail represents a rare event and therefore hardly measurable losses in the annual energy yield are observed. In Vienna during a time period of 20 years, 26 days with hail occur, other typical European conditions are described in Svabik (1998). Much more important is, where damage can occur by the impact of hailstones on the leading edge profile of the rotor blades which can take place with speeds of over 100 m/s. Laboratory investigations have found no damages to the material, but from installed WTGSs with an operation time of several years it is known that slight damage does appear. As an example the 1 KW WTGS at the St.Pöltener Mountain Refuge in Austria, 2481 meters above sea level, experienced during a hail-storm an over-speeding event which led to damage of the rotor blade nose that finally required an exchange of the blades.

3.4.3 Icing

Icing gives rise to the most frequent decrease in performances of WTGSs at mid- or northern latitudes by significantly influencing the aerodynamic and aeroeleastic behaviour of the blades. Another result is the possible damage to people and property from ice shedding away from the blades. Icing is therefore the subject of many studies (e.g. the EU/JOULE project WTGSO "Wind Energy Production in Cold Climates" or BOREAS III, 1996 and BOREAS IV, 1998). The WTGSO project addressed a wide range of icing problems producing icing maps of Europe, modelling of ice accretion on structures and blades, modelling of the effect of iced blades on power production and loads, experimental data from wind turbines operating under icing conditions, ice free anemometers, ice detectors and public safety.

Two prerequisites are necessary for the appearance of icing on the rotor blades: Firstly the surface temperature must lie beneath 0°C and secondly supercooled water droplets, i.e. liquid water at temperatures below 0°C must occur. It is valid that the smaller the drop diameter is the more strongly will be the supercooling, reaching -40°C at its lowest limit.

The icing process results from either

- Impingement of supercooled water droplets or wet snow on the blade surface by which the inner structure of the droplet is disturbed and the freezing point raised to 0°C. Sudden freezing is the consequence. Ice accretion is therefore found particularly on those parts of the WTGS, that are exposed to a frontal impact of the water droplets.
- Sublimation on the blades
- Energy balance favouring ice formation

3.4.3.1 Types of icing

In general one distinguishes 4 types of icing: *Clear-ice (glaze, blue ice)*, *rough-ice, hoarfrost* and *rime ice.*

Clear-ice forms a transparent icecap with a glassy surface that originates by the accretion of freezing rain with temperatures between 0°C and -4°C. The icecap adapts itself to the form of the enclosed object and can hardly be removed from it. The very smooth surface results from the fact that the droplets during the impact freeze not immediately completely because of the released heat (335 kJ/kg water) during the freezing process and so the water is evenly distributed across the surface by the flow.

Rough ice is produced if the rain contains crystals of ice, snow or sleet. The icecap looses its smooth transparent surface and becomes granulated and appearing whitish-opaque. This ice accretion occurs with air temperatures from -4°C to -9°C and is among the most frequent forms of icing. From the inherent snow and sleet a strong influence on the aerodynamics of the rotor blades can occur.

Hoarfrost appears, if fine water droplets with temperatures of less than -10°C impact the WTGS and instantly freeze completely. As the drops can no longer flow together the accretion grows against the airflow around edges in the form of humps. From the accreted snow crystals a rough surface develops appearing brittle and milky, also containing air bubbles. The profile-form of the blades is changed massively such the power output is greatly reduced. Furthermore, as fragments easy separate from the rotor blades, these can be hurled away up to a distance up to three rotor diameters during operation.

Rime ice is the most common type of in cloud icing and forms on the upwind side of structures. The most severe occurrence is found on widely exposed mountains and hills. Different types of rime may be distinguished in accordance with their density, hardness and appearance:

Hard rime is granular and adheres firmly on surfaces; its density ranges between 100 and 600 kg/m^3;

Soft rime is a fragile snow-like formation with a density less than 100 kg/m^3;

Metamorphosed rime is rime ice altered due to sublimation.

Rime icing has hardly any effects on the operation of WTGSs (Eichenberger, 1990).

3.4.3.2 The physical background of icing

The physical mechanisms associated with ice accretion are numerous and complex and can be divided roughly into 3 categories:

- Mechanical and meteorological processes, participating in the generation of liquid water within the air flow around the object as rain and fog formation (Langmuir 1944, 1995);
- Processes associated with the motion of supercooled water droplets that strike and produce icing on the accretion surface; these processes can be described by the equations from fluid and particle mechanics which determine the trajectory pattern of the droplets within the air flow;
- Thermodynamic mechanisms involved directly or indirectly in the energy budget (such as latent heat release, forced convection, evaporative heat transfer, exchange of thermal energy (List 1977, Lozowski 1980, Makkonen 1981, 1982)

The intensity of icing depends on aerodynamic and meteorological factors (WMO 1962). The aerodynamic factors include the collection efficiency of the profile for droplets and the boundary layer heating at the rotor blade. The collection efficiency depends on the curvature radius of the profile nose, on the speed and the angle of attack of the wind vector, and on the droplet size. A basis for the estimation of this efficiency is gives by the trajectories of the droplets. While small droplets are taken around the rotor blade with the flow, big ones hit the blades sooner because of their inertia. Additionally narrow edges and higher speeds yield a higher percentage of cached droplets with respect to those carried through a cross-section by the undisturbed flow. The percentage of droplet caught increases proportionately with upwind speed.

An insignificant heating of the rotor blade occurs from the friction on the upper- and undersides as well as by compression of the air at the front of the rotor blade (Schlichting, 1967) which amounts to

$$\Delta T = 0.87 v_0^2 / 2c_p \tag{3.37}$$

For a rotor blade cross section in a stream of 60 m/s, a heating of the blade surface by about 2.07°C results. This enables icing to start at approximately -2°C. As the speed increases with increasing radius the maximum kinetic heating takes place at the blade tips. However, this decreasing effect on icing is more than compensated for by the higher collection efficiency, therefore the ice accretion increases outward linearly.

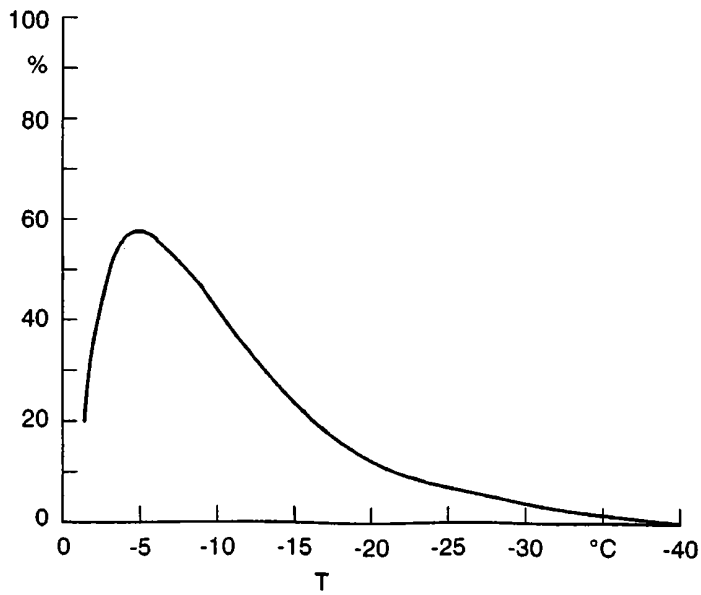

Figure 3.6: The relative frequency (in %) of observed cases (in %) with icing in relation to air temperature

As already mentioned, a prerequisite for icing is supercooled water droplets. Their number depends beside other factors on the air temperature. Between 0°C and -12°C the water particles are in the majority, in the range between -13°C to -20°C the number of ice and water particles is approximately equal, between -21°C and -40°C the ice particles prevail and below -40°C only ice particles exist. Because the ice particles in the air create no icing, the icing probability decreases strongly below -12°C. In aviation three quarters of the icing cases are observed above -15°C. The greatest icing probability lies between -4°C and -8°C. The amount of icing depends therefore strongly on the temperature. Because the freezing process of the liquid droplets is started by freezing nuclei and is dependent on their size, larger drops with a diameter of 1 mm are supercooled only down to -15°C, while smaller droplets with 10-20 µm diameter can reach -30°C. This means that essentially greater ice accretion is possible with temperatures just below 0°C, as the largest drops exist in this range. The relative air humidity plays a role in this respect too, as the ice particles grow during fog at the expense of water particles: This reduces the relative humidity to a value that corresponds to saturation above ice. The relative humidity of air is therefore a criterion for the ratio between water and ice particles as well.

In addition to the above mentioned studies the effects of ice accretion on the operation of a WTGS in the Swabian Alb, Germany, were investigated over a one year period. During this period icing occurred on 10-15 days with high wind speed and on 10-15 days with low wind speed. Usually the foremost parts of the blades were covered with ice up to 40 percent, but during freezing rain, icing also appeared over the entire blade depth. As a result the aerodynamics of the blade profile were extremely altered, the WTGS responded as stall-regulated with essentially less nominal power output. In order to examine the aerodynamic effects more accurately, plaster casts were taken of the frosted blade noses and were then tested in a wind tunnel, where premature flow separation and much higher resistance were determined.

Another problem is the imbalance from the burden of partial ice-load during the operation of a WTGS. This leads to strong vibrations and to premature fatigue of material or to fracture formation.

3.5 Lightning strikes

Heavy damage or even the destruction of the generator by lightning strikes represent a serious problem especially in mountainous regions. Two types of lightning impacts can be distinguished - the direct and the indirect impact. Direct impacts take place in the WTGS itself - usually the rotor blade - from where the discharge takes place over the rotor hub, the bearing, tower and foundation into the soil. The most serious damage involves the rotor blades and electric components. Indirect impacts take place over the medium-voltage grid, from where excess voltage waves propagate along the electrical distribution lines. Damage usually involves components which are insufficiently protected against over-voltage.

Table 3.3: Regional distribution of lightning damage in Germany, 1992-94 (Energiewerkstatt,1995)

	Coast	North-German Plains	sub-alpine mountains	all
WTGS number	584	455	263	1302
Years of operation	1251	936	465	2652
Observations (all)	85	64	109	258
Direct strike	25	16	22	63
Observations/WTGS-year	7%	7%	23%	10%
Direct strikes/ WTGS-year	2.0%	1.7%	4.7%	2.4%

In Germany under the framework of the Measurement- and Evaluation Programme during the period 1992 to 1994, 258 disturbances from lightning strikes on WTGSs were registered, with 195 indirect and 65 direct impacts (see Table 3.3). The essentially higher number of direct lightning-impacts in the mountain regions when compared to Northern Germany is as expected and agrees well with the spatial distribution of thunderstorm days per year (Svabik 1998).

4 SPATIAL DISTRIBUTION OF THE WIND SPEED ABOVE HOMOGENEOUS TERRAIN

In general the horizontal component of the wind velocity are typically two orders of magnitude larger than the vertical component, but they vary a great deal with height under the influence of the conditions in the boundary layer of the atmosphere and the underlying land surface. Therefore the information about the vertical profile of the wind in the atmospheric boundary layer and its physical properties forms the basis on which to assess wind power potentials. An overview of the main properties of this boundary layer is given in the following sections.

4.1 The atmospheric boundary layer

The part of the atmosphere that reacts to influences from the earth's surface with a time-lag of about one hour is called the atmospheric boundary layer (ABL). These influences consist of the friction of flow at the earth's surface, the heat transfer from the surface into the atmosphere and the orography of the landscape. On the basis of these conditions the daily temperature variation and turbulence effects in the ABL occur.

Above the ABL is the so-called free atmosphere that responds only very slowly to influences from the earth's surface and where friction can be neglected. Differentiation of the ABL into sublayers based on the occurring exchange mechanisms and the temperature stratification is given in the next table.

Table 4.1: Subdivision of the atmospheric boundary layer (Foken, 1984)

<table>
<tr><th colspan="2">Layer</th><th>Transport mechanism</th><th>Stability</th></tr>
<tr><td colspan="2">Ekman</td><td rowspan="3">turbulent</td><td rowspan="2">influenced by stability</td></tr>
<tr><td rowspan="2">Turbulent layer</td><td>Prandtl layer</td></tr>
<tr><td>dynamical sub layer</td><td rowspan="3">no influence by stability</td></tr>
<tr><td colspan="2">viscous sublayer</td><td>turbulent/molecular</td></tr>
<tr><td colspan="2">molecular sublayer</td><td>molecular</td></tr>
</table>

4.2 The basic governing equations of the ABL

In boundary-layer meteorology empirical and theoretical approaches for the description of the air flow are used due to the stochastic character of the turbulence. The theoretical background comprises basically the following equations: the three components of Newton's second law, the first law of thermodynamics, the equation of state and the continuity equation. The continuity equation accounts for the conservation of mass and the Navier-Stokes equations for the conservation of momentum. The first fundamental law of thermodynamics represents a form of the energy conservation and the moisture balance a form of the conservation of water in the atmosphere in all phases. The equation for ideal gases defines the condition of the medium on the basis of so-called state variables (Stull, 1988).

4.2.1 The ideal gas law

The state of the air as a gas is given by the state variables pressure p, density ρ and virtual temperature T_v

(4.1) $$p = \rho R_L T_v$$

where R_L is the gas constant of dry air. The virtual temperature for saturated (cloudy) air can be calculated from the water-vapour saturation mixing ratio r_{sat} and the liquid-water mixing ratio r_L, respectively:

(4.2) $$T_v = T(1 + 0.61\, r_{sat} - r_L)$$

For unsaturated air with mixing ratio r Eq.(4.2) reduces to $T_v = T(1+0.61\ r)$.

4.2.2 Conservation of mass

The conservation of mass is expressed in the form of the continuity equation:

(4.3) $$\frac{1}{\rho}\frac{dp}{dt} + \frac{\partial u_i}{\partial x_i} = 0$$

Because the compressibility of the air can be neglected in velocity ranges below the speed of sound the air is regarded in the boundary layer in good approximation as incompressible:

(4.4) $$\frac{\partial u_i}{\partial x_i} = 0$$

4.2.3 Conservation of momentum

The Navier-Stokes equations in tensor notation can be written as:

(4.5) $$\frac{\partial u_i}{\partial t} + u_j \frac{\partial u_i}{\partial x_j} = -\delta_{i3} g - 2\varepsilon_{ijk}\Omega_j u_k - \frac{1}{\rho}\frac{\partial p}{\partial x_i} + \frac{1}{\rho}\frac{\partial \tau_{ij}}{\partial x_j}$$

On the left side of Eq.(4.5) is the local change of speed (storage of momentum) and the advection term, on the right side the gravitational acceleration (gravity acts vertically), the Coriolis effect as well as the pressure gradient forces and the molecular friction term. With the assumption of incompressibility, the molecular friction term reduces to:

$$\frac{1}{\rho}\frac{\partial \tau_{ij}}{\partial x_j} = \nu \frac{\partial^2 u_i}{\partial x_j^2} \tag{4.6}$$

with the kinematic viscosity ν. Introducing the Coriolis parameter f_c Eq.(4.5) modifies to:

$$\frac{\partial u_i}{\partial t} + u_j \frac{\partial u_i}{\partial x_j} = -\delta_{i3} g + f_c \varepsilon_{ij3} u_j - \frac{1}{\rho}\frac{\partial p}{\partial x_i} + \nu \frac{\partial^2 u_i}{\partial x_j^2} \tag{4.7}$$

For neutral stratification (adiabatic temperature gradient) these three basic equations are sufficient. For the cases of unstable as well as stable stratification and moist air two further conservation laws have to be considered: the conservation of moisture (moisture balance) and the conservation of heat (first law of thermodynamics).

4.2.4 Conservation of moisture and the first law of thermodynamics

Under the assumption of incompressible air the moisture balance is

$$\frac{\partial q_T}{\partial t} + u_j \frac{\partial q_T}{\partial x_j} = \nu_q \frac{\partial^2 q_T}{\partial x^2} + \frac{S_{q_T}}{\rho_L} \tag{4.8}$$

with q_T the specific humidity of air, i.e. the entire water mass in all phases per unit mass of moist air, ν_q the molecular diffusivity for water vapour and S_{qr} S_{q_T} a net moisture source or sink term for all physical processes not already included in the equation.

The first law of thermodynamics describes the conservation of enthalpy, which includes contributions from both latent and sensible heat transport. Its formulation is

$$\frac{\partial \theta}{\partial t} + u_j \frac{\partial \theta}{\partial x_j} = \nu_\theta \frac{\partial^2 \theta}{\partial x_j^2} - RB - Q_H \tag{4.9}$$

with θ the potential temperature, ν_θ the thermal diffusivity, RB a term associated with radiation divergence and Q_H a term which accounts for latent heat release during phase transitions.

4.2.5 The equations in simplified form

In order to simplify Eq.(4.3) – Eq.(4.9) two approximations, the *shallow motion approximations* (MAHRT, 1986) and the *shallow convection approximations* are often used. The first represents the basis for the previously applied assumption of an incompressible boundary layer and states that the variations of the parameters, density, temperature and pressure, are essentially smaller than their average values. The second approximation consists of an additional assumption that the vertical temperature gradient is always smaller than g/R (=0.0345 K/m), stating that there is an upper limit for stability and that the vertical gradient of the

pressure deviation is smaller than the buoyancy term. By using these approximations and taking into account the Reynolds averaging (see Eq.(3.27)) for the physical parameters, finally the following system of equations (Stull, 1988) can be rewritten for Eqs.(4.1), (4.4), (4.7) – (4.9):

(4.10) $$\overline{p} / R_L = \overline{\rho} \overline{T_v}$$

(4.11) $$\frac{\partial \overline{u_j}}{\partial x_j} = 0$$

(4.12) $$\frac{\partial \overline{u_i}}{\partial t} + \overline{u_j} \frac{\partial \overline{u_i}}{\partial x_j} = -\delta_{i3} g + f_c \varepsilon_{ij3} \overline{u_j} - \frac{1}{\overline{\rho}} \frac{\partial \overline{p}}{\partial x_i} + \nu \frac{\partial^2 \overline{u_i}}{\partial x_j^2} - \frac{\partial \overline{(u_i' u_j')}}{\partial x_j}$$

(4.13) $$\frac{\partial \overline{q_T}}{\partial t} + \overline{u_j} \frac{\partial \overline{q_T}}{\partial x_j} = \nu_q \frac{\partial^2 \overline{q_T}}{\partial x_j^2} + S_{q_T} / \rho_L - \frac{\partial \overline{(u_j' q_T')}}{\partial x_j}$$

(4.14) $$\frac{\partial \overline{\theta}}{\partial t} + \overline{u_j} \frac{\partial \overline{\theta}}{\partial x_j} = \nu_\theta \frac{\partial^2 \overline{\theta}}{\partial x_j^2} - \overline{R} - \overline{L} - \frac{\partial \overline{(u_j' \theta')}}{\partial x_j}$$

Whereas no changes occur in Eq.(4.10) and Eq.(4.11) compared to Eq.(4.1) and Eq.(4.4), the remaining equations contain additional terms for the turbulent fluctuations.

Considering only flows above the lowermost 0.1 meter of the boundary layer another simplification is possible in Eq.(4.12) by neglecting the laminar friction term in comparison to the turbulent one. Eq.(4.12) then becomes

(4.15) $$\frac{\partial \overline{u_i}}{\partial t} + \overline{u_j} \frac{\partial \overline{u_i}}{\partial x_j} = -\delta_{i3} g + f_c \varepsilon_{ij3} \overline{u_j} - \frac{1}{\overline{\rho}} \frac{\partial \overline{p}}{\partial x_i} - \frac{\partial \overline{(u_i' u_j')}}{\partial x_j}$$

4.2.6 The Reynold's shear stress and the friction velocity

The last term in Eq.(4.15) can be considered as the turbulent friction. To ascertain this the averaged values of the products of speed fluctuations (Reynolds's shear stress) can be written as

(4.16) $$\tau_{ij} = -\overline{\rho u_i' u_j'},$$

as such the turbulent friction is formally analogous to the viscous friction. Another often used parameter to characterise turbulent momentum transport is the *friction velocity* u_*. It is defined as

(4.17) $$u_* = \sqrt{(\overline{u'w'})/\overline{\rho}}$$

4.2.7 The Boussinesq approximation

A clear and often used form of the boundary layer equations is the so-called *Boussinesq-approximation* in which density is replaced by a constant mean value, everywhere except in the buoyancy term in the vertical momentum equation Eq.(4.12), and which still satisfies the shallow convection conditions. For dry air (the moisture balance is not considered), using

(4.18) $$\frac{\bar{d}}{dt} = \frac{\partial}{\partial t} + \bar{u}\frac{\partial}{\partial x} + \bar{v}\frac{\partial}{\partial y} + \bar{w}\frac{\partial}{\partial z}$$

gives for the averaged condition under the assumption of a horizontally homogeneous turbulence

(4.19) $$\frac{\bar{d}\bar{u}}{dt} = -\frac{1}{\rho_0}\frac{\partial \bar{p}}{\partial x} + f\bar{v} - \frac{\partial \overline{u'w'}}{\partial z}$$

(4.20) $$\frac{\bar{d}\bar{v}}{dt} = -\frac{1}{\rho_0}\frac{\partial \bar{p}}{\partial y} - f\bar{u} - \frac{\partial \overline{v'w'}}{\partial z}$$

(4.21) $$\frac{\bar{d}\bar{w}}{dt} = -\frac{1}{\rho_0}\frac{\partial \bar{p}}{\partial z} + g\frac{\theta}{\theta_0} + \frac{\partial \overline{w'w'}}{\partial z}$$

(4.22) $$\frac{\bar{d}\bar{\theta}}{dt} = -\bar{w}\frac{d\theta_0}{dz} + \frac{\partial \overline{w'\theta'}}{\partial z}$$

In Eq.(4.21) the gravitational acceleration g was supplemented by a term describing the buoyancy of an air parcel (the ratio of the deviation of the potential temperature to the condition of equilibrium).

Because the inertial force is small in comparison to the Coriolis force, pressure gradient forces and turbulent friction terms, the equations for the horizontal wind under application of the geostrophic wind law can be written as follows (Holton, 1992):

(4.22.1) $$f(\bar{v} - \overline{v_g}) - \frac{\partial \overline{u'w'}}{\partial z} = 0; \qquad -f(\bar{u} - \overline{u_g}) - \frac{\partial \overline{v'w'}}{\partial z} = 0$$

and for the turbulent shear stresses

(4.23) $$(\overline{u'w'})_s = -C_d\left|\vec{v}\right|\bar{u}$$

(4.24) $$(\overline{v'w'})_s = -C_d \left|\vec{v}\right| \bar{v},$$

with $\left|\vec{v}\right|$ the amount of horizontal velocity vector, the stationary case for the equilibrium between Coriolis force, friction force and pressure gradient is obtained:

$$f \vec{k} x \vec{v} = -\frac{1}{\rho_0} \vec{\nabla} p - \frac{C_d}{h} \left|\vec{v}\right| v$$

4.3 The vertical profile of the wind speed in adiabatic stratification

For WTGSs the vertical course of the wind speed in the Prandtl-layer (approximately the lowermost 100 meters of the atmosphere) is of special interest. In general the height of this layer is defined by the condition that the change of the shear stress amounts to a maximum of 10 percent, therefore this layer is called *constant-flux-layer*. In order to estimate the average values for the parameters of the ABL at each height z, the related equations must be solved unequivocally. But this can not be achieved as Reynolds stress terms oppose as surplus terms the closure of the equation system. Introducing higher order terms for the estimation of the Reynolds stress leads to a system of more unknowns than equations. This problem is called *closure problem*. Although many kinds of closure models with different levels of complexity have been proposed, the simplest way for closing the turbulent flow equations is to relate turbulent fluxes directly to the mean variables i.e. parameterisation as a function of known quantities and parameters. A simple and often used approach based on this concept is the first order closure by the so-called K-theory and the concept of the mixing-length devised by Prandtl (Stull, 1988; Holton, 1992).

4.3.1 The K-theory and the concept of the mixing-length

The gradient transport theory or *K-theory* states that analogously to the molecular shear stress the Reynolds shear stress is proportional to the vertical velocity gradient:

(4.25.1) $$\tau_{xz} = \overline{u'w'} = -K_m (\partial \bar{u} / \partial z)$$

(4.25.2) $$\tau_{yz} = \overline{v'w'} = -K_m (\partial \bar{v} / \partial z)$$

The factor K_m is called the eddy viscosity, eddy diffusivity or turbulent-transfer coefficient. The essential difference to the molecular viscosity is that the eddy viscosity depends on the flow and not on the properties of the fluid.

In order to determine the eddy viscosity, Prandtl has proposed the *mixing-length hypothesis*: An air parcel with the speed u is moved upward an amount z' by a turbulent eddy, so u' is registered in the new height as horizontal speed fluctuation. This u' is proportional to the vertical transfer z' and the vertical gradient of the speed u:

(4.26) $$u' = -z' \partial \bar{u} / \partial z$$

Substituting Eq.(4.26) into the equation for the Reynolds's shear stress Eq.(4.25.1) yields

$$\overline{u'w'} = -\overline{z'w'}\partial\overline{u}/\partial z \tag{4.27}$$

With the assumption that w′ is proportional to u' it follows from Eq.(4.27) that

$$\overline{u'w'} = -c\overline{z'^2}\left(\frac{\partial\overline{u}}{\partial z}\right)^2 \tag{4.28}$$

Comparing this result with Eq.(4.25a) gives the eddy viscosity

$$K_m = l^2\left|\,\partial\overline{u}/\partial z\,\right| \tag{4.29}$$

with

$$l = (c\overline{z'^2})^{1/2} \tag{4.30}$$

The parameter l is termed *mixing-length* or, as a representative measure of the scale of turbulence, *turbulent length scale.* It is proportional to the variance of the average vertical displacement distance of the air parcel. The idea behind this concept is the average free path of the kinetic gas theory (Stull, 1988; Holton, 1992). Numerous proposals for describing $l(z)$ can be found in the literature. An often used example after Blackadar (1962) is given here as:

$$l(z) = \frac{\kappa z}{1+ \kappa z/l_A} \tag{4.30.1}$$

with l_A the *asymptotic length scale* that varies with stability.

4.3.2 The logarithmic wind profile

Because the Prandtl-layer shows in accordance with the definitions a constant vertical momentum transport for which the square of the friction velocity u_* can be regarded as representative value at a certain level (e.g. 10 m). From Eq.(4.25a) follows

$$u_*^2 = K_m\partial\overline{u}/\partial z = l^2(\partial\overline{u}/\partial z)^2 \tag{4.31}$$

With increasing height above ground level the mixing-length must also increase with z (Holton, 1992):

$$l = \kappa z \tag{4.32}$$

where κ is the von Karman constant. Its value must be determined empirically and lies between 0.35 and 0.42. Substituting Eq.(4.31) in Eq.(4.32) yields

$$u_*^2 = \kappa^2 z^2(\partial\overline{u}/\partial z)^2 \tag{4.33}$$

Solving this equation for the vertical gradient gives

$$\frac{\partial \overline{u}}{\partial z} = \frac{u_*}{\kappa}\frac{1}{z} \qquad (4.34)$$

Integrating Eq.(4.34) from a height z_0 at which u=0 until z the vertical profile of the wind speed results for neutral stratification:

$$\overline{u}(z) = \frac{u_*}{\kappa}\ln(z/z_0) \qquad (4.35)$$

The parameter z_0, the *roughness length*, is a measure for the roughness of the surface.

Eq.(4.35) is not valid in the lowermost part of the boundary layer however, because the roughness objects occur very densely and the K-theory is no longer valid. It is necessary therefore, to define a certain height, above which the logarithmic wind profile represents a realistic assumption. This height is named *zero displacement* or *displacement height* (d) and is dependent on the height of the roughness objects on the earth's surface. Eq.(4.35) can be written as

$$\overline{u}(z) = \frac{u_*}{\kappa}\ln[(z-d)/z_0] \qquad (4.36)$$

For very smooth surfaces such as water or snow d can be neglected.

4.3.3 The power law

Another more empirical approach is the power law according to Hellmann (in Molly, 1990):

$$\frac{u_2}{u_1} = \left(\frac{z_2}{z_1}\right)^{p'} \qquad (4.37)$$

A link with the logarithmic wind profile can be achieved if the exponent p' is determined as $p' = 1/\ln(10/z_0)$. Setting $z_0 = 0.01$ meter yields a value for $p' = 1/7$, that is only valid for smooth terrain.

4.4 The roughness length and its estimation

The simple parameterisation of the wind profile as considered above is valid only for flat homogeneous terrain as the presence of obstacles may greatly alter the profiles. Furthermore, because measurements of wind speed are made mostly at much lower heights than the hub-height of a WTGS it is necessary to know quite accurately the vertical profile of the wind speed at least up to this hub height. For this purpose the often unknown values of roughness length and displacement height must be estimated. Most WTGSs are erected in rural environments without large woody areas so that the displacement height can be neglected and the roughness length becomes the only measure of surface roughness. For higher precision over inhomogeneous terrain the roughness length must be determined for directional sectors - usually in 8 or 12 (Barthelmie et al., 1993).

4.4.1 Estimation of the roughness length from measurements at two heights

With neutral stratification measurements of the wind speed at two heights are sufficient in addition to the prevailing wind direction. In order to have truly neutral stratification it is recommended only to use this approach for wind speeds above 6 m/s, because strong mechanical mixing will then occur. Additionally, no larger obstacles or significant changes of the surface roughness on the windward side should exist as then no uniform boundary-layer profile is available.

Given u_1 the wind speed at height z_1 and the wind speed u_2 at height z_2 the logarithmic wind profile from Eq.(4.35) becomes

$$u_1 \ln(z_2) - u_1 \ln(z_0) = u_2 \ln(z_1) - u_2 \ln(z_0) \tag{4.38}$$

from which follows that

$$\ln(z_0) = \frac{u_1 \ln(z_2) - u_2 \ln(z_1)}{u_1 - u_2} \tag{4.39}$$

However as z_o is derived by means of the inverse logarithm, large errors can occur if the measurements show uncertainties.

4.4.2 Estimation of the roughness length by means of terrain classification

A simple, yet subjective method represents the method of terrain classification. Summarising the results stated in the literature, which were attained for z_o from measurements of wind speed and direction for several heights a table can be compiled where for each surface type a certain roughness length is assigned. From air surveys and maps (preferably from the standard scales 1:10.000 to 1:50.000) z_o can be derived by means of the surface types within a radius of some kilometres around the site. Unfortunately in the literature the tables for z_o differ considerably. The oldest table comes from Davenport in 1960 (Table 4.2) and was produced originally for the application of the power-law and was adapted later by Wieringa (1986, 1992) for the logarithmic wind profile (Figure 4.1). This is for wind energy purposes the most frequently used today. In Figure 4.1 a coarse division into four so-called roughness classes (Barthelmie et al., 1993; Troen et al., 1989) is shown which is used in the European Wind Atlas Programme.

Table 4.2: Roughness lengths derived from the terrain classification of Davenport (Wieringa, 1992).

Class	Surface	Landscape description	z_o (m)
1	Sea	Open sea, fetch at least 5 km	0.0002
2	Smooth	Mud flats, snow; little vegetation, no obstacles	0.005
3	Open	Flat terrain; grass, few isolated obstacles	0.03
4	Roughly open	Low crops; occasional large obstacles	0.1
5	Rough	High crops; scattered obstacles	0.25
6	Very rough	Orchards, bushes; numerous obstacles	0.5
7	Closed	Regular large obstacle coverage (suburb, forest)	1.0
8	Chaotic	City centre with high- and low rise buildings	>2

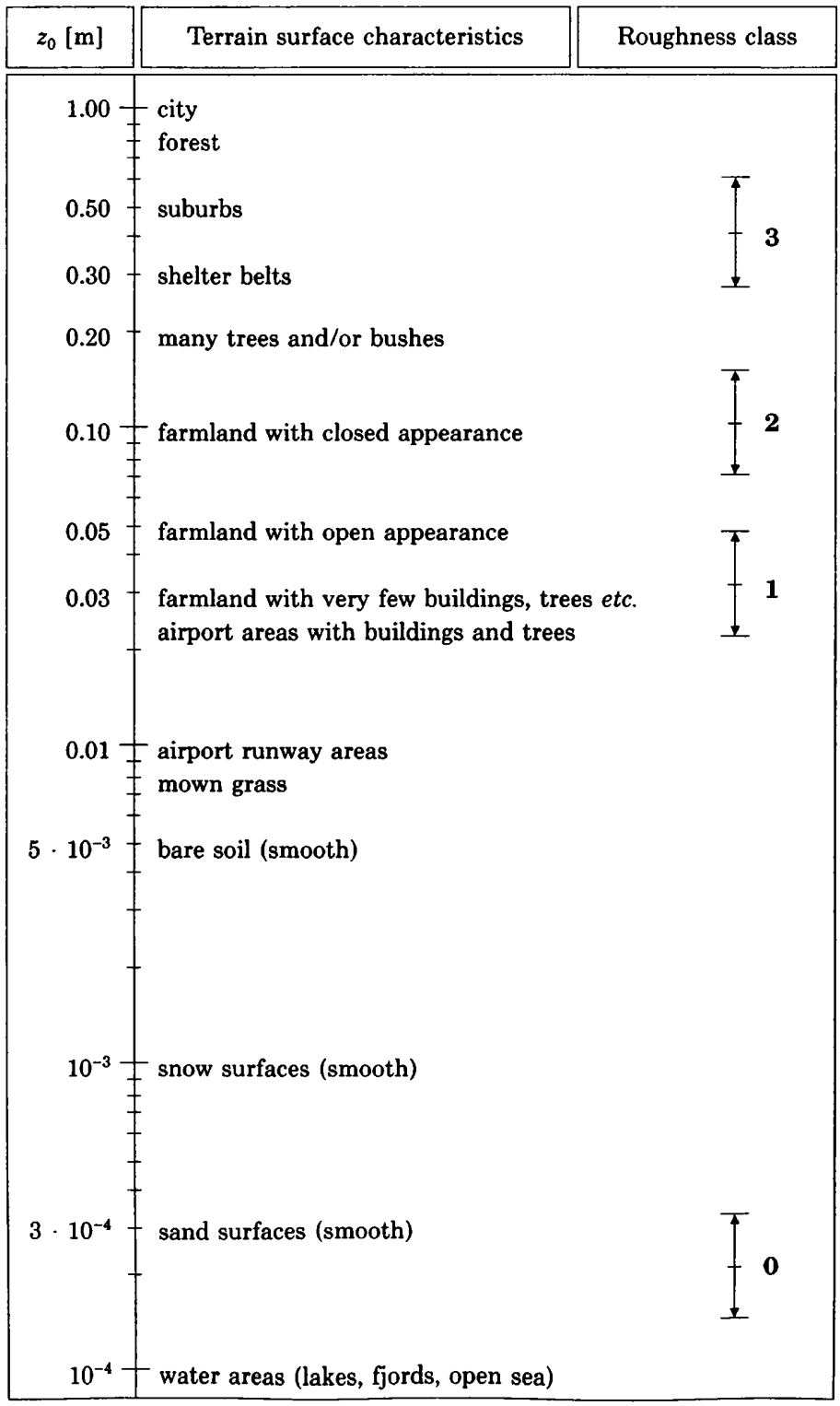

Figure 4.1: Roughness lengths in relation to the surface characteristics. On the right side, the simplified class division (Troen et al., 1989)

4.4.3 Estimation of the roughness length from the gustiness

In Beljaars (1987) and Wieringa, (1976, 1994) two methods were described that allow determination of z_o from data for a given turbulence condition of the wind vector.

Whereas Wieringa used the gust factor, Beljaars used the standard deviation of wind speed with the prerequisite that at least 20 values of the related speed and its standard deviation are available, thus

$$u = \frac{\sigma_u}{f} \ln(z / z_0) \tag{4.40}$$

where f is an empirical factor which is a function of the standard deviation and the friction velocity. For an averaging period of 10 minutes and a measurement frequency of 3 seconds Beljaars set $f = 2.2$.

The gust factor is defined in Eq.(3.36) with $G = u_{max}/u$ where u is the average wind speed during a time period T within u_{max} the maximum gust of duration t is recorded. It was shown (Beljaars, 1987) that the standard deviation of wind speed σ_u increases with increasing roughness and in neutral stability with the logarithmic wind profile such that $\sigma_u/u = \kappa\,(\sigma_u/u_*)\; 1/\ln(z/z_o)$ is valid. Further by Lumley & Panovsky (1964) it was shown that $\sigma_u/u_* \approx 2.5$ and hence $\sigma_u/u = 1/\ln(z/z_o)$.

Assuming that during moderate and strong winds the variation about the average is nearly Gaussian, the median gust factor is statistically related to σ_u after Wieringa (1994) by

$$\langle G \rangle / f_T - 1 = E(\frac{\sigma_u}{u}) = [1.42 + 0.3 \ln(-4 + 10^3 / ut)] (\frac{\sigma_u}{u}) \tag{4.41}$$

where E denotes the expectation of σ_u/u and ut the gust wave length. f_T is dependent on the averaging period of the measurements and for a 10-minute average $f_T = 1.1$ and for an hourly average $f_T = 1.0$. The estimation of the effective z_o can now be made by the inversion of the gust-model in Eq.(4.41). Using Eq.(4.40) in order to replace the standard deviation with z_o it follows that

$$z_o(i) = z \exp\left(\frac{-A f_T E(\frac{\sigma_u}{u})}{\langle G_m \rangle - 1 + A - f_T A} \right) \tag{4.42}$$

with i the direction sector (width = 30°), z the observation height and $\langle G_m \rangle - 1 = A(\langle G \rangle - 1)$ as recorded gust factor G_m is smaller than this for real wind. The attenuation factor A can be set (Wieringa, 1994) for a heavy cup anemometer to 0.86 (ut =110 m) and for a light cup anemometer to 0.93 (ut = 30 m).

From different studies (Barthermie et al., 1993) where both methods were compared with profile measurements it seems that the Wieringa approach results in more reliable z_o values.

4.4.4 Estimation of the roughness length from properties of the earth's surface

Because the estimation of z_o by means of terrain classification represents a subjective method and the alternative methods mentioned require additional measurements alternatives mostly based on the scaling of the surface structure need to be found. A solution to this problem stated frequently in the literature expresses z_o as a function of the geometrical sizes of single roughness elements. Lettau (1969) suggested:

$$z_0 = \frac{1}{2} h \frac{s}{S} \tag{4.43}$$

Where h is the height, s the front surface opposing the wind and S the specific area which results from the total basis area A and the number of roughness elements n such that $S = A/n$. Interestingly here however, only the height and width of the element are included, not their extend in the wind direction. This approach was examined by Kutzbach (in Oke, 1987), through distributing identical obstacles uniformly across an ice surface. The comparison with measurements yielded a good agreement proving the included base S was either not very small or very large.

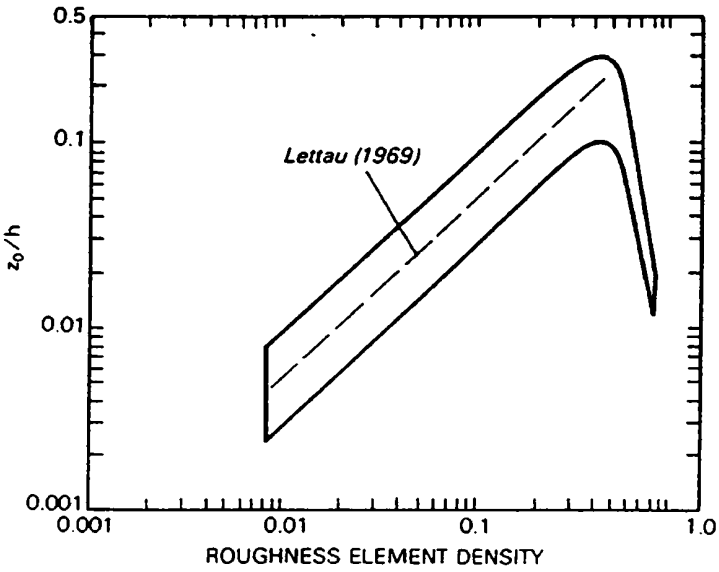

Figure 4.2: The relative roughness length with respect to the density of obstacles (Oke, 1987)

If the area S is very small the speed becomes virtually zero in the interposed spaces between the obstacles and the upper sides of the roughness elements which form a new surface with a smaller roughness as calculated in Eq.(4.43). If S is very large with few obstacles the calculation yields too small a value as the neglected roughness of the free surface in this case gains more influence.

Kondo et al. (1986) give an approach for non-uniformly distributed roughness elements. The relevant geometrical height h_r for the calculation of z_0 is defined both by the different obstacle heights as well as the dimension of the intervening free areas:

$$h_r = \frac{1}{A} \sum H_i g_i \tag{4.44}$$

with A the total area, H_i the height and g_i the base of the roughness element i. Empirically the following relationship between z_0 and h_r was found:

$$z_0 = 0.25 h_r \tag{4.45}$$

Comparing this approach with that of Lettau for a horizontally uniform ground surface by setting $H_i = H$ in Eq.(4.43), it follows that

$$z_0 = \frac{1}{4} H \frac{s}{S} \frac{l}{H} \tag{4.46}$$

where l represents the length of the obstacle in the wind direction. For the particular case of $l = 2H$ Eq.(4.43) results.

Raupach (1992) delivers a more complex approach that also takes the height of the displacement layer thickness into account. He distinguishes between the shear stress of the free surface and that one which results from differently formed objects. The starting point for consideration is the relationship of z_0 to the height h, the width b and the number of the roughness elements occupying the ground area S and a dimensionless number in the form

$$\lambda = nbh / S \tag{4.47}$$

Existing data show that z_0/h increases approximately linearly with λ up to a value of 0.1 to 0.15 which is reached for a λ from 0.1 to 0.3, but with λ further increasing z_0/h decreases again. The location of the maximum and the form of the curve described are dependent on the geometrical form of the obstacles. The existence of a maximum and the decrease of z_0/h are responsible for the invalidating Eq.(4.43) for a high density of obstacle elements.

Considering the shear stress within the layer that reaches up to the height of the obstacles the total shear stress can be seen as a combination of the shear stress on the ground τ_S and that of the roughness elements τ_R:

$$\tau = \rho u_*^2 = \tau_R + \tau_S \tag{4.48}$$

This τ is proportional to the air density, a specific drag coefficient of the object and the square of the speed at height h. Subtracting from these resistance force the shaded surfaces (in the case of the ground surface) and shaded volumes where bigger than the bases (in the case of the roughness elements), including the volumes of the roughness elements (as the speed is also zero within an area in the lee of the elements) the entire shear stress within the layer of thickness h can be written:

$$\tau = \rho U_h^2 \left[C_S \exp\left[-C_1 \left(\frac{U_h}{u_*} \right) \lambda \right] + C_R \exp\left[-C_2 \left(\frac{U_h}{u_*} \right) \right] \lambda \right] \tag{4.49}$$

where C_S is the drag coefficient of the (unobstructed) ground, C_R the drag coefficient of an isolated surface-mounted roughness element and U_h as a reference wind speed. It is helpful to consider the constants C_1 and C_2 as of magnitude 1 and to set them equal. U_h / u_* is also a function of the shear stress. For the solution of Eq.(4.49) it can be considered as an implicit function of τ and with $U_h / u_* \equiv \gamma$ and $C_1 = C_2 = c$ it follows that

$$\gamma = (C_S + \lambda C_R)^{-1/2} \exp(c \lambda \gamma / 2) \tag{4.50}$$

With

$$x = c\lambda\gamma / 2 \tag{4.51}$$

and

$$a = (C_S + \lambda C_R)^{-1/2} c\lambda / 2 \tag{4.52}$$

an equation of the following form results

$$x\exp(-x) = a \tag{4.53}$$

which can be solved iteratively giving the following expression:

$$\frac{z_0}{h} = \frac{h-d}{h}\exp(\Psi_h)\exp(-\kappa\gamma) \tag{4.54}$$

The profile influence function or stability function Ψ_h can assume a value between 0.62 and 1.03 and is set here $\Psi_h = 0.74$ (Raupach, 1992). The unknown displacement layer thickness is then

$$d = h\left(\frac{(C_R/C_S)\lambda}{1+(C_R/C_S)\lambda}\right)\left(1 - c_d\left(\frac{b}{h\lambda}\right)^{1/2}\gamma^{-1}\right) \tag{4.55}$$

which finally enables the calculation of z_0/h in dependence on λ. From measured data results, best agreement of this relationship is found when $c_d = 0.6$.

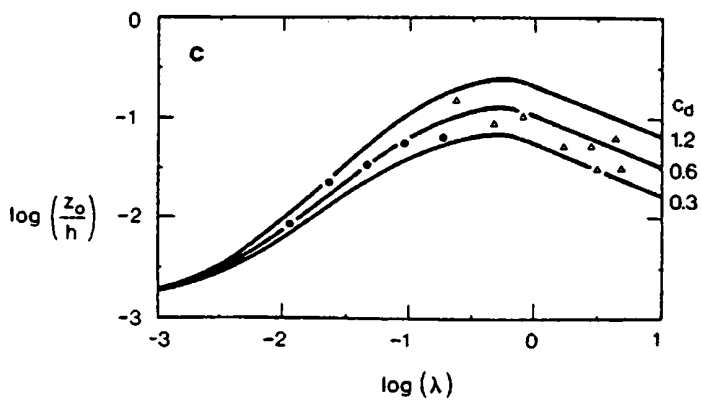

Figure 4.3: Predicted values of the relative roughness length on λ for $C_R = 0.3$; $C_S = 0.003$, and different values of c_d (Raupach, 1992)

4.5 The vertical wind profile in non-adiabatic stratification

If temperature decreases more strongly with height then in the adiabatic case unstable stratification occurs. Because an air parcel which is transported to a higher level is there warmer than its surroundings is accelerated further due to the inherent buoyancy developed. From this process a reinforcement of the momentum transport originates and consequently a stronger velocity gradient in the lowermost layer above the ground develops than in the adiabatic case. If temperature decreases less with height as in the adiabatic case (or even increases with height in the case of an inversion) stable stratification results. In this case, the mechanical momentum transfer is damped and a weaker velocity gradient occurs in the lowermost layer. In order to take these deviations of the logarithmic wind profile into account it is necessary to formulate an additional term which describes the dependence of the wind profile on temperature stratification. This can be achieved for example using. the *Monin-Obuchov length* (Holtslag, 1984).

4.5.1 The Monin-Obuchov length

The turbulent heat flux is independent of the height under stationary conditions and can be written in the form.

$$Q_H = c_p \rho \overline{w'T'} \tag{4.56}$$

Neglecting the Coriolis force in Eq.(4.15), for a temporal variation of the vertical component w of the wind speed the buoyancy becomes most influential. A length scale comprising of the three turbulence governing properties g/T_o, u_*, and $Q_H/c_p \rho$ is by dimensional analysis the Monin-Obuchov length L:

$$L^* = -u_*^3 / (\kappa \frac{g}{T} \overline{w'T'}) \tag{4.57}$$

Because the potential temperature θ is directly proportionally to the temperature, T can be simply replaced by θ in Eq.(4.57) in order to determine the turbulent heat flux with Eq.(4.14). With stable stratification the turbulent heat flux is negative in the z-direction and therefore $L^* > 0$. With unstable stratification the turbulent heat flux is positive and therefore $L^* < 0$. The velocity gradient for the non-dimensional function $\Phi(z/L^*)$ is given by (Holtslag, 1984):

$$\frac{du}{dz} = \frac{u_*}{\kappa z} \Phi(z / L^*) \tag{4.58}$$

from which follows in the adiabatic case by comparison with Eq.(4.34) that $\Phi = 1$ which is an important boundary condition for the determination of the function $\Phi(z/L^*)$ because in this case the average turbulent heat flux is zero and therefore $z/L^* = 0$.

4.5.2 The vertical profile of wind speed in stable stratification

In the case of stable stratification for the function $\Phi(z/L^*)$ usually a linear approach is chosen:

$$\Phi(z / L^*) = 1 + a_1 \frac{z}{L^*} \tag{4.59}$$

where the constant $a_1 = 4.7$ after Businger et al. (1971) and $a_1 = 5.0$ after Dyer (1974). Integration of Eq.(4.58) from 0 to z yields

$$u(z) = \frac{u_*}{\kappa}\left[\ln(z/z_0) - \Psi(z/L^*)\right] \tag{4.60}$$

The function $\Psi(z/L)$ derived from Eq.(4.59) as

$$\Psi = -a_1 \frac{z}{L^*} \tag{4.61}$$

The negative sign leads to an enlargement of the terms in brackets of Eq.(4.60) that yields an increasing attenuation of the wind in the lowermost layer in connection with a smaller friction velocity. This can be observed frequently in the diminution of the ground wind after sunset when temperature inversion starts caused by the negative radiation balance at the ground.

4.5.3 The vertical profile of the wind speed in unstable stratification

A more complex formulation for describing stability is usually necessary for unstable stratification

$$\Phi(z/L^*) = \left[1 - a_2(z/L^*)\right]^{-1/4} \tag{4.62}$$

with an empirical constant a_2 with values between 15 and 16. Integration yields:

$$\Psi(z/L^*) = 2\ln\left(\frac{1+x}{2}\right) + \ln\left(\frac{1+x^2}{2}\right) - 2arctg(x) + \pi/2 \tag{4.63}$$

with

$$x = \left[1 - a_2(z/L^*)\right]^{-1/4} \tag{4.64}$$

In the literature various functions for $\Phi(z/L^*)$ can be found (see e.g. WMO No.575).

4.5.4 The concept of the internal boundary layer

The vertical profiles of the wind speed as described in the forgoing paragraph are valid only for uniform surface properties in the flow direction. In heterogeneous terrain the question arises how the vertical profile is influenced by surface areas with different roughness. Above an extended surface a wind field appears in balance with the given roughness. If there is a change in roughness, a new equilibrium downwind of the line between the two roughness areas is established. The boundary layer near the ground consists then of two layers one close to the surface influenced by the new roughness and the other on top of it dominated still by the original roughness. This is in principle the concept of the *internal boundary layer*. The horizontal distance x (*fetch*) downwind from the point at which the two different surfaces meet has an essential influence at which height the change of the vertical profile takes place. The height of the internal boundary layer δ_i at which the roughness of the immediate surroundings of a site is valid can be written as a function of the fetch x and the two roughness lengths z_{01}, z_{02} (upstream, downstream roughness):

(4.65) $$\frac{\delta_i}{z_{01}} = a\left(\frac{x}{z_{01}}\right)^b$$

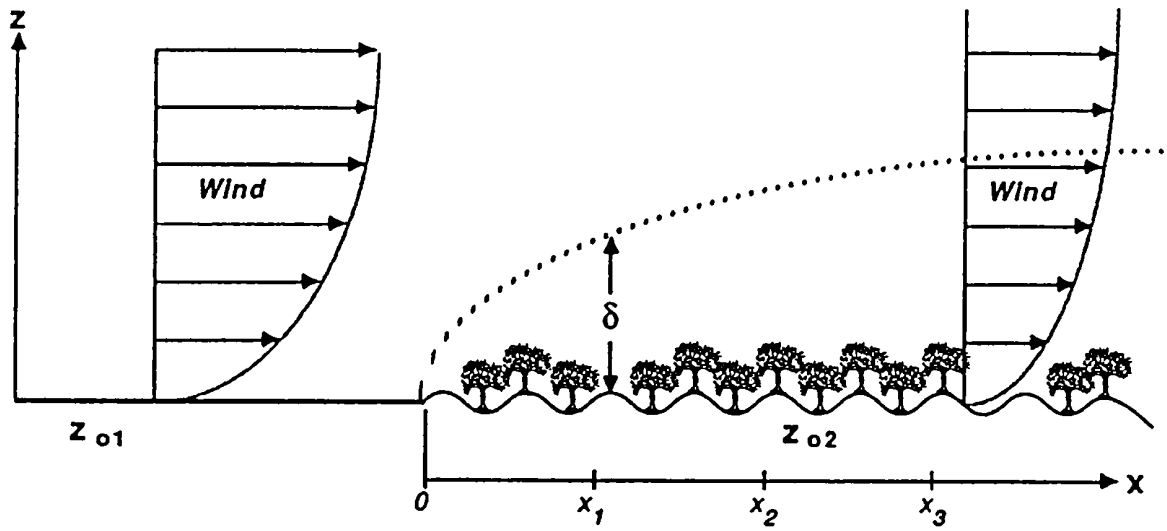

Figure 4.4: Increases of the internal boundary layer height δ as a function of the fetch (Stull, 1988)

The exponent b = 0.8 for neutral stratification, being larger for unstable stratification and smaller when stable. The parameter a can is formed as a function of the two roughness lengths:

(4.66) $$a = 0.75 + 0.03\,\ln(z_{02}/z_{01})$$

4.5.5 Comparison of extrapolation procedures to hub-height from a lower level

The hub-height of new generation WTGSs in the performance range around 1 megawatt lies over 60 meters above ground level. This requires a high measurement technique and financial expenditure. In a study of the German Wind Energy Institute (DEWI) for the AEOLUS II generator with 80 meter rotor diameter and 92 meter hub-height, wind speed values which were extrapolated from measurements at lower heights were compared with measured values in 5 levels up to 126 meters. For extrapolation the logarithmic wind profile, the power law and the logarithmic wind profile with stratification correction after Monin-Obuchov were used. In Figure 4.5 the relative deviation (= [calculated–measured value]/measured value) is shown. The underestimation of the measurement by means of the power law (*Hel*) as well as the logarithmic profile (*Log*) is confirmed whereas the Monin-Obuchov approach (*Obu*) has only a relative deviation of 2 percent. With very low wind speeds all three models gave quite high erroneous values. As a consequence of these findings a survey of the power characteristic seems possible by means of extrapolation of the wind speed with consideration being given to temperature stratification, though further locations should be included in the validation.

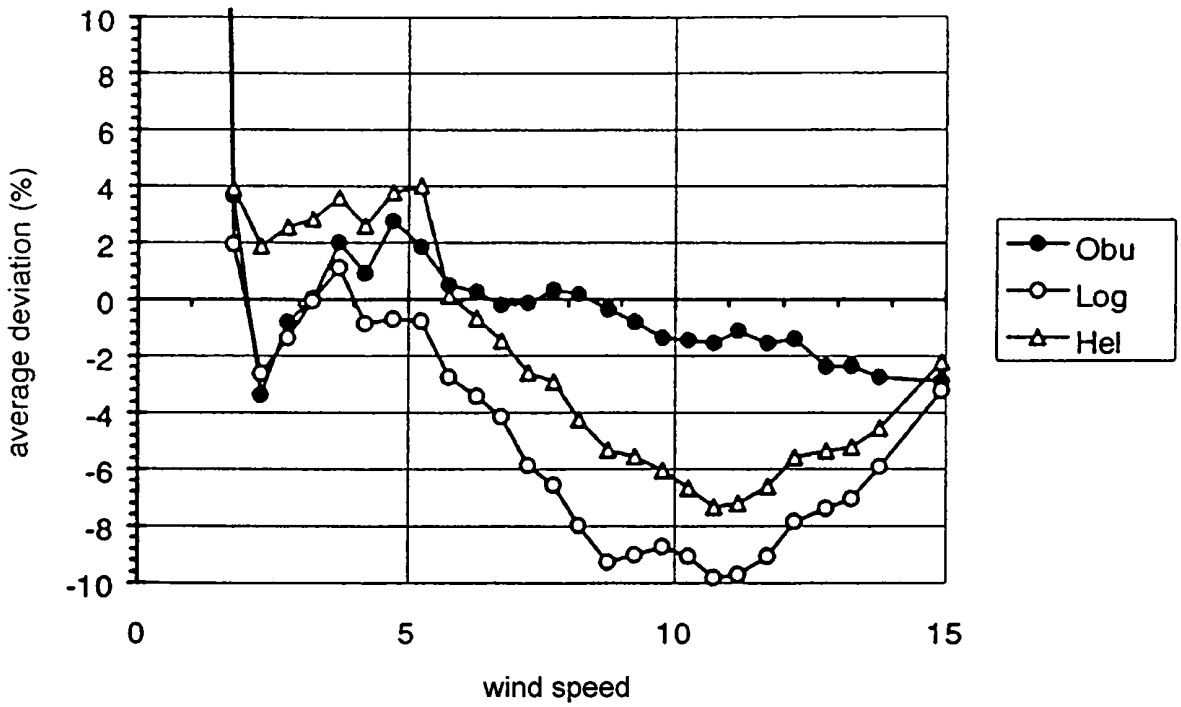

Figure 4.5: Average relative deviation over the measured wind speed at a height of 92 meters; for annotation see text (Strack et al., 1996)

4.6 The representativeness of wind measurements

It is a fact that wind measurements at 10 meters height are very often corrupted by the specific surroundings of the measuring site. Hence the question arises are such measurements "climatologically" representative and the data can be used equally optimal for different purposes. We know well the regulations for anemometer measurements (WMO No.8, VI.6.6. 1973): *"Measurements of wind for synoptic purposes should refer to a height of 10m in an unobstructed area, and should consist of the mean of values taken over a period of about 10 minutes".* And further on for non-ideal sites: *„When a standard exposure is unobtainable, the anemometer should be installed at such a height that its indications are reasonably unaffected by local obstructions in the vicinity. This will usually necessitate placing the anemometer at a height exceeding 10m by an amount depending on the extent, height and distance of the obstructions, but it is impracticable to give any general rule for determining this since local conditions differ so widely".*

The definition of representativeness is difficult due to the applications that may have their own conditions in time and space for which then the data have to be representative (Wieringa, 1994). This imposes that some kind of generalisation is necessary to achieve a regional representativeness that holds for different applications.

4.6.1 Exposure correction method for wind measurements

A good compromise for wind measurements at a site (together with accurate meta data about the site itself) is for a wind speed u>5m/s with a 150 meter fetch as a minimum, no obstacles (with height H) nearer than 15 times H and the anemometer height $z \geq 20\, z_o$. Then the following simple relationship for two heights of the wind profile is valid:

$$u_2/u_1 = \ln(z_2/z_o)/\ln(z_1/z_o).$$

With the assumptions

u_s in z_s	in moderately open terrain, z_{os},
u_r in 10m	potential wind above a flat reference terrain, $z_{or} = 0.03$,
u_b in z_b	resulting wind from the upwind meso-scale (≤10 km) roughness effects but without influence of the local roughness elements
z_b =*blending height:*	height above which there is no influence from a local z_o,

the objective exposure correction method from Wieringa (1976) can be applied. Taking into account that at the earth's surface the maximum height of roughness elements are usually in the range of 20-30 meters and knowing that the individual effect of an obstacle is smoothed out considerably for $z \approx 2H$ (WMO 1964) the blending height can be set at $z_b = 60$ m. With these assumptions a transformation is possible in the form (geometrical relations in Figure 4.6) of having only geometrical quantities on the right hand side of the following equation:

(4.67) $$u_r / u_s = [\ln(z_b/z_{os})\, \ln(z_r/z_{or})] \,/\, [\ln(z_s/z_{os})\, \ln(z_b/z_{or})]$$

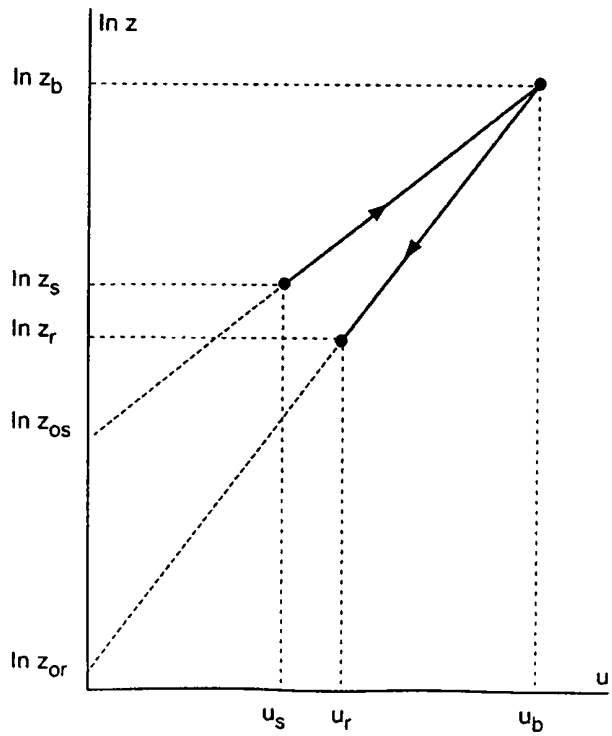

Figure 4.6: Transformation model for exposure correction (after Wieringa 1994)

The advantages in using the potential wind instead of original wind data are -„standardisation“ of so called „design values“ and having representative input data for models and other applications. The disadvantages are that the procedure is applicable only for well kept stations with detailed information about the surroundings, that homogenisation of the series is necessary in case the station is moved to another site or changing surroundings and for wind speeds $u>5$ m/s.

5 FLOW FIELDS AND OROGRAPHY

Inhomogeneous terrain formations can change the wind field in comparison with a homogenous surface in two ways. Firstly, a change in the pressure field can be evoked dynamically by the orography on an existing flow and secondly, pressure gradients can be generated, even in wind still periods, at the upper level of the boundary layer caused by thermally induced winds from varying energy absorption of the earth's surface depending on hillside inclination and orientation - the so-called thermal induced winds. The first part of this section deals with the influence of topographic elevations on a flow which results from the spatial pressure distribution, the second part with thermally induced flows.

5.1 Flows over and around hills

Flows above and around elevations are strongly dependent on the height and shape of the hill or mountain, as well as the velocity of flow and prevailing temperature stratification. The different flow forms can be distinguished by the resultant forces to be considered. Firstly some characteristic properties of the flow and atmosphere are discussed.

5.1.1 The Brunt-Väisälä frequency and the atmospheric wavelength

If an air parcel is lifted in a stable stratified flow a restoring force is generated that tries to bring back the parcel to the original location caused by differential buoyancy of the air parcel and its surroundings. On the basis of this restitution force oscillations of the air parcel occur in the vertical with the so-called *Brunt-Väisälä* or *buoyancy frequency* (Stull, 1988; Holton 1992):

$$N_f = \left(\frac{g}{\theta} \frac{d\theta}{dz} \right)^{1/2} \tag{5.1}$$

where $\theta(z)$ is the potential temperature at the original position z. If a stable stratified flow is lifted with the speed u by a hill or mountain then in front, above and behind this elevation waves are formed. The *atmospheric wavelength* λ_a results from the Brunt-Väisälä frequency and the flow velocity u as

$$\lambda_a = 2\pi \frac{u}{N_f} \tag{5.2}$$

Taking an average value of 0.0035 K/m for the vertical gradient of the potential temperature an average value and for the velocity u = 10 m/s the atmospheric wavelength emerges as approximately 5 kilometres.

Which wave form develops during the flow over the mountain is dependent on the relationship of the characteristic horizontal extend L of the mountain to the atmospheric wavelength

$$\frac{L}{0.5\,\lambda_a} = \frac{L \cdot N_f}{\pi \cdot u} \tag{5.3}$$

5.1.2 Wave regimes of flows over hills

The following considerations will focus for simplicity on two-dimensional elevations such that the wind vector has only two components u and w. Concentrating only on mountain ranges limited laterally, the effects resulting from Coriolis acceleration can be neglected. Starting with the boundary layer equations and the non-averaged Boussinesq-approximation (Holton, 1992) (c.f. paragraph 4.2.7) without the Coriolis term we have

(5.4) $$\frac{du}{dt} = -\frac{1}{\rho}\frac{\partial p}{\partial x}$$

(5.5) $$\frac{dw}{dt} = -\frac{1}{\rho}\frac{\partial p}{\partial z} - g$$

(5.6) $$\frac{d\theta}{dt} = 0$$

and using continuity equation for an incompressible medium (cf. Eq.4.4) the governing equations for the deviation from the basic state are obtained by use of Reynolds averaging and linearization, neglecting effects of rotation yields:

(5.7) $$\left(\frac{\partial}{\partial t} + \bar{u}\frac{\partial}{\partial x}\right)u' + \frac{1}{\rho_0}\frac{\partial p'}{\partial x} = 0$$

(5.8) $$\left(\frac{\partial}{\partial t} + \bar{u}\frac{\partial}{\partial x}\right)w' + \frac{1}{\rho_0}\frac{\partial p'}{\partial z} - g\frac{\theta'}{\bar{\theta}} = 0$$

(5.9) $$\frac{\partial u'}{\partial x} + \frac{\partial w'}{\partial z} = 0$$

(5.10) $$\left(\frac{\partial}{\partial t} + \bar{u}\frac{\partial}{\partial x}\right)\theta' + w'\frac{d\bar{\theta}}{dz} = 0$$

Eliminating the pressure disturbance by subtracting Eq.(5.7) from Eq.(5.8), and subsequently u' and θ' with the help of Eqs.(5.9) and (5.10) one derives the conditional equation for w''

(5.11) $$\left(\frac{\partial}{\partial t} + \bar{u}\frac{\partial}{\partial x}\right)^2\left(\frac{\partial^2 w'}{\partial x^2} + \frac{\partial^2 w'}{\partial z^2}\right) + N_f^{\,2}\frac{\partial^2 w'}{\partial x^2} = 0$$

This wave equation describes the so-called *internal gravity waves* in the general form also allowing for temporal changes. In the case of flowing over high mountains this temporal change is not possible and stationary wave are formed (Holton, 1992), because of the average horizontal wind speed and terrain height (the cause for the flow lifting) being constant. Therefore Eq.(5.11) simplifies to

$$\frac{\partial^2 w'}{\partial x^2} + \frac{\partial^2 w'}{\partial z^2} + \frac{N_f^{\,2}}{\bar{u}^2} w' = 0 \tag{5.12}$$

Parts of this equation can be neglected according to the horizontal extend of elevation. For hills, whose length is smaller than the atmospheric wavelength in flow direction, no waves develop and the third term in Eq.(5.12), responsible for wave development, can be neglected. The remaining terms yield the Laplace-Equation

$$\frac{\partial^2 w'}{\partial x^2} + \frac{\partial^2 w'}{\partial z^2} = \Delta w' = 0 \tag{5.13}$$

This form results from the requirement that the gradient field of a scalar potential (in this case the vertical deflection), that fulfils the non-vortical condition, must also be non-divergent. Therefore, flows that fulfil the Laplace equation are named *potential flows*. As these flows are also valid in the case of stable stratification the solutions for Eq.(5.13) will be discussed in section 5.1.4.

In the case that the horizontal extent of the hill reaches approximately the atmospheric wavelength a non-hydrostatic wave regime is established and all terms in Eq.(5.12) must be considered. Then waves are generated which extend themselves in the horizontal and vertical directions also. The harmonic wave solution of Eq.(5.11) for the decay or growth of the vertical deflection in relation to x and z has the form

$$w'(x,z) = \mathbf{Re}[\hat{w}\exp(i\Phi)] = w_r \cos\Phi - w_i \sin\Phi \tag{5.14}$$

with $\hat{w}$ a complex amplitude having a real part w_r and an imaginary part w_i. The phase Φ is a linear combination of x and z and can be written as

$$\Phi = kx + mz \tag{5.15}$$

with k the wave number in the x–direction and m the wave number in the z-direction. While the horizontal wave number is always real and therefore in the x-direction has sine-shaped waves forms, the vertical wave number $m = m_r + m_i$ may be complex so that in this case an exponential decay or growth of the vertical deflection takes place depending on whether m_i is positive or negative. The differentiation, if sine-shaped waves developed vertically direction or if an exponential decay or growth occurs, results from the so-called *dispersion relationship*:

$$m^2 = N^2 / u^2 - k^2 \tag{5.16}$$

If the horizontal velocity of flow is smaller than the ratio of Brunt-Väisälä frequency to the horizontal wave-number, m is real and waves are generated in the z-direction. In this case the lines, which can be drawn through points at different heights with the same phase, are not vertical but deflected from the local vertical through an angle α (Blumen, 1990). The cosine of this angle results from the ratio of the horizontal wave number to the amount of the wave number vector thus

$$\cos\alpha = \pm k / \left|\vec{k}\right| \tag{5.17}$$

where the wave number vector has the x-component k and the z-component m. The tilt of the phase lines for internal gravity waves depends only on the ratio of the wave frequency to the buoyancy frequency and is

independent of wavelength. In the reverse case m is imaginary and no waves are propagating in the z-direction. These two cases are shown in Figure 5.1 and Figure 5.2.

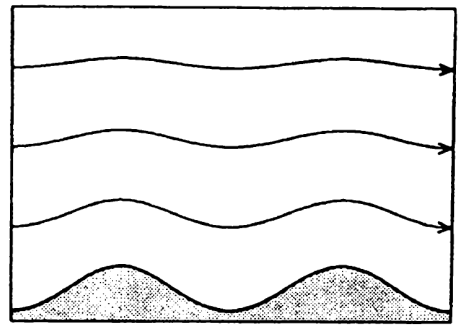

Figure 5.1: Waves with exponentially decreasing amplitude in the z-direction (Holton, 1992)

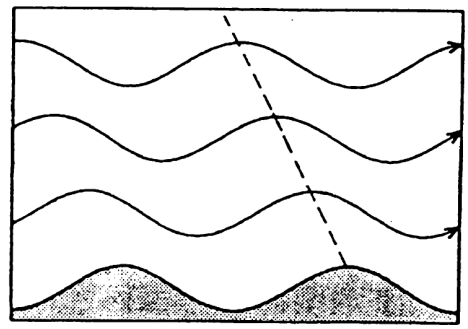

Figure 5.2: Waves propagating in the x- and in z-directions. The dashed line connects points of equal maximum upward displacement (Holton, 1992)

If the horizontal extent of the elevation is larger than the atmospheric wavelength but not so large that Coriolis-effects need be taken into account, then the horizontal wave number k is smaller than the ratio of the Brunt-Väisälä frequency to the horizontal flow velocity. Looking at the dispersion equation Eq.(5.16) shows that the square of the wave-number k can be neglected when compared to the other quantities. From this it follows that the vertical deflection does not depend on x and Eq.(5.12) simplifies to:

$$\frac{\partial^2 w'}{\partial z^2} + \frac{N_f^{\,2}}{u^2} w' = 0 \tag{5.18}$$

The waves resulting from this equation are termed *hydrostatic wave regime*, a representation of which is given in Figure 5.3.

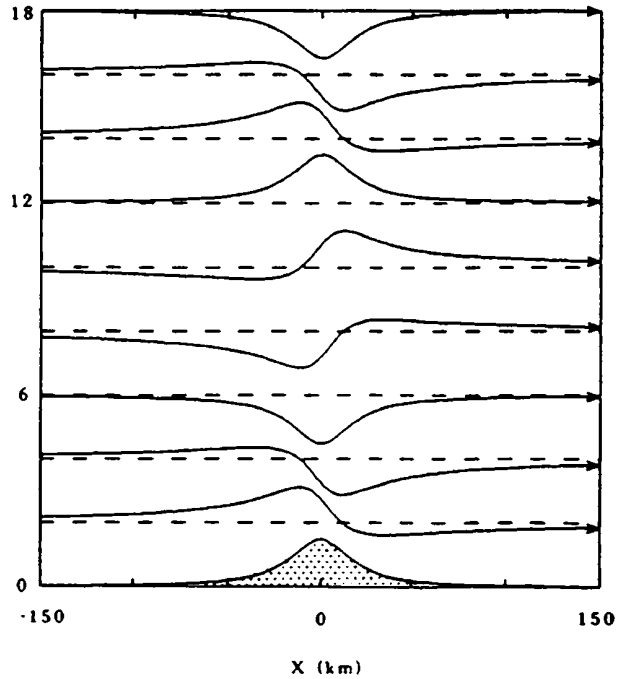

Figure 5.3: Hydrostatic waves above an elevation wider than the atmospheric wavelength (Blumen, 1990)

5.1.3 Non-linear effects of mountain flows

Non-linear effects such as the blocking of flow on the windward side of a hill, the lateral flow around a single hill or canalising the flow between two hills appear when the linearization of the boundary layer equations in paragraph 5.1.2 is no longer valid. Another non-linear effect, that leads to high wind speeds in the lee of a mountain range, is the breaking of vertically extending gravity waves. More about this subject can be found in Mason et al. (1995), Oke (1987), Stull (1988), and Blumen (1990).

The characteristic parameter for the appearance of non-linear effects is the *Froude-number* and is defined by the ratio of inertial to buoyancy forces as

$$Fr = U / N_f L_h, \tag{5.19}$$

where L_h is a characteristic length scale, usually the half-width of the hill at half-hill height (H/2) and U is the characteristic velocity in the boundary layer. A Froude-number significantly smaller than 1 emerges if the flow is affected by buoyancy forces, which can happen in a very stable stratified atmosphere. In this case the flow has insufficient kinetic energy to raise the necessary potential energy for lifting. The consequence is a blocking on the windward side of the hill and a lateral flow-around. The nearer the Froude-number approaches 1, the more thinly the layer is in which blocking and lateral flow-around takes place, and consequently the flow above this layer overflows the elevation. Thus waves are generated starting from a sufficient horizontal extent of the overflowed part of the elevation, whereas no waves appear in the low layer. This phenomenon is named *lee-wave separation.* The ratio of the layer-depth z_w of the part of the flow, that can overflow the hill, to the hill height z_{hill} is approximately equal to the Froude-number ($z_w/z_{hill} \approx Fr$) for this range of values (Stull, 1988). The blocking phenomenon and lee-wave separation is represented in Figure 5.4 and Figure 5.5.

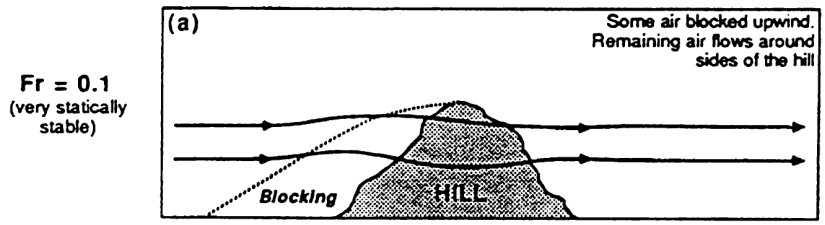

Figure 5.4: Blocking of flow on the windward side of a hill with a small Froude-number (Stull, 1988)

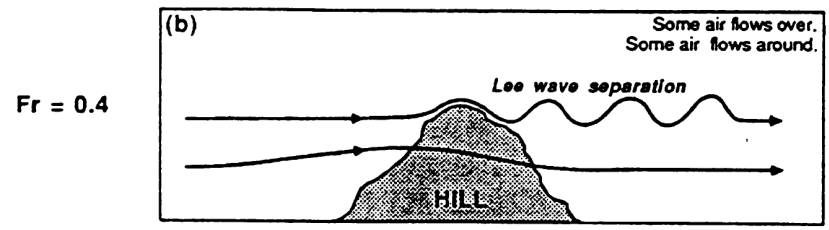

Figure 5.5: Lee-wave separation with a Froude-number < 1 (Stull, 1988)

For large Froude-numbers the familiar balance between inertial effects and turbulent friction can be observed. The ratio U/N_f is typically 1 km, so for hills with $L_h \leq 1$ km may be free of buoyancy effects during the day and when winds are strong. Hills with $L_h \sim 5$ km are always affected by stratification to some degree.

Blocking and canalising is of great importance for wind energy use: the first because this was not taken into account until now for most commonly used wind field models, resulting often in a small overestimation of the energy yield to the windward side of hills; the second (the canalising) as effective canalising is only possible in very stable stratification (with wind speeds mostly below the cut-in speed) or for sufficient heights of the hill sides. Thus it follows that high yields are only possible, if the canal axis corresponds to the main wind direction.

Another non-linear effect, the breaking of vertically propagating gravity waves (see Figure 5.6) gives a theoretical base to interpret the appearance of high wind speeds in the lee of mountain ranges, as was observed for example by Steinhauser (1952) of wind measurements from stations at the foot of the *Smaller Carpathian Mountains*. The critical layer in the lee of a mountain, where refraction takes place can be considered as a boundary at which the vertically propagating waves are reflected in the direction of the earth's surface from which high wind speeds occur.

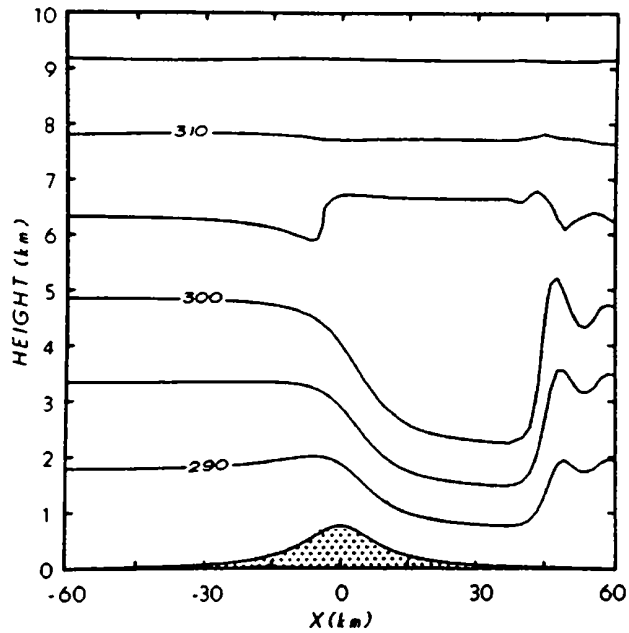

Figure 5.6: The isentropics for a flow with a critical layer at 7/12 of the vertical wavelength (Blumen, 1990)

The modification of the equations for shallow-water waves provides a second theoretical base for describing the formation of high wind speeds. The momentum conservation equation and the continuity equation in such a layer are given by:

$$u\frac{\partial u}{\partial x} + g\frac{\partial D}{\partial x} + g\frac{\partial h}{\partial x} = 0 \tag{5.20}$$

$$\frac{\partial (uD)}{\partial x} = 0 \tag{5.21}$$

with D the layer thickness and h the hill height. Substituting Eq.(5.21) into Eq.(5.20) to eliminate u yields

$$\left(1 - \frac{1}{Fr_m{}^2}\right)\frac{\partial (D+h)}{\partial x} = \frac{\partial h}{\partial x} \tag{5.22}$$

where the modified Froude-number Fr_m is defined as

$$Fr_m{}^2 = u^2/(gD) \tag{5.23}$$

If $Fr_m > 1$ (super-critical case), the layer thickness increases with increasing hill height and the wind speed decreases on the basis of the continuity equation. In this case the kinetic energy of the flow is changed into potential energy for lifting the flow. At the crest of the hill the speed is lowest and the layer thickness greatest. On flowing away the contained energy is converted again into kinetic energy.

If Fr_m <1 (sub-critical case), the layer thickness decreases with increasing hill height and at the hill top the speed is greatest. In this case potential energy of the layer is changed during the lifting into kinetic energy and on flowing away again into potential energy.

As an explanation for the speed amplification in the lee of mountains this theory describes well the change from the sub-critical to the super-critical flow condition on the hill top. This change is made possible, if the wind speed is increased continuously towards the hill top by gravity waves.

A weak point of this theory is the assumption of a free surface on the one hand (i.e. the restriction of the vertical energy exchange to the layer thickness D) because gravity waves enable a vertical energy exchange up to the tropopause and on the other hand the assumption that the greatest speed is reached in gravity waves on the hill top.

A third theory for leeward velocity amplification (Blumen, 1990) considers two layers with different atmospheric wave numbers. At the boundary between these layers one part of the upwardly propagating waves is reflected. For an optimal superposition between the upward and the reflected, downward propagating waves, high flow velocities occur on the lee side. The highest speeds are reached, if the vertical wave number equals twice the height of the tropopause (Figure 5.7).

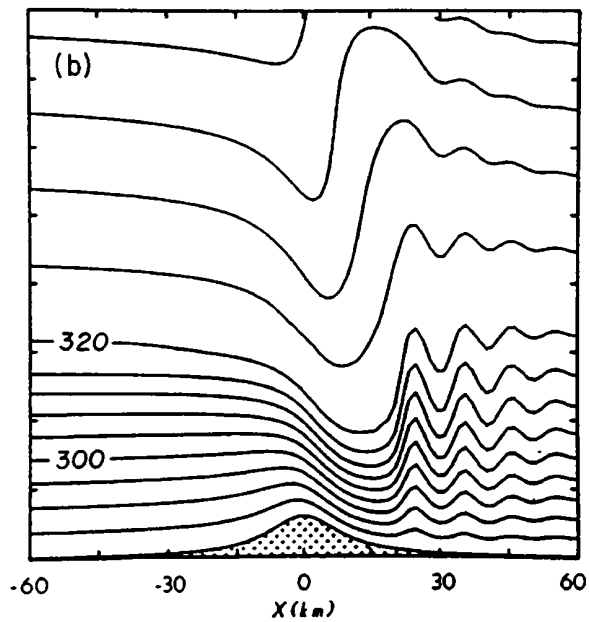

Figure 5.7: The isentropics of a flow over a mountain ridge with a two-layer atmosphere (Blumen, 1990)

5.1.4 Overflow of hills during neutral stratification

In the case of flows over hills, whose horizontal extend is smaller than the atmospheric wavelength and their height is at least one magnitude smaller than the length the Laplace-equation Eq.(5.13) can be used for the determination of the friction-free flow. For simplicity only the two-dimensional case will be treated here in more detail, i.e. the first differentiation of the velocity components u and w with respect to y as well as the terrain height h are all set equal to zero (Hoff, 1987). The terrain height h is only a function of x and has a maximum H (the summit height) at x=0. The z-coordinate will be considered in the following as the height over the ground.

The basic idea of all theories for the overflow of smaller hills is the subdivision of the flow into an inner layer, which is influenced massively by the friction, and an outer layer that is characterised by a velocity enhancement (as it appears in the friction-free case) and forms the buoyancy for the flow velocity in the inner layer. The procedure for the solution of this problem is firstly to solve the Laplace-equation in order to get the velocity components for the friction-free case. From this, one derives the amount of speed amplification in relation to the undisturbed basic flow, the hill height and the form of the hill. The undisturbed basic flow in the friction-free case is a height-independent flow parallel to the x-axis such that no vertical velocity component appears. The wind vector above the hill can be written formally as the sum of the undisturbed basic flow U_∞ and a speed amplification dependent on x and z (Hoff, 1987):

$$U(x,z) = U_\infty + \Delta U(x,z) \tag{5.24.1}$$

$$W(x,z) = 0 + \Delta W(x,z) \tag{5.24.2}$$

Because only the horizontal wind speed component is of interest for WTGSs this will be taken into consideration in the following. A method for the determination of the amplification term in Eq.(5.24.1) is the application of the *theory of thin airfoils*, in which potential flows for the condition that $H<<L$ are described by a superimposition of the basic flow, with lined up flow sources and sinks that correspond to the local hillside inclination. Normalising the *hill-function h(x)* with H (the hill height) and all other dimensions with a longitudinal length scale L ($=L_h$ in Eq.(5.19)) which is usually the half-width of the hill, the horizontal speed amplification results in:

$$\Delta U(x,z) = U_\infty \frac{H}{L}\sigma(x/L, z/L) \tag{5.25}$$

The amplification is directly proportional to the basic flow and to the ratio of the height to the characteristic length of the hill as well as to its form. This is represented in Eq.(5.25) by the so-called form-parameter $\sigma(x/L, z/L)$. The form parameter is obtained from the above mentioned theory of thin airfoils as:

$$\sigma(x/L, z/L) = \frac{1}{\pi}\int_{-\infty}^{\infty} f'(s/L)\frac{x/L - s/L}{(x/l - s/L)^2 + (z/L)^2}d(s/L) \tag{5.26}$$

The function $f(x/L)$, which appears in Eq.(5.26) as first derivative, is the standardised hill-function with the height H = 1 and approaches zero for very large values of x. Taking the half-length as a characteristic length of the hill

$$L \equiv L_{1/2} = x_{right}(h = H/2) - x_{left}(h = H/2) \tag{5.27}$$

the form parameter being obtained at the top of the hill. On the basis of a symmetrical Gaussian bell curve the form parameter equals 0.939 and for an inverse polynomial

$$f(x/L) = \frac{1}{1 + (x/L)^2} \tag{5.28}$$

the form parameter is 1. The pressure disturbance, caused by the higher velocity, results from the Bernoulli-equation

(5.29) $$\frac{\rho}{2}U_\infty^{\,2} + p_\infty = \frac{\rho}{2}U^2 + p$$

while neglecting the square of the flow term as:

(5.30) $$\Delta p \cong -\rho U_\infty \Delta U$$

The behaviour of the different parameters of the friction-free flow is illustrated in Figure 5.8a to Figure 5.8d for a hill with the form of an inverse polynomial. The decrease of the form parameter is clearly shown (and with it the speed-up effects with height) and additionally the disappearance of the gradient for the pressure disturbance at the highest point of the hill, whereby on the windward side an acceleration from the pressure disturbance and to leeward a retardation of the flow occurs. In the case of steeper hillside inclinations, this course of pressure disturbance is responsible in connection with the retarding effect from ground friction for the flow separation.

In order to take the uniform surface friction into account the friction-free flow must be replaced in Eq.(5.24.1) and Eq.(5.25) by a height dependent flow. While however, in the friction-free case the flow is described by Eq.(5.25) up to the height $z = 0$, this is not possible for the flow with friction, because the friction has a dominant role in the force balance within the previously mentioned inner layer and the potential theory loses validity.

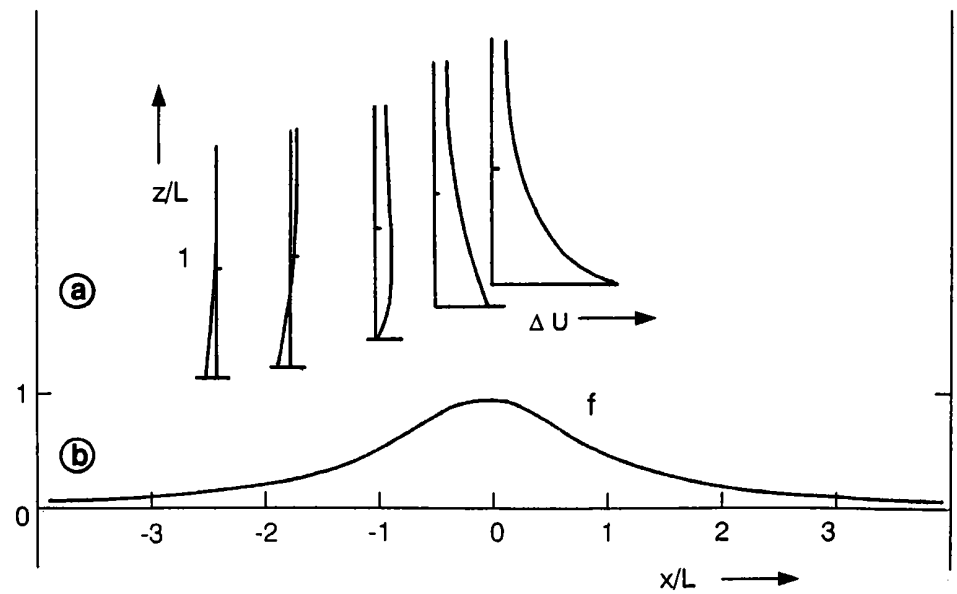

Figure 5.8: The behaviour of different parameters with respect to x/L on the inverse-polynomial hill after Hoff (1987); (flow from the left)
(a) Speed-up-profile of the frictionless flow with x/L=-2.4, -1.75, -1 and -0.5
(b) horizontal profile of the inverse polynomial hill standardised by H and L

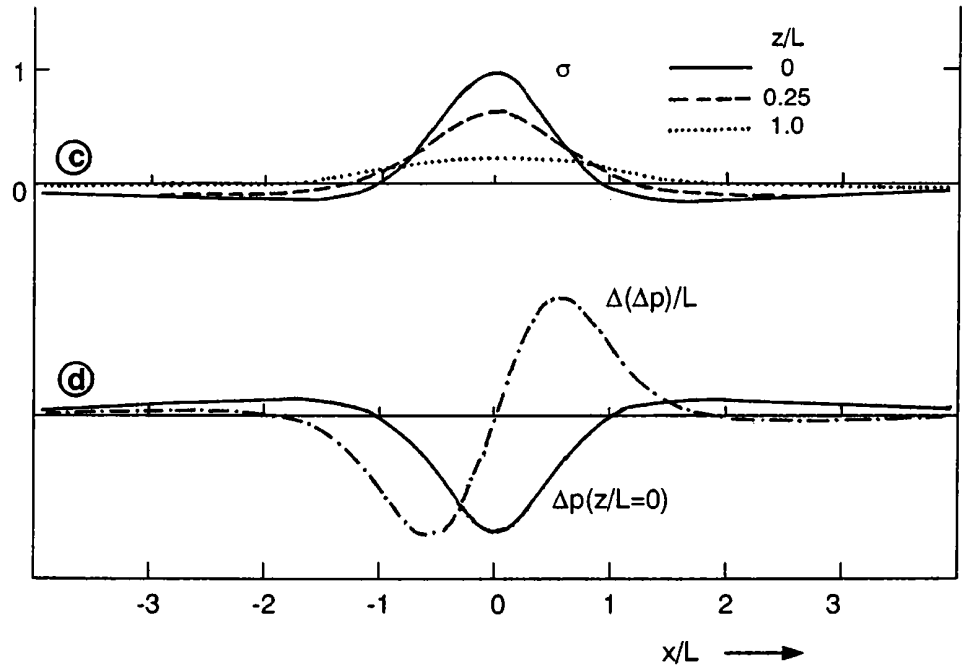

Figure 5.8 (cont.): The behaviour of different parameters with respect to x/L on the inverse-polynomial hill after Hoff (1987); (flow from the left):
(c) form parameters $\sigma(x/L)$ for $z/L = 0$, 0.25 and 1.0;
(d) near-surface pressure disturbance (full line) and the pressure gradient smoothed over L (dashed line)

However, for the calculation of the flow in the outer layer the flow in the inner layer must be described first. A schematic representation of this two-layer concept for flows across a hill is given in the next figure.

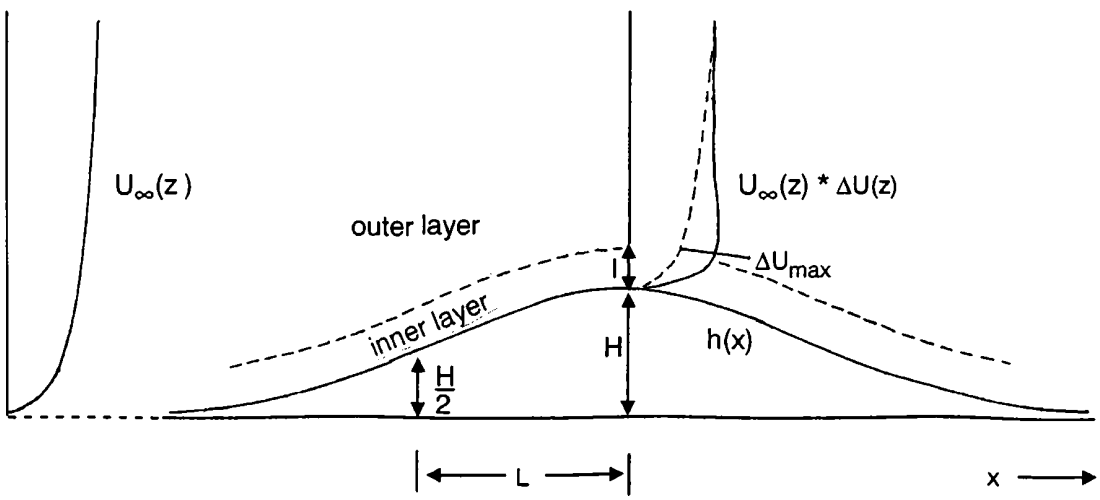

Figure 5.9: Two-layer concept for flows across a hill with static friction (Hoff, 1987).

With the application of the logarithmic wind profile from Eq.(4.35) the solution for the speed amplification in the outer layer which lies above the inner layer with the still unknown layer-thickness l is given by

$$U(x,z) = U_\infty(z) + U_\infty(L)\frac{H}{L}\sigma(x/L, z/L) \tag{5.31}$$

As scaling velocity for the horizontal speed increases, the velocity was chosen for the height H, which represents the typical effect height of the obstacle.

For the flow around hills the relevant forces are, as mentioned above, advection, pressure gradient and friction. The pressure gradient directly on the ground must be equal to the friction, because for advection the necessary velocity vanishes here. Under the assumption that the pressure disturbance is hardly modified by the inner friction layer, the required layer thickness l' of the inner layer can be gained from equating the change of the shear stress $\Delta\tau$ within the depth l' with the advection at the lower boundary of the outer layer:

$$U_\infty(l')\frac{\Delta U(l')}{L} = \frac{1}{\rho}\frac{\Delta\tau}{l'} \tag{5.32}$$

If one uses the shear stress velocity instead of the friction velocity, the right hand side of Eq.(5.32) is given after splitting off the friction velocity into an undisturbed term and an additional term, with a subsequent linearisation as:

$$\frac{\Delta(u_*^2)}{l'} \cong 2u_{*\infty}\frac{\Delta u_*}{l'} \tag{5.33}$$

Using for the undisturbed term

$$u_{*\infty} = U_\infty(l')\frac{\kappa}{\ln(l'/z_0)} \tag{5.34}$$

and for the disturbed term

$$\Delta u_* = \Delta U(l')\frac{\kappa}{\ln(l'/z_0)} \tag{5.35}$$

after some reshaping the conditional equation for the layer thickness l' this becomes:

$$l'\cdot\ln^2(l'/z_0) = 2\kappa^2 L \tag{5.36}$$

Beside this equation there are others in the literature (Hunt et al., 1975; Britter et al., 1981) for which the logarithm is not squared as e.g.

$$l'\cdot\ln(l'/z_0) = 2\kappa^2 L, \tag{5.37}$$

and which result from the application of the concept of the mixing-length under the constraints that $\Delta U(l') = u_* / \kappa$. While Eq.(5.36) gives a height l' which returns approximately the vertical location of the maximum velocity increase, Eq.(5.37) is, physically seen, arbitrarily. With known l the determination of the horizontal velocity amplification at the hill crest (where the gradient of the pressure disturbance becomes zero) is made possible by the following equation:

$$U(z < l', x = 0) = U_\infty(z) + \frac{\Delta u_{*0}}{\kappa} \ln(z / z_0) \tag{5.38}$$

The new parameter Δu_{*0} represents the disturbance of the near-surface shear stress at the hill crest. This results from equating the amplification at the height l of inner and outer layer to

$$\Delta u_{*0} = u_{*\infty} \frac{\ln(L / z_0)}{\ln(l' / z_0)} \frac{H}{L} \sigma(\frac{x}{L} = 0,\ z = l') \tag{5.39}$$

from which the velocity in the inner layer can be calculated:

$$U(z < l', x = 0) = U_\infty(z) + U_\infty(z) \frac{\ln(L / z_0)}{\ln(l' / z_0)} \frac{H}{L} \sigma(\frac{x}{L} = 0, z = l') \tag{5.40}$$

Under the assumption that the maximum increase takes place at the height l' and the hill has the form of an inverse polynomial (σ=1) we get:

$$\Delta U_{\max} \cong U_\infty(L) \frac{H}{L} \tag{5.41}$$

In using the height l' from Eq.(5.36) and considering the Jackson-Hunt theory (Hunt et al., 1975) the maximum increase emerges as:

$$\Delta U_{\max} \cong \left[U_\infty^{\,2}(L) / U_\infty(l')\right] \frac{H}{L} \tag{5.42}$$

This value is indeed higher than that from Eq.(5.41), because the height used for of the inner layer is greater in Eq.(5.42). Another often used parameter is the so called *speed-up*:

$$\Delta S = \frac{U(x,z) - U_\infty(z)}{U_\infty(z)} = \frac{\Delta U(x,z)}{U_\infty(z)} \tag{5.43}$$

From Eq.(5.41) it follows that the maximum of this speed-up occurs when

$$\Delta S_{\max} = \frac{U_\infty(L_e)}{U_\infty(l)} \frac{H}{L} \tag{5.44}$$

or under application of Eq.(5.42) the maximum speed-up is:

$$\Delta S_{max} = \left(\frac{U_\infty(L)}{U_\infty(l')}\right)^2 \frac{H}{L} \tag{5.45}$$

In later works the Jackson-Hunt theory was widened by an additional middle layer and the height of the maximum speed-up was assumed with l/3, which led to an improved reproduction of measurements by the theory.

A still unsolved problem in the representation of the vertical profile of the horizontal wind speed is the elimination of the salient point appearing in the course of the height l' versus Δu (see Figure 5.10), that originates at the connection of the profiles of inner and outer layer after Eqs.(5.40) and (5.31). Hence, the following conditions must be fulfilled: The profile curve should change into the outer layer asymptotically for $z/l' \to \infty$ and the wind profile of the inner layer near the ground should have an osculating curve where $z = z_0$. Such a profile is given by

$$\Delta U(0,z) = U_\infty(L)\frac{H}{L}\sigma(0,z/L)P(z) \tag{5.46}$$

with

$$P(z) = 1 + \frac{\ln(z/l')}{\ln(l'/z_0)}\exp[-(z-z_0)/l'] \tag{5.47}$$

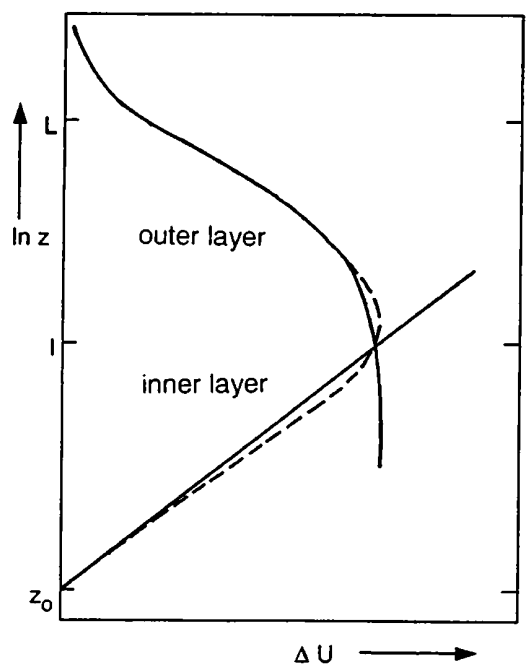

Figure 5.10: Speed-up at the top of a hill, schematically (Hoff, 1987)

For three-dimensional elevations the calculation of the speed-up is more complicated, also curvilinear coordinate systems are often used that follow the stream lines. Therefore only the results derived from the Jackson-Hunt theory are given here:

(5.48.1) $\Delta S_{max} \cong 1.6H/L$ for axis-symmetrical hills

(5.48.2) $\Delta S_{max} \cong 0.8H/L$ for 2-dimensional terrain steps

(5.48.3) $\Delta S_{max} \cong 2.0H/L$ for 2-dimensional mountain ridges

However, these equations lose their validity if the hillside inclination becomes too large. In this case a region forms with separate flow in the lee of the highest point a region forms with separated flow (see paragraph 5.1.3). While in the above equations the pressure field is derived from the form of the hill, during flow-separation the region beneath the flow-separation must be considered in addition to the true elevation for the calculation of the pressure field, which leads to a shift of the summit into the windward side and to an elongation of the horizontal extension of the overflowed structure. By the shift of the geographically highest point to the windward side three-dimensional, axis-symmetrical hills with large hillside inclinations reach for example a maximum speed-up of only 1.25 *H/L* (Bradley et al., 1986).

The horizontal extent of the so-called separation-bubble includes all points of *h(x)*, for which

(5.49) $$\left.\frac{\partial U}{\partial z}\right|_{z=0} < 0$$

is valid. This happens specifically when the flow to the wind ward side is slowed down in the acceleration region by friction such that overcoming the positive pressure gradient by the flow is no longer possible behind the highest point. As a consequence the smaller the ratio of the hill height to the roughness length is, the sooner a flow-separation appears in the lee. Another important criterion for the appearance of flow-separation is the hillside inclination represented as a measure of adequate approximation

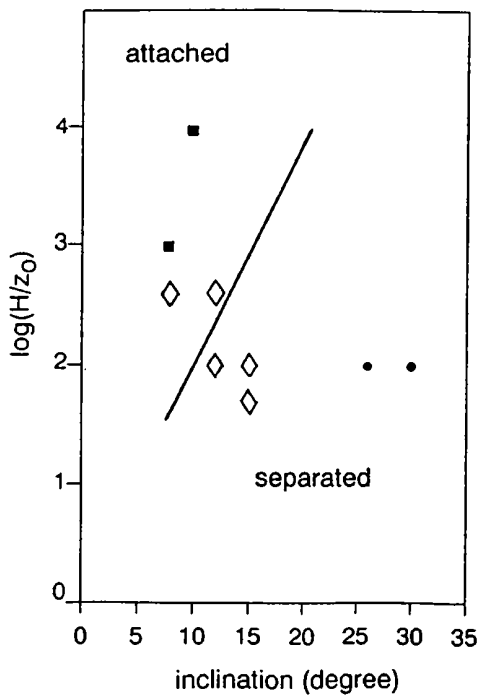

Figure 5.11: Flow separation with respect to hill height and hillside inclination (Petersen 1990)

for the curvature of the pressure disturbance with respect to x. The stronger the increase of the positive, lee side pressure gradient is (see Figure 5.8.d), the more difficult becomes to overcome, such that in the case of a sharp edged hill crest (which is equal to an infinitely large curvature of the pressure disturbance) flow-separation always appears. The dependence of flow-separation on the two mentioned causes is shown in Figure 5.11. It follows that flow-separation appears for a given roughness length and hillside inclination of 10 to 20 degrees or more.

There are two possibilities for testing the theoretical findings: Firstly, a large-scale field experiment with high technical and consequently financial expenditure, secondly, a wind-tunnel experiment. While for the first case, discovering a suitably formed hill with uniform surface roughness over a distance of approximately 5 kilometres would be difficult, in the second case it is realising a ratio of the hill height to roughness length. Because in wind tunnel hill heights of only one to two meters can be reached the roughness must be scaled for a realistic model of the flow conditions and consequently, has to be very small. This leads to the problem that for inferior roughness no realistic turbulent boundary layer is formed, therefore flow investigations in the wind tunnels are usually restricted to the case of forested hills which are of little use for wind energy purposes (Britter et al., 1981).

Extensive and well documented field experiments were performed e.g. in Scotland at the Askervein Hill (Walmsley et al., 1996), in Australia on the Black Mountain and in Canada at Kettles Hill (see Taylor et al., 1987). While Askervein Hill and Kettles Hill have only very low roughness, the Black Mountain is forested (Table 5.1). All three hills are approximately two dimensional, i.e. the length of the hill is essentially smaller than the width (Bradley et al., 1986; Hoff, 1987).

The results of these field experiments confirm in the case of low roughness the validity of Eq.(5.36) for the height of the inner layer and the maximum velocity increase. Only the forested Black Mountain delivers a layer-thickness l, which corresponds to Eq.(5.37). But this could be explained by the very steep hill and possibly separated flow in the lee falsifying the results. A summary of the results of all three field experiments with theoretical calculations for comparison is given the following table.

Table 5.1: Comparison of the layer thickness l' from theory with measured values h_{umax} (all parameters in m); after Bradley (1986)

Field experiment	Roughness	Height H	L	l'*	l'**	$h_{u\,max}$
Black Mountain	1.14	170	275	28	14	27
Askervein Hill	0.03	116	215	12	3.2	3
Kettles Hill	0.01	100	520	22	4.5	5

(*) after Eq.(5.37); (**) after Eq.(5.36)

The calculations of the velocity amplification agree well with the measurements on the up-wind side and at the highest point, only in the lee an overestimation of the wind speed occurs by neglecting each form of flow separation, which can happen in small areas of terrain with hillside inclinations of more than 20°. Figure 5.12 shows the comparison of the calculation by means of a three-dimensional model based on the Jackson-Hunt theory with measured data from the Askervein Hill.

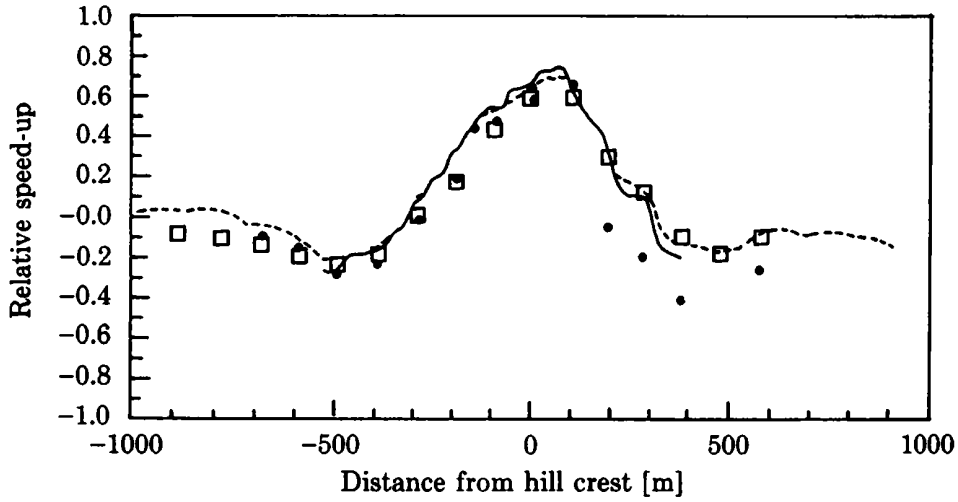

Figure 5.12: Measured data compared with calculated values of the MS3DJH/3 model (Troen et al., 1989)

5.2 Thermally induced flows

In complex terrain further phenomenon as thermal induced flows have to be considered too: Hillside winds blow parallel to the inclination of the hillside and consist of an up-slope flow along the hill side blowing during the day, and down hillside flow blowing during the night. Valley winds blow parallel to the longitudinal-axis of the valley, during the day in a downward direction and in the night in the up-valley direction.

5.2.1 Hillside winds

Hillside winds originate by positive as well as negative buoyancy forces, which result from the fact that the air is warmer or colder than the air on the hillside for the same height at some horizontal distance to the hillside. A warmer air layer near the hill side develops during the day with direct solar irradiation. In this case the strongest up-slope flows are to be expected. On the other hand a strong cooling of the ground and of the near surface air layers takes place in the night during clear sky conditions due to the negative radiation balance so that in these cases the strongest hillside down flows occur.

In order to gain a better understanding of the physics of hillside winds one can look again at the basic equations for conservation of momentum, the first law of thermodynamics and the continuity equation, expressed for simplicity in natural coordinates (*s, n*). With the s-component parallel to the hillside, the n-component vertical to the hillside and α the inclination it can be written:

$$\frac{du}{dt} = -\frac{1}{\rho_0}\frac{\partial(p-p_a)}{\partial s} - g\frac{d}{\theta}\sin\alpha - \frac{\partial\overline{u'w'}}{\partial n} \tag{5.50}$$

$$\frac{dw}{dt} = -\frac{1}{\rho_0}\frac{\partial(p-p_a)}{\partial n} + g\frac{d}{\theta_0}\cos\alpha \approx 0 \tag{5.51}$$

$$\frac{d\theta}{dt} = -\frac{1}{c_p \rho_0}\frac{\partial R}{\partial n} - \frac{\partial \overline{w'\theta'}}{\partial n} \tag{5.52}$$

$$\frac{\partial u}{\partial s} + \frac{\partial w}{\partial n} = 0 \tag{5.53}$$

with

$$\theta = \theta_0 + \gamma z + d(s,n,t) \tag{5.54}$$

and

$$\frac{\partial p_a}{\partial z} = -\rho_a g \tag{5.55}$$

The driving force of the hillside wind is the buoyancy term, i.e. the second term on the right hand side of Eq.(5.50). The ratio of the deviation of the potential temperature to the total value is governed by Eq.(5.52) in which the radiation term and the turbulent heat exchange is included. The value of sinα enables differentiation of different hillside wind regimes. If $\sin\alpha < 0.001$ no sufficient hillside incline is given for the developing of hillside wind. With $\sin\alpha$ between 0.001 and 0.1 an increase of the boundary layer occurs with little hillside winds with a maximum in the afternoon. With $\sin\alpha > 0.1$ a thin convective boundary layer develops with strong hillside up-flow reaching its maximum at midday. Noteworthy is the fact that the theoretical models for the flow over hills claim to be valid for a range up to the flow separation (up to an angle of approximately 20 degrees), hillside winds in these models are however completely unconsidered and therefore represent a possible error source.

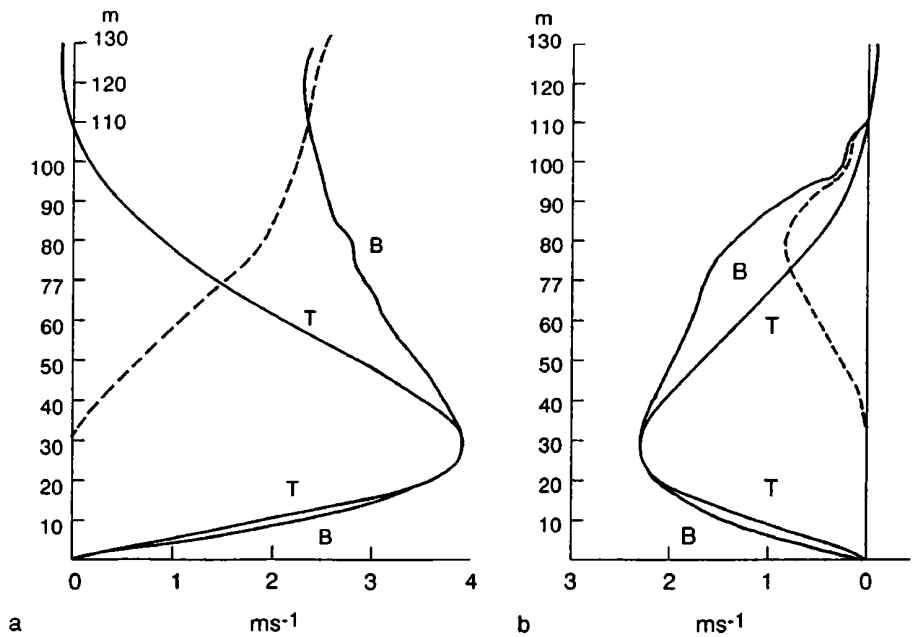

Figure 5.13: Measured (B) and theoretical (T) vertical profile of (a) a up-slope flow and (b) hillside down-slope flow; (the dashed lines show the difference between measurement and calculation)

5.2.2 Valley and mountain winds

Valley winds are caused from the pressure gradient which develops from the stronger daily course variation of the temperature in the upper part of the valley versus the lower parts or the plains before the valley mouth. From this, an up-valley wind results during the day with a maximum around 3:00 p.m. and a down-valley wind (mountain wind) during the night with a maximum around 3:00 a.m. For example during weather situations with weak pressure gradient differences in the valley of the Inn in Landeck (Austria), for a village 156 km valley-upward, a 3.6 times stronger daily course variation of the temperature occurs as compared with the small city of Rosenheim (Germany) which lies out on the open plains. This leads to valley winds of up to 4 m/s in the summer and to mountain winds of up to 7 m/s in the winter, as measured on the Isel mountain near Innsbruck, Austria. The frequency of valley winds occurring reaches approximately 30 percent in the Inn valley. From this it is evident that valley winds are interesting for wind energy purposes in conjunction with other reinforcing factors as channelling of the main wind direction.

A simple method for the estimation of the strength of valley winds is given by the *topographic amplification factor* (TAF). The basic idea is founded on the effects from the daily course of temperature in different valley sections and the pressure gradient change with regard to the solar insulation and its ability to warm air volumes in the section. While over the plains a very large volume warms up (similarly to be cooled) an essentially smaller volume is similarly effected in the upper part of the valley due to the decreasing surface. The topographical amplification factor between a valley section and the plains is defined as follows:

$$TAF = \frac{A(D)/V_{vally}}{A(D)/V_{plain}} \tag{5.56}$$

Here $A(D)$ is the horizontal surface at height D above the valley floor through which the solar energy reaches the underlying volume V. The volume to be warmed upon the plains is simply $D \times A(D)$. Another way to define TAF is given by using the valley cross section instead of the volume:

$$TAF = \frac{W/A_{vally}}{W/A_{plain}} \tag{5.57}$$

The quantity W is the width of the cross section at height D and A is the vertical cross-section surface. For a valley, according to the form, the following TAF results for $W=2D$: $TAF = 1.27$ for a concave, $TAF = 2$ for a triangular and $TAF = 4.66$ for a convex valley cross section, as it is shown in the following

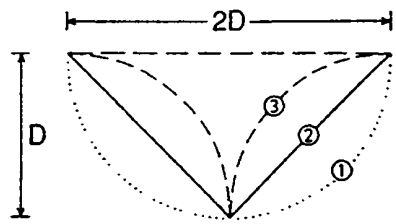

Figure 5.14: Form of the valley cross section for 3 different amplification factors (see text; Blumen 1990)

However, beside the topography further factors play a role for the strength of the valley winds. Differences in the albedo can reinforce or reduce the daily course of temperature between the plains and the end of the valley and a stable stratified atmosphere can restrict the height D to a lower level than the topographically pre-determined one. This leads to a greater daily course than expected from the topographical amplification factor for convex valleys.

6 MODELLING OF WIND FIELDS

6.1 Introductory remarks

A prerequisite in the siting procedure of wind power plant location of a single installation as well as for a wind farm is the knowledge of the possible annual energy yield and also therefore the local wind field. Only then can the information be used to verify the economic feasibility of a WTGS. Furthermore, for the assessment of optimal sites for a WTGS installation within a domain, numerical flow models providing an objective interpolation algorithms for the wind vector must be applied. As discussed in paragraph 4.6, the frequency-distribution of the wind speed at hub-height and the height-reduced air density as well as installation-specific parameters must be well known, such as the power curve and the technical availability. Ideally the measurements of wind vectors should be taken at hub-height over a time period of at least two years for statistical reasons (representativeness). In practice these measurements are rarely available as the present common converters have hub-heights between 30 and 65 meters, and measurements at this height are technically difficult and therefore very costly. This is why estimation by means of mathematical-physical models on the basis of long-term time series measured by an existing meteorological network is necessary. To apply models instead of or in addition to in-situ measurements is nearly an imperative because of the financial and temporal constraints (Dobesch et al., 1996).

It would not be pragmatic to give a thorough presentation of the great number of models in use here. An extensive overview can be found in Lalas et al. (1996) chapters 6-9 and in Physick (1988) for models over complex terrain. So we can distinguish between different numerical model designs according to the physical principles considered. These models can be roughly divided into two general categories, namely in *diagnostic (or kinematic) models* and *prognostic (or predictive, dynamic, primitive equations) models.* Diagnostic models take an initial set of observations scattered over a domain and try to reproduce a complete flow field over the whole period of observations, satisfying some physical constraints (mostly mass conservation). Prognostic models forecast the state of the flow field future - based on an initial state of the atmosphere and given boundary conditions. In this category the codes called *JH-models* (after Jackson&Hunt, 1975) can be included too (despite the fact that they are neglecting their time-dependence). But Troen claims in Lalas et al. (1996) that the JH models are to be preferred to the mass-consistent method. We will keep with this opinion in the following.

The solution of the full set of equations in the prognostic models is still a laborious task and the more elaborate the model is, the more reliable the input data must be to exploit the offered advantages - but often such data are not available. Alternatively, the relative simplicity of diagnostic models makes them attractive for many practical purposes especially as observed data from the domain of investigation can be easily taken into consideration. Thus Pennel (1983) found that in some cases improved mass-consistent models could outperform the more complex dynamical models.

Two main types of diagnostic models can be distinguished. One type relies on the Jackson&Hunt (1975) theory (cf. above) from which a more simplified approach can be found in Troen et al. (1986). Typically representative models are found in Mason and Sykes (1979), Walmsley et al. (1986) and that used in the European Wind Atlas (Troen et al., 1989). Another type is the so-called mass-consistent approach. Here only the equation of mass conservation is used to correct an initial "guess" of the flow field (e.g. by spatial interpolation between observed wind vectors in the domain under consideration for the given orography). Representations of these models are the *NOABL* (Traci et al., 1977, 1978; Phillips, 1979) and many variants as *AIOLOS* (Tombru et al., 1990) and its latest version *WINDS* (Ratto et al., 1990), *COMPLEX* (Bhumrakar et.al., 1980; Endlich et al., 1983), *ZAWINOD2* (Dobesch et al., 1999) and others.

From a more practical point of view roughly three categories of calculation procedures can be identified:

The first group includes simple one-dimensional calculation procedure for the vertical extrapolation of the wind speed to hub-height from measured data at lower levels (mostly 10 meters above ground level), based on the conditions for plain terrain and therefore usually the logarithmic wind profile is applied and, eventually, the stability of the atmosphere or changes in surface roughness are taken into account. The application of these procedures is restricted however to plain surfaces. Typical of this group are the *ALWIN* procedure, developed by DEWI (German Wind Energy Institute), as well as the Danish *WAsP* (Troen et al.,1989) without the orography module.

The second group comprises models in which slightly inhomogenous terrain can be taken into account, in accordance with the theory of Jackson&Hunt. Other models of this category are the BZ code (integrated in *WAsP*) and the *MS3DJH/3R* model family (Walmsley et al., 1986) together with the MS-Micro/2 code - a microcomputer implementation of the MS3DJH/3R code.

The third group includes wind field models for inhomogeneous terrain, which are based either on the fulfilment of the continuity-equation (the so-called *mass-consistent models*), or, additionally, on the conservation of momentum and on a non-hydrostatic atmosphere, (the so-called *non-hydrostatic models*). Mass-consistent variational-analytical models are far spread and exist in many versions e.g. in Sherman (1978) or above mentioned *ZAWIMOD2* with a variation-analytical base. Representative of the non-hydrostatic models is the *GESIMA* model (Mengelkamp, 1991) from the German Research-Centre Geesthacht. It should be mentioned that for single points in the calculation procedures of the first and second group by repeated application, area-related information can be achieved in the case of a regionally uniform wind field.

As examples the *ZAWIMOD2* and the Danish *WAsP* (which forms the basis for the European Wind Atlas) and *GESIMA* model are introduced in the following paragraphs.

6.2 Mass-consistent models with variational-analytical base

One can simplistically look at this model category, as an intelligent interpolation-extrapolation of measurements in non-homogenous terrain: Wind vector measurements from the domain of investigation are used for an estimation of the so-called *initial wind field*, the three-dimensional wind field for each node of the surface grid. To fill in the gaps between and beyond the single measurement points must be extrapolated in the vertical and horizontal directions. In the vertical direction the above mentioned logarithmic wind profile can be applied with or without additional terms for the stability of the atmosphere or the power-law is used. Above the height of the Prandtl-layer the wind vector can be considered in good approximation as constant. In the horizontal direction, the estimated values for the wind vector at the grid points are obtained in the simplest case by a weighted average of the measurements. The weights are given by the reciprocal value of the square of the horizontal distance from the grid points to the points with measurements (Barnard, 1991; Dobesch et al., 1999).

$$\vec{v}_0(x,y,z) = \left(\sum_{m=1}^{M} (\vec{v}_0(x_m,y_m,z)/r_m^{\,2}) / \sum_{m=1}^{M} (1/r_m^{\,2}) \right) \tag{6.1}$$

The quantities x, y, z are the co-ordinates of the grid point for which the interpolated wind vector is calculated, x_m, y_m, z those of the grid point at the height z for the measuring station, M is the number of stations used and r_m the horizontal distance of the grid point from the station M. Because the vertical wind speed is not available routinely, the vertical wind component is set to zero for the entire model domain.

In the next step the initial wind field is modified so that firstly, the u, v, w components fulfil the continuity-equation and secondly, the modification within the investigated space must be a minimum (Sherman, 1978). These conditions are fulfilled, if

(6.2)

$$E(u,v,w,\lambda') = \int_V \left[\alpha_u{}^2 (u-u_0)^2 + \alpha_v{}^2 (v-v_0)^2 + \alpha_w{}^2 (w-w_0)^2 + \lambda' \left(\frac{\partial u}{\partial x} + \frac{\partial v}{\partial y} + \frac{\partial w}{\partial z} \right) \right] dxdydz$$

becomes a minimum. Here u, v w are the modified wind vector components, u_0, v_0, w_0 the components of the initial wind field, α_u α_v α_w weight factors, which were set equally for the horizontal components ($\alpha_u = \alpha_v = \alpha_1$, $\alpha_w = \alpha_2$) and which decide the extent of the modification to the individual components, and λ' is here the Lagrange-multiplier. The function E() in Eq.(6.2) becomes a minimum, if u, v, w fulfil the Euler-Lagrange-equations:

(6.3) $$u = u_0 + \frac{1}{2\alpha_1{}^2} \frac{\partial \lambda'}{\partial x}$$

(6.4) $$v = v_0 + \frac{1}{2\alpha_1{}^2} \frac{\partial \lambda'}{\partial y}$$

(6.5) $$w = w_0 + \frac{1}{2\alpha_2{}^2} \frac{\partial \lambda'}{\partial z}$$

Applying the continuity equation to Eqs.(6.3) - (6.5) a second order differential equation, the *Poisson-equation*, for the Lagrange multiplier results:

(6.6) $$\frac{\partial^2 \lambda'}{\partial x^2} + \frac{\partial^2 \lambda'}{\partial y^2} + \left(\frac{\alpha_1{}^2}{\alpha_2{}^2} \right) \frac{\partial^2 \lambda'}{\partial z^2} = -2\alpha_1{}^2 \left(\frac{\partial u_0}{\partial x} + \frac{\partial v_0}{\partial y} + \frac{\partial w_0}{\partial z} \right)$$

The squared ratio of α_1 / α_2 enables simulation of different stability conditions in the atmosphere for the flow in complex terrain. If the ratio is very small a stronger modification takes place in horizontal direction so that the w-component remains small. This corresponds to the case of a stable stratified atmosphere, with which a flow-around of the elevation is more likely than an overflowing. The larger the ratio is chosen, the more strongly overflowing is simulated in the model, which corresponds to the case of neutral as well as unstable stratification. Sherman (1978) gives for neutral stratification $\alpha_1 / \alpha_2 = 0.0001$ but in the literature other values can be found. Other models allow it to fix the weight factors for each wind field to be calculated so that with omission of a measuring station and simultaneous calculation of its data from adjacent data, the error between calculated and measured data for all stations becomes a minimum (Barnard, 1991).

The Poisson equation is solved with the boundary condition $\partial\lambda'/\partial n = 0$ for the closed border of the topography which is approached by a so-called *block-orography*, and $\lambda' = 0$ for the open boundary in this case of the free atmosphere. Since the block orography consists of vertical and horizontal surfaces, whose dimensions correspond to the grid-point distance, the grid mesh must be a narrow one in order to reduce larger errors. This can be avoided by introducing terrain-following co-ordinates but for the price of a much higher computational expense. Numerically the Poisson-equation then is solved for λ', in that one replaces the differential-quotients by final differential ratios (a three-point difference with the exception of border points). From the results for λ' the modified wind components at each grid point can be estimated with the help of the Euler-Lagrange equations.

6.3 The European Wind Atlas (*WAsP*)

The European Wind Atlas Analysis and Application Program (*WAsP*, Troen et al., 1989) has already a broad user community. It was developed at the end of the nineteen eighties, supported by the European Union within the framework of the Joule-Thermie Programmes, with the goal to achieve on the basis of long-term measured data of wind vectors at standard meteorological heights an overview of the available regional wind resources and to give at certain locations an estimation of the annual energy yield to be expected. By the use of long-term data the statistical representativity should be increased. From another account the model assumptions should guarantee transferability of these data over larger horizontal distances. Because each measurement is influenced by the immediate surroundings, as nearby obstacles, specific roughness and orographic conditions (and are therefore only valid for the point of the measurement itself), these factors have to be eliminated as a first step in order to gain a regionally representative wind climatology. As a second step, from this climatology the wind-climatological characteristics at any location up to a distance of 100 kilometres from the measuring location can be determined under consideration of the new environmental conditions. With these factors the frequency-distribution of the wind speed by means of the Weibull-distribution (c.f. paragraph 7.2) is established, giving the possibility to estimate the annual energy yield at the chosen location using the power-curve and the technical availability of the WTGS. Figure 6.1 represents these two steps descriptively, for which the European Wind Atlas has a collection of the regionally representative wind climatologies for different countries compiled.

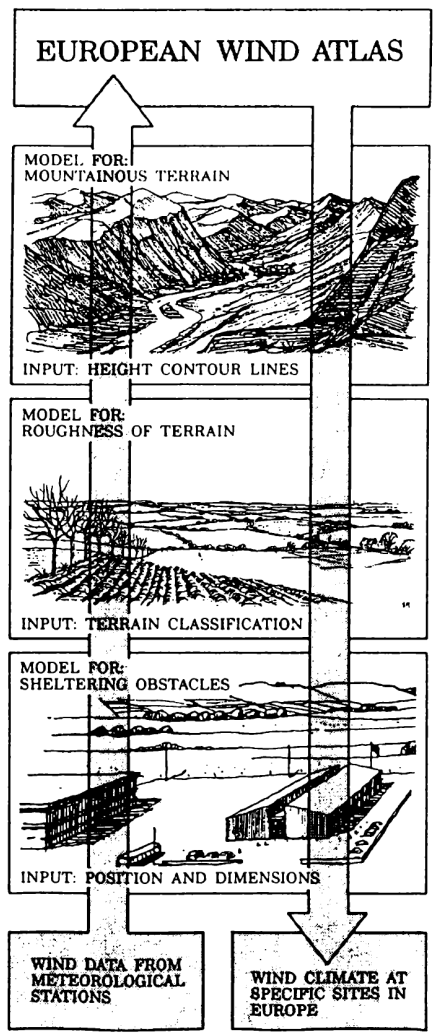

Figure 6.1: Methodology of the wind atlas procedure (Troen et al., 1989)

The way the transferability of the measured data is given for a distant location is dependent on the orography and its influences on the regional wind field. While in the large plain areas of Denmark or Northern Germany the regionally representative wind climatology has a radius of up to 100 km, this is reduced to a maximum of 50 km or even less in the plains near to large mountain ranges. If the measuring site is in a mountainous area, transferability on the basis of the assumption made in the *WAsP* model is no longer valid. In order to explain the reason for this, the following individual model modules of *WAsP* are described shortly. Interestingly the models do not interfere directly with the data but rather rely on the frequency-distribution of the wind speed, separated into 12 sectors with a range of 30° each. The correction for a differently stratified boundary layer is not performed in the final version.

6.3.1 The obstacle model

While the hub-heights of the presently used WTGSs make them slightly susceptible to the immediate screening from obstacles, the attenuation of the wind speed in the neighbourhood of the stations where the wind vector is measured in the usual climatological height of 10 meters must be taken into consideration separately. Whether an obstacle provides shelter at this specific site or not depends on: the distance (x) and direction of the position vectors from the origin (point with measurement) to the two nearest situated corners points of the obstacle, the height (h) and the length in flow direction (L) as well as the porosity (P) of the obstacle and the anemometer height. The porosity is defined by the relationship of the obstacle-free gaps to the total surface of the obstacle: The gaps are equally zero for example in the case of a concrete wall and so the porosity is also zero; if the obstacle consists of a row of trees the porosity lies according to the size of the gaps between 0 and 1 and is set usually ≈0.5. The basis for the model of the velocity attenuation by obstacles originates from a work of Perera (1981), in which these reduction-coefficients are derived from wind tunnel measurements for infinitely long fences and shelter belts crosswise to the flow direction. The reduction by such obstacles is represented in Figure 6.2.

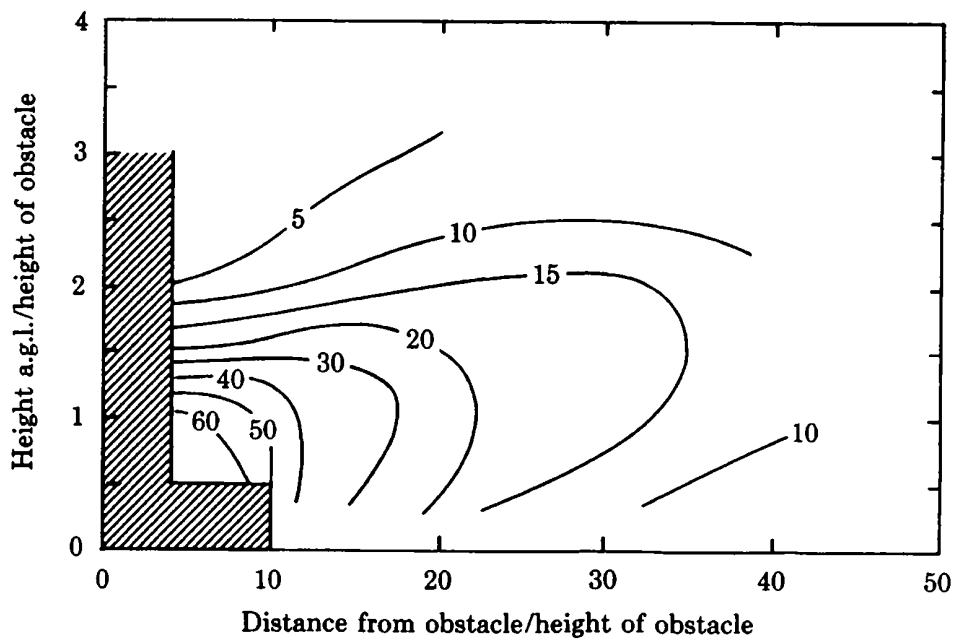

Figure 6.2: Reduction of the wind speed (R_l) in percent due to a two-dimensional obstacle. In the shaded area the sheltering depends on the detailed geometry of the obstacle (Perera, 1981).

The effect of porosity P (with $0 \leq P \leq 1$) is approximately accounted for by multiplication with $(1-P)$. If beside the porosity P also the lateral dimension of the obstacle is regarded by a factor R_2 the corrected speed u_{corr} with the reduction-coefficients R_1 and R_2 is

$$u_{corr} = u\left[1 - R_2 \cdot R_1(1-P)\right] \tag{6.7}$$

The quantity R_2 has to be introduced because the shelter from an obstacle with a finite lateral dimension decreases due to mixing in the wake. Furthermore the effect in the average wind speed in a given azimuth sector is decreased too because of the finite angular dimension of the obstacle as seen from the site. Therefore in a given sector the reduction in average wind speed is, derived from simple geometrical considerations,

$$R_2 = \begin{cases} (1 + 0.2\,x/L)^{-1} & \text{for } L/x \geq 0.3 \\ 2\,L/x & \text{for } L/x \leq 0.3 \end{cases} \tag{6.7.1}$$

6.3.2 The roughness model

The logarithmic wind profile can be applied only if the upwind terrain is reasonable homogeneous. But an unique roughness-length is only available in the rarest cases. However, it is possible for small-scale terrain inhomogenities to model the change of surface stress which occurs when flows are crossing a change in surface roughness. In this case an internal boundary layer grows downwind from the change. Considering a point at a distance x (the fetch) downwind of this change the internal boundary layer has grown to a height h (Panofsky 1973), similar to Eq.(4.72).

$$\frac{h}{z_0}\left[\ln(h/z_0') - 1\right] = 0.9\frac{x}{z_0} \tag{6.8}$$

where z_0' is the bigger of the upwind (z_{o1}) and the down wind (z_{o2}) roughness length. It can be empirically found that the change of the friction velocity is well modelled using the relation

$$u_{*2}/u_{*1} = \ln(h/z_{o1}) \,/\, \ln(h/z_{o2}) \tag{6.8.1}$$

With the knowledge of the height h the vertical profile can be considered as a profile composed from three logarithmic parts where the lowermost part reaches approximately one tenth, the middle part up to one third of the internal boundary layer height. However, this approach requires the restrictive condition by the existence of several roughness changes that this one lying further away must have the double distance as that lying closer to the measuring station (Troen et al., 1989).

6.3.3 The orographic model

The orographic model (BZ-model) of the *WAsP*-programme is used to correct orographically induced disturbances in the flow field due to terrain inhomogenities. Because the *BZ model* is based as the whole *MS3DJH* model family on the theory of Jackson&Hunt (1975) it provides only for hills with a height up to 200 meters and a hillside inclination of up to 20 degrees for realistic results. In this geometrical range a good approximation for the speed-up can be calculated by means of the application of polar co-ordinates and a zooming grid.

As presented already in section 5.1.4 a potential flow with the resulting flow perturbations is determined initially. For this case it is assumed that the Laplace equation is fulfilled, if the vector field of the wind is non-vortical, i.e. the velocity perturbation $\vec{u}'(u,v,w)$ is related to the potential χ by

$$\vec{u}' = \nabla\chi \tag{6.9}$$

For the three-dimensional case the potential results under the assumption that the disturbance potential vanishes at the outer boundary R (= outer model radius). A general solution can be expressed in polar co-ordinates in terms of a sum of the products of Fourier-Bessel series with the argument $c(n,j)r/R$ for each n and of Fourier series with the argument $\exp(in\varphi)$ (φ = azimuth) with the coefficients $K_{n,j}$. These coefficients are estimated by the kinematic boundary condition on the ground (hillside-parallel flow):

$$w_0 = \left.\frac{\partial\chi}{\partial z}\right|_{z=0} = \vec{u}_0 \cdot \nabla h(r,\varphi) \tag{6.10}$$

where w_o is the terrain-induced vertical velocity and h the height of terrain. By defining the model centre to coincide with the point of interest it is possible to concentrate the model resolution there and also to restrict the calculations to the perturbation at this point. For the centre point (r=0) the following solution is found:

$$\nabla\chi_j = \frac{1}{2}(1,i)K_{1j}\frac{c_j^1}{R}\exp\left(-c_j^1\frac{z}{R}\right) \tag{6.11}$$

In a second step the influences of friction are taken into account in the inner layer with the layer thickness l. For the calculation of l in the BZ model, Eq.(5.36) is used but the speed-up according to Eq.(5.42) should lead to an overestimation of the speed amplification after Hoff (1989). However, the comparison with measured data of the Askervein Hill shows a good agreement of theory and measurement (Troen et al., 1989).

6.4 The GESIMA model

This non-hydrostatic model is based beside the conservation of momentum and the continuity-equation also on the conservation of energy and the moisture balance, and uses the so-called flow-form of terrain following co-ordinates whose vertical component is a function of the terrain height and the upper boundary of the model space. To account also for small-scale circulation that result from dynamically generated pressure differences (blocking or canalling effects), the pressure is partitioned into three parts, the basic pressure - defined by the temperature field, the hydrostatic and the non-hydrostatic pressure deviation. The hydrostatic part is determined from the hydrostatic basic equation and the non-hydrostatic from the Poisson equation. The Reynolds' shear stress is parameterised by means of the K-theory and the velocity at the upper boundary of the model is given by the geostrophic wind.

In order to assess the average annual wind energy potential at a certain point or on a surface the two-dimensional frequency-distribution of the geostrophic wind must be known in N speed-classes and K directional sectors. By means of this frequency-distribution $f_{k,n}$ the average wind energy flow can be determined for each place:

$$E = \frac{1}{2}\rho \sum_{k=1}^{K} \sum_{n=1}^{N} f_{k,n} \left(u_{gk} \frac{\sqrt{u_n^2 + v_n^2}}{V_{GEO}} \right)^3 \tag{6.12}$$

u_{gk} is the average geostrophic wind in the class k, V_{GEO} is the amount of the geostrophic wind at the upper boundary of the model, and u_n and v_n are the components of the wind vector for the simulation with V_{GEO} from the directional sector N.

Although a great step was made with the GESIMA model in the direction for realistic representation of wind fields in complex terrain by means of models only, a low spatial resolution is only possible now due to the enormous computing capacities required.

6.5 Model comparison

To relate measurements of wind velocity on hills some attempts have been made to relate them to topographic features. A list of such measurements is given in Taylor et al. (1987). On the basis of such data sets especially those from Askervein Hill, or Kettles Hill (Barnard, 1991; Bradley et al.,1989 and paragraph 5.1.4) many comparisons between different models can be found in the literature which are not easy to follow as often modifications were made during the use and adaptations for the models to better fit to the given conditions. A good overview is given in Walmsley et al. (1990) or Walmsley et al. in Lalas (1996) where the results of 3 codes based on the JH theory and one mass-consistent (*NOABL*) code based on a data set from the Blashaval Hill experiment in Scotland were examined. The results show a good agreement with each other and fell within the observed range of variation from the observations. However, gradual differences arose from the given orography and the treatment of the roughness in the upwind fetch. In another study Guo et al.(1990) adapted the *COMPLEX* and *NOABL* models resulting in a new model, called *MC-3*. Troen states (in Lalas et al., 1996) that the mass-consistent codes fall naturally short in the treatment of the flow physics but have advantages in the ability to incorporate directly a number of data in the analysis and, consequently, the advantages of both model types should be linked which was achieved in the *LINCOM* model (Troen, 1987, unpublished). In these studies the guidelines from the method after Walmsley et al. (1982 and 1989) were used showing a slightly better adaptation of the model results to the given wind field.

7 SITING AND ENERGY YIELD

7.1 The importance and requirements of siting

In Europe for modern WTGSs typical values of rated power are 600 W/m^2 but for the same rated power it can vary by 50 percent (Lalas et al., 1996). The specific energy is on average 600 KWh/m^2/year but with the best WTGSs on very good sites over 1200 KWh/m^2/year can be reached. For instance a wind speed increase of only 1 m/s (say from 7 to 8 m/s) would result in a remarkable performance improvement so the electricity cost drops and the capacity factor (function of technical availability - see paragraph 6.6 - and wind resource at the specific site) would increase to 35 percent (typical 20 percent in Europe, for good sites 50 percent can be reached). This means a 20 percent increase of energy yield for a 12 percent increase in wind speed. Therefore the importance of an accurate siting becomes paramount. Due to the fact that the wind energy flux is proportional to the cube of wind speed, which can be written formally as

$$P \propto \frac{1}{2}\rho \int_{u_{in}}^{u_{out}} f(u)u^2 du \tag{7.1}$$

(with P the energy flux and $f(u)$ the frequency of occurrence of wind speed u; cf. paragraph 2.1) in the siting procedure a careful identification of locations with higher wind speeds compared to other locations within a given domain is required which is a crucial task in the exploitation of wind power.

Ideally for the estimation of energy yield for a specific WTGS over its lifetime time series of wind vector (minimum 1 year) at hub height should be available together with its mechanical and technical availability (cf. paragraph 2.5 and 2.7). But measurements at hub height are very rare and one usually has to rely on the data from a meteorological network in a certain standard height. Very often such data are measured at stations where location was usually chosen by criteria other than suitability for wind energy issues. Therefore the data needs to be corrected before an extrapolation to hub height can be done. Both were discussed in more detail in chapter 4 (paragraph 4.3).

7.1.1 General considerations

Wind energy systems as other energy systems have to be planned carefully to achieve reliability and low cost. They are by their nature very sensitive to meteorological phenomena because these do not only influence normal operation (by the given wind conditions) but can disrupt the service, augment demands or require consideration for environmental reasons (WMO, WCAP-13).

Meteorological information for wind energy use should contain high resolution spatial maps of regional wind climatologies derived by special algorithms. As a prerequisite models for transforming measured wind data into objective meso-scale representative values must be used because measured meteorological data very often are unrepresentative (and even of questionable quality, cf. paragraph 4.4). Furthermore short term forecasts of wind speed (24-48 hours) for scheduling and dispatching may be a favourable method to optimise wind energy buying and selling by the wind farm operators. These forecasts have to be highly accurate local forecasts with an uncertainty of less than 15 percent and should be based on a numerical weather prediction with downscaling algorithms as given in the MOS or LAM forecast products and for a time step of at least 3 hours or less.

As a consequence the data representativeness must be given high priority. This can be achieved through the improvement of measurements by strictly observing WMO regulations (e.g. WMO No.8, VI.6.6, 1973) without any compromises on the exposure of measuring equipment; documentation about the meta

data and objective correction/reduction procedures for wind data with knowledge of shading by obstacles, orography and environmental roughness of the site in question (cf. paragraph 6.3). Necessary additional information and skills must be available too, e.g. DEMs (digital elevation models with a resolution of 100 x 100 meters or less), GIS tools together with land use models and remote sensed data for assessing the areal environmental conditions of the site and representative data models such as digital databanks together with certain geostatistical algorithms for areal interpolation of necessary parameters.

A verification of the findings can be made from ground based measurements (with a temporary or station network), by comparison with long-term observations (from a climate network, GCOS, etc.) and by simulation models. Fostering and improving the LAM and/or MOS analysis and forecast products can provide the user with wind climatologies on the basis of high resolution (in time and space) data sets.

7.1.2 Meteorological data

Basically, for siting and yield estimation the following data and information must be available (with regard to the exposure of measuring devices and representativeness of data, see above and paragraph 4.6), defined or derived:

Measurements/observations:

- Time series of wind speed and wind direction (hourly or 10-minute averages)
- Maximum winds or gustiness
- Lightning frequencies
- Ice accretion
- Meta data from station

Climatologies:

- Two-dimensional probability distribution based on the time series (wind rose)
- Absolute maximum of wind speed, gust and strength frequencies
- Wind speed on a monthly, seasonal and yearly basis and its variations
- Duration curves of expected percentage of wind speed above certain thresholds
- Average air density
- Two dimensional probability distribution of air humidity and air temperature (below 0° C)
- Number of hours with heavy rain
- Number of days with thunderstorms, lightning events and icing

Wind resource assessment usually refers to the calculation of average wind speed and its probability distribution in different directional sectors over several years (ideally 10 - 20 years). Accurate determination of the wind speed is of paramount importance. Additionally, special emphasis has to be put on strong and extreme wind events and their frequency as well as on lightning strike frequency and icing conditions because these can heavily influence power output or even the life span of WTGSs (cf. paragraph 3.4).

Before a specific site for the installation of a WTGS can be determined a region must be found by certain prospecting procedures where the wind speed is high. For this purpose one has to investigate the given wind regime of a region, as far as it is unaffected by surface friction and the topographic features. This can be done e.g. by rawinsonde measurements aloft using the geostrophic wind approach (cf. paragraph 3.2). It is accepted that this geostrophic wind is rather constant over distances of the order of 100 km. Another method for generalising point measurements is the *exposure correction method* (cf. paragraph 4.6.1) with which a *potential wind* is calculated (at a *blinding height*) well above local surface inhomogenities and which is then typical for a distance of up to 50 km. For the micro-siting one can either measure the wind vector at the site of interest (but this is expensive and time consuming); or try to extrapolate the local wind field from other measurements in the region; or deduce it from numerical simulation on a grid. For the two

last mentioned procedures a wide range of computer codes and models of different complexity and data requirements are in use (cf. chapters 4, 5 and 6). The spectrum stretches here from simple mass-consistent models that generate wind fields, consistent with kinematic constraints imposed by the available data and the domain of interest, to the most developed models which solve the non-hydrostatic set of the fundamental equations of motion in the atmospheric boundary layer including different parameterisation scales for turbulence.

7.1.3 Some aspects of predicting the wind resource on land and offshore

As in the forgoing chapter described, for wind farm development, it is essential to have a good estimate of wind speeds from the proposed site. On land, this can be achieved in a relatively straightforward manner by e.g. installing a mast and measuring wind speeds for a period of around a year. Then, by statistical comparison of the long record from a nearby anemometer station maintained of a meteorological measuring network, an evaluation of the long-term potential can be carried out (Woods et al. 1997).

Monitoring wind speeds offshore as part of the site evaluation is generally not feasible, simply because of the cost of mast installation and monitoring. however, in the far offshore (away from the effects of land), wind speeds vary much less in space than is the case onshore. This makes modelling wind speeds a more straightforward exercise. Possible approaches include using reanalysis data from the National Centres for Environmental Prediction (NCEP, Kalnay et al., 1996; see http://wesley.wwb.noaa.gov/reanalysis.html). These gridded data go back to 1948 at a daily (or better) resolution and are continually up-dated. The grid resolution is around 210 km. Horizontal winds are a model output, and could be used directly to estimate wind speed. However, it is generally considered that the models used to generate the NCEP reanalysis data simulate sea level pressure more accurately than horizontal wind speeds. Sea level pressure data can be used to calculate the geostrophic wind speed. Then, using a boundary layer model such as WA^{S}P (described in Section 6.3), hub-height wind speeds can be calculated from the geostrophic winds.

Close to land, the wind field over the sea becomes much more complex due to the thermal and dynamic effects of the land on the overlying air. At the same time, it is likely for some time to come that offshore wind farm construction will concentrate in the near-shore zone, because installation and maintenance costs will be lower than in the far offshore. Modelling winds in the near-shore zone is not straightforward. A number of empirical and theoretical formulae have been developed to model the development of internal boundary layers at the coastal discontinuity (cf. paragraph 4.5.4), and the increase in wind speed as air moves away from the land. These formulae, and methods for evaluating wind speeds in the near offshore, are reviewed by Barthelmie et al. (1996).

7.2 Estimation of energy yield

If reliable wind measurements are available at a particular site and the procedures accounting for different surface roughness in certain wind direction sectors at the measuring sites are applied, as described in paragraph 4.4, the energy yield of a WTGS in the time period dt results from the product of power and the time interval:

$$dE = P(t)dt \tag{7.2}$$

Integration over time T (e.g. 1 year) gives:

$$E_T = \int_0^T P(t)dt \tag{7.3}$$

After Eq.(7.3) and Eq.(2.4) one obtains

$$P(t) = \frac{1}{2} F \, c_{pr}(t) \rho(t) u^3(t) \tag{7.4}$$

with $c_{pr}(t)$ the actual over-all efficiency of the WTGS for the time t and F the area of the rotor cycle. If the turbine stands still or does not reach the intended performance because of icing, crosswinds or reduced air density, c_{rp} is not identical to the power-coefficient c_p from the power curve. For simplification the air density is usually regarded as a pure function of height and the other deviations from c_p during unaffected operation are considered by means of the technical availability. The available energy then can be written as

$$E_T = \rho_{rel} \cdot T_A \cdot \int_0^\infty f(u) P_N(u) du \tag{7.5}$$

with

$$P_N(u) = \frac{1}{2} \rho_0 F u^3 c_p \tag{7.6}$$

Here ρ_{rel} is the relative density and T_A the *technical availability*, which currently can be assumed as 0.95. To calculate the energy yield using Eq.(7.6) as well as the power curve $P_N(u)$, the likelihood-density-function $f(u)$ must be known. It can be estimated by adaptation to the measured frequency-distribution of the wind speed with two parametric Weibull-distribution, which belongs to the Gamma-distribution family. The mathematical form of this distribution is:

$$f(u) = \frac{k}{A}\left(\frac{u}{A}\right)^{k-1} \exp\left(-\left(\frac{u}{A}\right)^k\right) \tag{7.7}$$

The two Weibull parameters are usually named *scale parameter A* and *shape parameter k*. The dependence of $f(u)$ on different values of the shape parameter is illustrated in Figure 7.1. For $k > 1$ the maximum of $f(u)$ lies at values $u > 0$, while for $0 < k < 1$ it decreases monotonically. The Weibull-distribution can be reduced to two other theoretical distribution, namely with $k = 1$ the *exponential-distribution* and with $k = 2$ the *Rayleigh-distribution* which is sometimes used to describe wind data as for the multitude of German and Danish sites, and therefore it is often used by WTGS manufacturers for the estimation of the energy yield. However, for non-homogenous terrain the values of the form parameter lie between $1.3 < k < 1.8$, which results in a greater energy yield in comparison to the Rayleigh-distribution of the same average value.

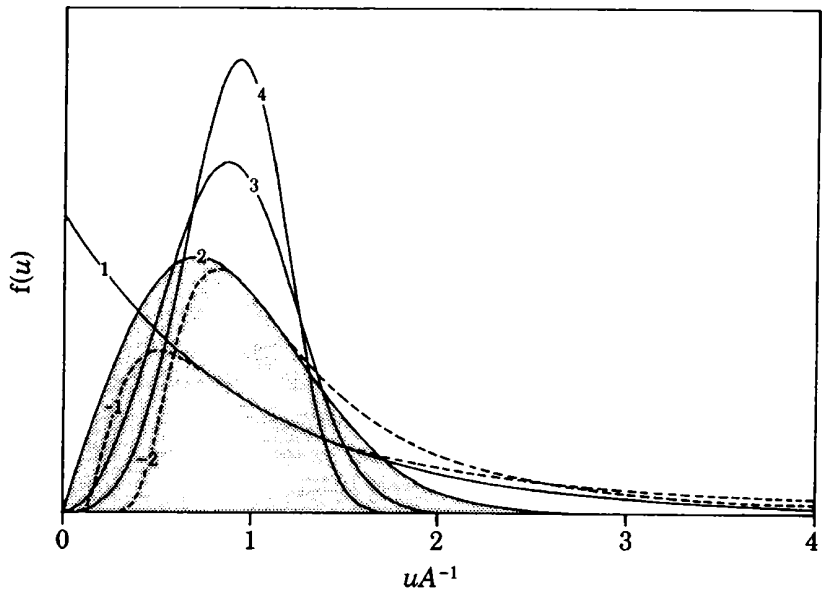

Figure 7.1: The Weibull-distribution for different values of the shape parameter and for the scaled wind speed uA^{-1} (Troen et al., 1989).

The cumulative likelihood density function for all speeds smaller than a threshold u_x is given by:

$$\int_0^{u_x} f(u)du = 1 - \exp\left(-(u_x / A)^k\right) \tag{7.8}$$

The frequency of the appearance of the speed-class $[u_1, u_2)$ becomes:

$$\int_{u_1}^{u_2} f(u)du = \exp\left(-(u_2 / A)^k\right) - \exp\left(-(u_1 / A)^k\right) \tag{7.9}$$

To adapt for a real distribution the mean value and the variance are necessary:

$$\mu = A\Gamma(1+1/k) \tag{7.10}$$

$$\sigma^2 = A^2\left[\Gamma(1+2/k) - \Gamma^2(1+1/k)\right] \tag{7.11}$$

If the histogram based on the measured data corresponds well in all speed classes to a Weibull-distribution any fitting method can be used. Because this is not always the case a method must be chosen which delivers the best fit in the operational range of the WTGS. Therefore, adopting the suggestions given in the European Wind Atlas (1989), the following assumptions are made: Firstly, the entire wind energy in the Weibull-distribution and in the observed distribution agree and secondly, the frequency of velocities above the cut-in speed are equal for both distributions. The average power is given by:

$$P = \frac{1}{2}\rho A^3 \Gamma(1+3/k) \tag{7.12}$$

If the wind climate of a site is known the velocity at which the WTGS reaches its highest efficiency as well as the distribution of the highest power density should preferably by in proximity. The highest efficiency should be reached at

$$u_{opt} = A\left(\frac{k+2}{k}\right)^{1/k} \tag{7.13}$$

In general u_{opt} lies between 1.4 and 2 times the value of the average wind speed. It should be mentioned here that often a wind distribution cannot be adequately represented by a Weibull distribution. In particular, when the wind climate has a large proportion of thermally generated winds. In such a case the best approximation may be the sum of 2 Weibull distributions, one representing the synoptic content and the other the thermal.

7.3 Verification and uncertainty

To verify the forecast of an energy yield at a certain site is an important but complicate task as the yield data are mostly available (if ever) for a relative short period in comparison with the measurement period from which the forecast was derived. Additionally, they are strongly dependent which basic station and measurements were used (if no site-specific measurements have been available) relative to the site where the WTGS was eventually erected. An example in the following table (from Gerdes et al., 2000) shows this clearly and the importance of areal interpolation procedures

Table 7.1. Energy yield forecast with respect to measurements at different locations for Northern Germany in comparison with the measurement at a 130 meter mast; (*) from Eelde, Bremen, Helgoland

Station	Bremen	Eelde	Helgoland	130-m mast	interpolated (*)	
Period	1970-1978	1970-1978	1971-1980	1993-1997		
Energy yield	797	1.067	1.051	947	881	MWh/a
Forecast/actual yield	87	116	114	103	96	%

As a further example an examination of the accuracy of the *WAsP* model is given here that is described thoroughly in Penner (2000). Several error sources were identified, especially for the evaluation of the site. Three of these error sources are meteorological and one from manufacture. Possible meteorological errors are the selection of the right basic station (because from this station the wind climatology is derived), an erroneous roughness length and the change of roughness elements in the upwind direction. This can lead to errors of up to 35 percent in the estimation of energy yield. How far this is dependent on the roughness length is shown in Figure 7.2. Errors in roughness length up to 25 percent result only in small errors of the energy yield, but with larger deviations from the actual roughness theses errors increase rapidly, that shows clearly the necessity for an objective evaluation of roughness. A variation in the horizontal distance of roughness changes of 5 percent creates a small deviation in energy yield (0.3 percent). A frequent error which is of concern to the manufacturer, is the specification of the power curve based on theoretical calculations instead of measurements which leads to an overestimation of the energy yield.

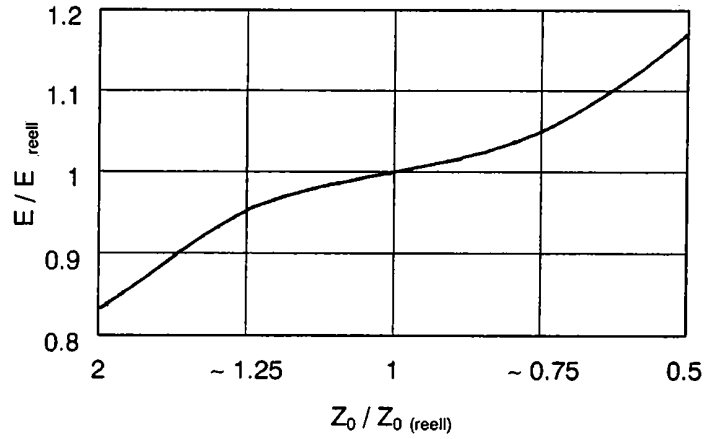

Figure 7.2: Relative energy yield deviation due to errors in roughness (Penner, 2000)

In as much as a model after Jackson&Hunt achieves better results than a mass-consistent variational analytical model with much less physical reliance depends strongly on the type of the terrain. The discussions on model results are extensive and readers who wish to gain more information about this should consult the appropriate literature such as e.g. Barnard (1991) or Lalas (1996).

A study about uncertainty in the course of energy yield forecast was made by Strack et al.2003. The uncertainty resulting from data from a meteorological network having not the quality to comply with the requirements for wind energy calculations amounts about 10% and more of the energy yield. High quality wind measurements with uncertainties of 1-2 % will cause an error of about 3-5 % in the energy yield. Another error is introduced by too short measuring periods which are not representative climatologically. Using the already mentioned MCP procedure carefully such errors can be reduced to approximately 4 % if suitable long-term reference data are available. Another factor is the surface roughness influencing wind speed and its height variation essentially. Experience is needed to assign the proper roughness length to the given surface properties. A quantification method is given e.g. in the WA^{S}P package (Troen et al.1989), other methods are described in Dobesch et al. (2001). Since part of the input is empirical it is often not possible to separate the uncertainty in the terrain roughness from the uncertainty in the wind field modelling. As well this is valid for the sensitivity of the energy yield from the orographic features around the site, especially when adjusting measurements for site-specific influences and transferring them to other sites. In more complex terrain some model can not applied any more without introducing significant errors in the results. Generally, because of the complexity of air flow over inhomogeneous terrain it is difficult to assess results from flow calculations always properly. Power curves for wind turbines contribute to the overall uncertainty and can amount to 6-8 %, depending on the wind conditions and power curve measured according to IEC (1998).

The overall uncertainties resulting from the possible errors described above may reach up to 30% in case only data from a meteorological station in some distance from the site are used, not taking into account properly the features of the physical environment of the site itself. This can be reduced to 10 - 12 % by means of high quality measurements at the site. It is a good opportunity for improving accuracy in energy yield forecasting if another wind farm already in operation is within the model domain. With the wind measurements and operational data of this turbines the accuracy in this case will be quite good even without on-site wind measurements (Strack et al. 2003).

In summary it may be said that by a careful analysis of the influencing factors to identify and minimize uncertainties for a specific site und turbine, giving such a base for effective project planning, risk management and the verification of the project.

7.4 Wind farms

The optimum layout of wind farms depends mainly on two facts (beside the general constraints that normally apply to construction and operations of WTGSs), namely the intended energy yield by the selected number and power output of turbines and the available land area. To optimise the requirements for the first fact the spacing of the turbines as far apart as possible in the prevailing wind direction would be ideal but on the other hand, land use and the cost of connecting wind turbines to the electrical grid require to space them closer together.

As already outlined in chapter 2.2, the wind leaving from the turbine in operation must have a lower energy content than the wind arriving in front of the turbine. Therefore each wind turbine will slow down the wind behind it and casts a wind shade in the downwind direction. This is called the *wake effect.*

Usually, as a rule of thumb, turbines in wind farms are spaced somewhere between 5 and 9 rotor diameters apart in the prevailing wind direction, and between 3 and 5 diameters apart in the direction perpendicular to the prevailing winds. Typically, the energy loss due to the wake effect is somewhere around 5 percent. To estimate this loss more precisely the following considerations have to be applied.

7.4.1 Energy Loss from the wake effect

With knowledge of the wind turbine rotor, the wind rose, the roughness in the different sectional directions and the Weibull distribution the energy loss can be calculate due to wind turbines shading one another. Following Mortensen et al.(1993) the reduced wind speed (the speed in the wake V; see Figure 7.3) can be calculated by

$$V = \left[1 - \left(1 - \sqrt{1 - C_t}\right)\left(\frac{D}{D + 2kX}\right)^2\right] \tag{7.14}$$

where U is the undisturbed wind speed, $(1\text{-}C_t)^{1/2} = U_r/U$, C_t the turbine thrust coefficient, D the rotor diameter, X the axial distance from the rotor to the point of calculation, and k is the wake decay constant.

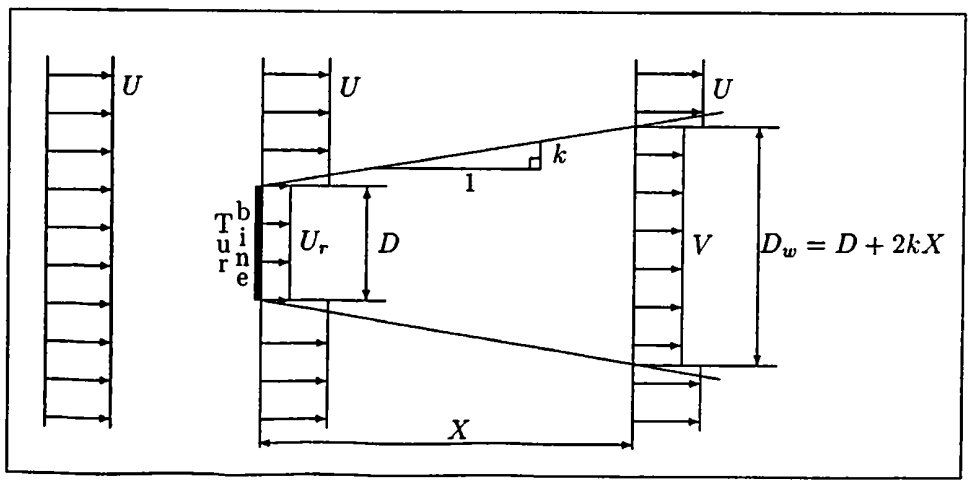

Figure 7.3: Flow field in the wake of a WTGS in the distance X (annotation see text); after Mortensen et al.(1993)

The decay constant is defined as

$$k = A'/\ln(h/z_0) \tag{7.15}$$

where A' is another constant ($A' \approx 0.5$). Normally a wake decay constant of 0.05 to 0.1 will give satisfactory results, but the smaller the estimated turbulent intensity, the smaller A' should be used. Again it should be noted that differences in surface roughness can make it necessary to use sector-specific decay constants. The thrust coefficient is defined as

$$C_t = 2\,F_T/\rho\pi r^2 U^2 \tag{7.16}$$

with F_T the thrust force, ρ the density of air, and r the rotor radius.

A simple wake model presented Ainslie (1988). He used for the turbulent intensity $I = 1/\ln(z/z_0)$ (cf. Eq.(3.29)). Then a look up table of maximum velocity deficit ratio was created for various values of C_t and I at distances downstream up to 100 diameters of the rotor, assuming that the wake has a Gaussian shape.

Frandsen et al.(1996) gave on the basis of the power-law relationship a velocity deficit

$$\delta u = 0.176\,C_t^{0.83}/(I^{0.63}x_d^{0.77}) \tag{7.17}$$

with x_d the distance downstream of the rotor plane in diameters. The added turbulence (taken as constant over full wake width) due to the wake of upstream turbines can be calculated after Hassan et al.(1991) with

$$\delta I = 1.31\,C_t^{0.71}\,I^{0.68}\,(x/x_n)^{-0.96} \tag{7.18}$$

where x is the distance downstream of the rotor plane and x_n is the near wake length. In Frandsen et al.(1996) a similar estimation of the added turbulence is given as

$$\delta I = [1.2\,C_t x_d^{-2}]^{0.5} \tag{7.19}$$

Several methods for the effect of multiple wakes on a turbine can be used. The resultant wake velocity deficits are in the case of

Square root of the sum of squares of δu	$(1-u_i/U)^2 = \Sigma(1-u_{ij}/u_j)^2$
Energy balance	$U^2 - u_i = \Sigma(u_j^2 - u_{ij}^2)$
Geometric superposition	$u_i/U = \pi u_{ij} / u_j$
Linear Superposition	$(1- u_i/U) = \Sigma(1- u_{ij}/u_j)$;

where U is the wind speed, u_i the velocity at the i-th turbine, u_{ij} the velocity at the i-th turbine due to the wake of the j-th turbine. The summations are over the j turbines upstream of the i-th turbine. Some specific tests to examine these wake combination methods have been performed by a series of wind tunnel experiments by Hassan et al.(1990) and Smith (1990).

The aerodynamic power reduction caused by the reciprocal shading if the WTGSs is usually expressed (Hau, 1996) in terms of the "*aerodynamic field efficiency (AFE)*". It is defined as the ratio of the power output of the whole wind farm to the sum of undisturbed power out put of all the single WTGSs comprising the wind farm. In a real wind farm there is always AFE < 1, its value dependent beside on the technical properties of the WTGSs themselves, on the field geometric of the wind farm (number of WTGSs and land area), the turbulence intensity and the probability distribution of wind direction. The turbulence intensity is important insofar that the loss of momentum in the wake of a WTGS is filled up after a certain distance by momentum transport from the flow in the surrounding and this is strongly dependent on the turbulence intensity. This means the higher the turbulence intensity is the more rapidly the momentum loss is filled up again. The turbulence intensity of the real atmosphere usually lies between 10 to 15 percent above land and around 5 percent above the sea. This effect is enhanced in a wind farm by the rotation of the rotors. This shows the necessity of having a good estimation about the turbulence conditions in the area. A wind farm has a somewhat different power characteristic too: after reaching the cut-in-speed the plants in the first row will start up, then followed by the next row and so on. From a certain flow velocity which lies above the rated velocity specified for a single WTGS within the wind farm, all WTGSs will operate with rated power. In this case the field efficiency of the farm is 100 percent. Because the aerodynamic rotor drag is equivalent to the momentum loss in the wake, it is a measure for the dimension of the wake area. Therefore rotors with high aerodynamic drag, as e.g. stall regulated ones, are disadvantageous compared with rotors with a high tip speed ratio.

The optimal geometry of the grid of a wind farm is dependent on the field geometry and the given grid connection. The electrical losses are a direct consequence of the grid design (voltage level, length and cross section of cables, numbers of transformers, etc.). For large wind farms the electrical loss until the grid should be not more than 5 percent and can be significantly lower if the output of the WTGSs is on a higher voltage level (e.g. 20 kV).

7.4.2 Experiences with wind farms (on- and offshore)

The power output of a single WTGS, even for the "big" ones with 2-3 MW, is low compared with a conventional power plant. The decentralized arrangement of WTGSs in densely populated areas reaches quickly its limits. Additionally, areas with technical usable wind energy potentials are in most countries limited to certain regions. On account of this there is a need to concentrate a larger number of WTGSs in these regions independently of their own energy demand. Beside this the spatial concentration of WTGS has many technical advantages for construction, operation and maintenance of such wind farms. Many experts believe therefore that under commercial conditions a minimum of 10 to 20 WTGSs are necessary. Due to the need of space of such wind farms agricultural areas can be used ideally in countries where only limited space is available as it is mostly the case in Europe. An alternative are off-shore wind farms.

But not only areas with a good wind potential are favourable for wind farms, (governmental) subsidies or offered tax credits or paying for the "green energy" on the scheme of "maximum avoided costs" were also necessary in the past (and today) to promote wind energy as it was the case in the U.S.A. (PURPA, cf. chapter 1.4). In Europe one of the first wind farm was constructed near Tandpipe in Jütland, Denmark. In Great Britain the begin of extensive use of wind energy was started by the "Non Fossil Obligation Program" (NFFO) between 1990 and 1994. Large wind farms can be found too in Spain (e.g. near Tarifa) and Portugal. But now in may part of the world wind farms are under operation and planned as in India and in China. Especially here great attempts were made in the last few years. So e.g. the Huitengxile wind farm in Inner Mongolia will be pushed from 5 MW in 1995 to 200 MW in 2005 and even to 600 MW in 2010.

With offshore wind farms experiences are quite short because there are until now only a few working operationally. One of the fist (actually the forth worldwide) was the Swedish Bockstigen farm (Lange et al., 1999), West off the coast of Gotland island, operating since March 1998. This farm resulted from a demonstration in the EU-THERMIE program framework and can stand as a model for many other offshore wind farms to be constructed. This wind farm consists of five 550 kW turbines which were especially adapted for the offshore conditions. The speed control system was optimized so it performs two main functions: Firstly, at low wind speeds (up to 20% of rated power output) the WTGS operates as frequency converter. The turbines generators run with variable speed to increase the power output. Secondly, At medium or high wind speeds the WTGSs are directly grid coupled where the power converter operates as a precision blind current source. The lessons learned from this farm are that wind, wave and sea current conditions at the site have to be carefully investigated as well as the given conditions for the anchoring of the sea cables and the monopile foundation. Additionally, measurements were performed at the Bockstigen turbines as well as at turbines of identical type of land for direct comparison of the power output between onshore and offshore WTGSs.

Beside all this technical aspects the perspectives of environmental protection have to be considered thoroughly and with high accuracy as it has been done e.g. during the planning for the Borkum-West offshore wind farm in Germany (Erdmann et al.2000). All possible sphere of influences on the living environment during the construction phase and the operation were investigated and measure were recommended where such influences were identified and a monitoring concept was developed to assess and document the environmental impact now and in future (see the following chapter 8).

8 ENVIRONMENTAL IMPACT OF WTGSS

Each energy system has, in varying degrees, associated with it positive and negative impacts on the environment. Traditional energy planning and cost/benefit analysis has ignored until now environmental externalities (the environmental damages on air and water quality, land use, global climate and biodiversity) but increasing efforts were made recently, leading to impact-pathway approaches, estimating e.g. the damage from a fossil fuel plat in terms of the value of the reduced life span and well-being of persons impacted by the plant's emissions. In 1995 a study "Externalities of Energy" (*ExternE*) sponsored by the European Commission in the UK, made a comprehensive effort to quantify monetary values of environmental externalities for a wide range of fuel cycles (coal, oil, gas, hydro, nuclear and wind) including the following environmental impacts: global warming, acidification, land use, occupation and public accidents, bird mortality, noise, visual amenity and radio interference. Though wind energy itself produces no gaseous emissions, during its construction and installation impacts are generated. This has been quantified by the above mentioned study for two wind farm sites in UK.

Table 8.1: Environmental externality values for wind-generated electricity and its external costs in 1/10 Euro-Cent/kWh (ExternE, 1995)

noise	global warming	acidification	occupational / public accidents		visual amenity
0.07 - 1.1	0.15	0.7	0.26	0.09	not quantified

With these numbers wind energy's environmental impact appear no higher than any other fuel and considerably lower than those of fossil fuels. In addition, the impacts from wind energy are local, relatively predictable and primarily aesthetic, compared to other energy generating systems. So the environmental benefits of the generation of electricity by wind turbines are clearly shown in having no pollutants at all during operation, such reducing the carbon dioxide content of the atmosphere and, additionally, reducing the dependency on conventional fossil and nuclear fuels. In the following some of the mentioned possible impacts such as sound emission, the visual impact and electromagnetic interference are investigated.

8.1 Sound emission from wind turbines

The aerodynamic noise produced by WTGSs can perhaps best be described as a 'swishing' sound (Boyle, 1996). It is affected by the shape of the blades (especially the trailing edge and the tip shape), the interaction of the air flow with the blades and the tower, and the turbulent wind conditions that can cause unsteady forces on the blades which then radiate noise. Noise nuisance is usually more of a problem in light winds because for higher winds the noise from the WTGSS is partially masked by the background noise.

The sound heard from a source in the landscape is strongly dependent on the distance, the height of the source and the topographic features of the landscape itself and also on the conditions in the atmosphere (wind speed and direction and stratification of the air mass). But for most contemporary turbines available, sound emission is only a minor problem due to new designs of quieter rotor blade tips. The sound intensity falls with the square of the distance from the sound source where, additionally, sound absorption or reflection may play a role at a particular site. So typically a minimum distance of about 7 rotor diameters or 300 meters is given to the nearest neighbours. There is always some background noise in the landscape, and at winds speeds around 4-5 m/s the noise from the leaves of trees, masts and fences etc. will gradually mask any potential sound from WTGSs. Generally, very little sound is heard upwind of wind turbines which makes it necessary to use the wind rose to chart the potential dispersion of sound in different directions. Further, the distinction between noise and sound is a highly psychological phenomenon. In fact, studies

indicate that people's perception of noise from wind turbines is governed more by their attitude to the source of the noise, rather than by the actual noise itself (from S. Krohn, 1998, Web site of the Danish Wind Turbine Manufacturers Assoc.)

Two main sources of noise emission from WTGSs exist, namely aerodynamic and mechanical sources:

In the *aerodynamic case* of sound emission, when the wind hits different objects at a certain speed, it will make a sound creating a random mixture of high frequencies or it may cause a surface to vibrate and these structures in turn emit their own sound. Most of the noise from the rotor blades will originate from the trailing (back) edge. Since the tip of the blade moves substantially faster than the blade root, great care is taken about the design of the rotor tip. Despite the fact that much improvement in this area has already been done, research for quieter rotor blades continues.

The *mechanical case* of sound emission which may originate in the gearbox, shafts and generator of a WTGS is not a big problem, due to the technological development in WTGSs construction. The same is the case for resonance of different components. Additionally, sound insulation is sometimes applied which can be useful to minimise some medium- and high-frequency noise effects but is hardly ever used.

To quantify the noise level at a certain location in the vicinity of a turbine e.g. the Danish Noise Directives (Danish Ministry of the Environment, 1991) can be used as follows:

$$L_p = L_{wa} - 10\,\mathbf{log}(2\pi r^2) - a\,r \tag{8.1}$$

where L_p is the sound pressure level in dB (decibel), L_{wa} the source emitting noise, r the distance between source and receiver and a an attenuation coefficient. If L_{wa} exists as a single, broadband sound power level then a = 0.005 dB/m. The Noise Directives also include a 5 dB penalty for the presence of tones in the noise emission. Therefore the noise load L_p is defined as

$L_r = L_p$ if there are no clearly audible tones, or

$L_r = L_p + 5$ if clearly audible tones are present.

If L_{wa} exists of octave band data, i.e. $L_{wa} = [L_{wa}(i)]$, where i = 1,2,..n, then

$$L_p = 10\,\mathbf{log}\left[\sum_{i=1}^{n} 10^{Lp(i)/10}\right] \tag{8.2}$$

with

$$L_p(i) = L_{wa}(i) - 10\,\mathbf{log}(2\pi r^2) - a(i)\,r.$$

The attenuation coefficient $a(i)$ is given in the next table.

Table 8.2: Attenuation coefficient due to bandwidth of emitted sound

Octave Band (Hz)	63	125	250	500	1000	2000	4000	8000
$a(i)$ dB/m	0.00	0.00	0.001	0.002	0.004	0.007	0.017	0.056

The sound emission of e.g. m turbines in a wind farm can be calculated with Eq.(8.2) by summing the L_p of the m single turbines.

Usually the sound power level ($L_{wa,ref}$) is provided for a reference wind speed of 8 m/s in 10 meters height (u_{10}). Therefore the sensitivity of L_{wa} to wind speed is needed. Using u_{10} as reference speed in the reference height the value of L_{wa} in Eq.(8.1) or Eq.(8.2) must be replaced with

$$L'_{wa} = m\,(u_{10} - 8) + L_{wa,ref} \tag{8.3}$$

where m is the slope of $d(L_{wa})/d(u_{10})$.

8.2 Shadow casting from wind turbines

The visual perception of a WTGS is determined by a variety of factors, including turbine size and design, number of blades, layout of the wind farm etc. One specific factor is the flickering effect. When the sun is visible WTGSs will cast a shadow on the neighbouring areas and the rotor blades chop the sunlight, causing a flickering (blinking) effect while the rotor is in motion. This may be quite annoying for people. Therefore the potential flicker effect has to be estimated and upon this the turbines placed where this effect is bearable for the neighbours. Shadow casting is generally not regulated explicitly by planning authorities. But in Germany there has been a court case in which it was decided to tolerate 30 hours of actual shadow flicker per year on a certain neighbouring area.

This shadow flicker effect can be predicted quite accurately using astronomy and trigonometry producing either a likely, or a "worst case" scenario, i.e. a situation where there is always sunshine, when the wind is blowing all the time, and when the wind and the turbine rotor keep tracking the sun by yawing the turbine exactly as the sun passes.

8.2.1 Basic considerations

The disturbing effect of the shadow cast by WTGSs for residents originates mainly from the shadow of the rotor blades, rotating with a speed less than 100 U/min. The narrow, slowly moving shadow of the tower corresponds to the shadow of high buildings and is normally not felt as disturbing. These effects definitely originate from three factors:

- the difference of the radiation-intensity between shadow-minimum and –maximum; this is defined by the technical parameters of the height and the rotor blade's cord length of the WTGS, by the astronomic parameter of sun elevation angle and the geometrical situation between observers, the WTGS and the sun;
- the temporal course of the intensity change, which is governed by the speed of rotation of the rotor and the geometrical situation of observers, the WTGS and the sun;
- the daily/yearly duration of the shadow casting resulting from the first factor under additional consideration of the climatological values for the location.

For the human eye the allowable difference between shadow-minimum and -maximum of a wind turbine is given here after DEWI (1998). A lower limit for the sun elevation angle is quoted as 3°: In the atmosphere an attenuation of the direct solar radiation occurs by scattering and absorption through the air particles (Dirmhirn, 1964). This attenuation increases exponentially with the penetrated air-mass as well as with decreasing sun elevation (see Table 8.3). So the attenuation of the intensity with an angle of 3° at 200 meters a.s.l. amounts to approximately 80 percent of the radiation with a sun elevation of 41.8°

(*standard value*). With increasing height the attenuation decreases and at a height of 1000 meters a.s.l. the attenuation (with 3° of elevation angle) is only 68 percent of the *standard value* (see Table 8.4). As a consequence of this, a diminution of the minimal sun elevation angle can be assumed with respect to the height a.s.l. of about 0.5° per 500 meters.

Table 8.3: Penetrated air-mass with respect to the sun elevation (at sea level)

Sun elevation	90	70	60	50	40	30	20	15	10	5	3 (°)
True air-mass	1.0	1.06	1.15	1.3	1.55	2.0	2.9	3.8	5.6	10.4	15.4

Table 8.4: Dependency of the penetrated air-mass on the height above sea level.

Height	0	900	1900	2900	4000	5400 (m)
True air-mass	1.0	0.9	0.8	0.7	0.6	0.5

The attenuation of the radiation intensity is additionally influenced by the water vapour and dust content of the atmosphere.

For typical construction heights the distance between the WTGS and the observer is more than 1000 meters for the quoted height angles. With these distance however no kernel-shadow occurs (100 percent masking of the sun disk by the rotor blades).

At a further low threshold, a masking of the sun disk by 20 percent is observed at the rotor blades. This value depends on the rotor blade cord length of a specific WTGS and leads to intensity differences between 0 and approximately 20 percent. No intensity difference exists, if the focus of the rotor circle and the sun disk are in a line. By the superimposition of the two, the intensity attenuating effects and the entire intensity difference amounts to less than 10 percent.

Regarding the temporal course of the intensity change, at present no investigations have taken place.

In all present standards, no differentiation is made where a kernel shadow or a diffuse shadow is found. It is essential that consideration be given however, for example, a residence that lies 200 to 250 meters to the north of an installation experiences 30 hours extreme kernel-shadows (high sun elevation) per year, or when positioned 700 to 750 meters south east of an installation when subject only to a diffuse shadow with less than 10 percent intensity change (low sun elevation, low masking). It is possible therefore that standard values be set up with regard to the sun elevation and the share of the masked sun disk. So it appears realistic to reduce the possible annual shadow duration hours to zero if more than 80 percent masking of the sun disk through the rotor blades occurs, and to increase this duration in five-hour steps to 30 hours per year with 20 percent masking. Additionally, the greatest allowable elevation angle of 15° could be accepted as a guideline with a masking of more than 40 percent. With this elevation angle, the attenuation reaches at 200 meters only 40 percent of the *standard value*. Summarising the effects of sun elevation and masking, the intensity difference for 80 percent masking and 15° amounts to approximately 50 percent of the value at 41.8° and 100 percent masking.

Table 8.5: Recommendation for a guideline of the maximum annual shading duration (in hours)

Masking	80%	70%	60%	50%	40%	30%	20%	10%
0° to 3° -	-	-	-	-	-	-	-	-
3° to 15°	0	5	10	15	20	25	30	-
> 15°	0	0	0	0	5	10	15	-

8.2.2 Geometrical data of WTGSs

The construction height determines the shadow casting and therefore this height has to be considered especially because of the considerable heights of future WTGSs that will rise between 85 and 100 meters.

The rotor blade depth determines the percent share of the masked sun disk within a pre-determined distance. The rotor blade is broadest at the root and narrowest at the blade tips, the average rotor blade depth reaches approximately 70 to 80 percent of the rotor blade depth at the root. The average rotor blade depth should be taken for the calculation of the masking, since travel across the sun disk is more likely with the outer part of the rotor blade due to the comparatively greater length. These data can be found in the published information of the rotor blade manufacturers.

If no exact data are available for the rotor blade, the average rotor blade depth can be appraised using the following formula:

Rotor blade depth (m) = 0.0306 times diameter (m) – 0.0377

The rotation speed effect decreases for technical reasons (the acoustic power level increases to the 5^{th} power of the blade tip speed) with greater diameter. For example WTGSs with three rotor blades and 30 meter diameter have a rotation speed of approximately 40 r/min and WTGSs with more than 60 meter diameter rotors have approximately 18 – 20 r/min. Two bladed installations with a rotor-diameter of 30 meter reach rotation speeds of approximately 70 r/min. The frequency of shadow casting is 2 Hz comparable to a three wing installation of the same size.

8.2.3 Distances for the shadow casting

The decisive distances on the basis of the construction height of the WTGS and the sun elevation angle on plain surfaces can be calculated from the geometry of the ray path. The increase of the distance takes place linearly in dependency on the construction height and for height angles of 2°, 2.5°, 3° and 15° as shown in the following table:

Table 8.6: Influence distance in meters (m) for different height angles and construction heights

Elevation	Height 50	60	70	80	90	100	110	120	m
2°	1432	1718	2005	2291	2577	2864	3150	3436	m
2.5°	1145	1374	1603	1832	2061	2290	2519	2748	
3°	954	1145	1336	1526	1717	1908	2099	2290	
15°	187	224	261	299	336	373	411	448	

The influence distance of any construction height can be calculated by means of the following formulas:

Sea level height ≥ 1000 m (height angle 2°):	E = 28.636 * B
Sea level height ≥ 500 m (height angle 2.5°):	E = 22.904 * B
Sea level height < 500 m (height angle 3°):	E = 19.081 * B
Minimal spacing (height angle 15°):	E = 3.732 * B

E = influence distance; B = construction height

The stated elevation angles of the sun and the respective distances can only be reached at 48.2° degrees of latitude in certain directional sectors however.

Clockwise from North (0°=360°) the relevant areas for shadow casting are:

0° - 24°	Shadow casting for less than 3.732 construction heights distance possible
24°–108°	Shadow casting with a height angle of 15° possible
50° - 124°	Shadow casting with a height angle of 2-3° possible
124° - 236°	No (relevant) shadow casting possible
236° - 310°	Shadow casting with a height angle of 2-3° possible
252° - 336°	Shadow casting with a height angle of 15° possible
336° - 360°	Shadow casting for less than 3.732 construction heights distance possible

8.2.4 Distances on the basis of the masking of the sun disk by the rotor blades

The distance *E(d)* from the WTGS, for which the rotor blades yield a masking *d* of the sun disk can be calculated from the distance earth-sun *ES* (= 149 504*10^3km), the shadow width *S(d)* and the rotor blade depth *T* as follows:

(8.4) $$E(d) = ES * T / S(d)$$

The shadow width in 10^3 km as well as the ratio *ES* and *S(d)* for different degrees of masking can be found in the following table:

Table 8.7: Shadow width (10^3km) and ratio ES/S(d) with respect to the degree of masking (%)

Masking	80	70	60	50	40	30	20
Shadow-width	956	814	685	562	445	331	220
ES/S(d)	156.4	183.7	218.3	266.0	336.0	451.7	679.6

8.3 Visual intrusion in the landscape

The visibility of turbines in the landscape may be of some problems where landscape protection and visual amenity are valued highly in the society. To quantify this more or less subjective impressions, different ways accounting for visibility exist. The points of visibility can be the nacelle, the blade tip or a point on the tower. In the case of a wind farm a simple way is to count the number of turbines and which of the mentioned points are visible from locations in the vicinity of the wind farm site. For example, the visibility count can be made by summing up (with possible weights) if the nacelle, the tip and/or the tower can be seen. Therefore if the whole turbine is visible the count for that turbine is e.g. 3. Simply, the maximum count for a whole wind farm using this method is 3 times the number of turbines (without

weighting). If only the topography is used in the calculations, ignoring visual sheltering effects from buildings, trees and other structures, the theoretical maximum visibility of turbines is given for a certain point in the vicinity. Additionally, exclusion zones can be specified where beside the topography features like forests obscure the turbine(s).

8.4 Electromagnetic interference

Sometimes a reflection of the electromagnetic radiation can occur if a WTGS is positioned between radio, television or microwave transmitter and receiver. This is due to the reflected wave interfering with the original signal causing a distortion which is dependent on the blade material and the surface shape of the tower. The most likely form of interference is on television viewing but this can be dealt with relatively easily by the installation of relay transmitters or by connecting through a cable television service (Boyle 1996). Microwave links, VHF Omnidirectional Ranging (VOR) and Instrument Landing Systems (ILS) are very susceptible to interference.

8.5 Résumé

As a summary of this chapter it can be said that technologies that use natural energy will have some local impacts such as visual intrusion or disruption of local ecosystems. This means that the local impacts associated with energy technology should be minimised and any remaining local impacts should be traded off against the global environmental benefits of the technology. Furthermore, extracting more energy from natural resources than the local ecosystem can cope with must be avoided. In this matter environmentalists, climatologists and hydrologists are requested to monitor these developments through an effective observation on large scales as well as on local scales and an adequate information system.

9 REFERENCES

Ainslie, J.F. (1988): Calculating the Flowfield in the Wake of Wind Turbines. J. of Wind Engineering and Industrial Aerodynamics, 27, 213-224.

Aspliden, C.I., D.L. Elliott, L.L. Wendell (1986): Resource Assessment Methods, Siting and Performance Evaluation. Physical Climatology for Solar and Wind Energy, 321-376.

AWEA, American Wind Energy Association (2005): Global Wind Energy Market Report

Barnard, J.C.(1991): An Evaluation of three models designed for siting wind turbines in areas of complex terrain. Solar Energy, 46, 283-294.

Barthelmie, R.J., T.D. Davies, J.P. Palutikof (1993): Estimation of sector roughness lengths and the effect on prediction of the vertical wind speed profile. Boundary Layer Meteor.,63, 19-47.

Barthelmie, R.J, J.P. Palutikof (1996): Coastal wind speed modelling for wind energy applications. Journal of Wind Engineering and Industrial Aerodynamics, 62, 213-236.

Beljaars, A.C.M.(1987): The Measurement of Gustiness at Routine Wind Stations - a Review. Instruments and Observing Methods Report No.31, WMO.

Bhumrakar, C.M., R.L. Mancuso, F.L. Ludwig (1980): A practical and economic method for estimating wind characteristics at potential wind energy conversion sites. Solar Energy 25, 955-965.

Blumen,W., ed.(1990): Atmospheric Processes over complex terrain.

Boeswirth, L.(1993): Technical Hydrodynamics (in German).

Boyl, G., ed.(1996): Renewable Energy . Power for a Sustainable Future. Oxford Univ.Press.

Bradley, E.F., P.J. Mason, P.A. Taylor (1986): Boundary-Layer flow over low hills. Boundary Layer Meteorol.,39, 107-132.

Britter, R.E., J.C.R. Hunt, K.J. Richards (1981): Air flow over a two-dimensional hill: Studies of velocity speed-up, roughness effects and turbulence. Quart.J.R.Met.Soc. 107, 91-110.

BTM Consult Aps. (2005): World Market Update 2005.

Businger, J., J. Wyngaard, Y.Izumi, F. Bradley (1971): Flux profile relationships in the atmospheric surface layer. J.Atmos.Sci.,28,181-189.

DeRenzo, D.J.(1979): Wind Power. Recent developments. In Energy Technological Review No.46, Noyes Data Corporation, Park Ridge.

DEWI (1998): Schattenwurf von Windenergieanlagen: Die Geräuschabstrahlung von MW-Anlagen in den Schatten gestellt?. DEWI-Magazin Nr.13.

Dirmhirn, I.(1964): The radiation field in the environment. Akad. Publishing House Company, Frankfurt/Main.

Dobesch, H., G. Kury (1996): Methods and Foundations of Optimal Siting for the exploitation of Wind Energy. Wetter und Leben, 48, 1-2, pp.33-48 (in German).

Dobesch, H., G. Kury eds. (1997): Wind Atlas of the Central European Countries of Austria, Croatia, Czech Rep., Hungary, Slovak Rep. and Slovenia; Austrian Contribution to Meteorology and Geophysics, Vol.16, Publ.No. 378.

Dobesch, H., H.V. Tran (1999): The Diagnostic Wind Field Model ZAWIMOD2. Austrian Contribution to Meteorology and Geophysics, Vol.22, Publ.No.389.

Dwenger, N.(1995): Spezielle Auslegungskriterien für Windturbinen im Binnenland. Proceedings: Wind Energy Applications in Non-Flat and Complex Terrain.

Dyer, A.J.(1974): A review of flux-profile relations. Boundary Layer Meteor.,7, 363-372.

Eichenberger, W.(1990): Aviation weather science (in German).

Elliott, D.(1997): Energy, Society and Environment. Technology for a sustainable future; in Routledge Introductions to Environment Series, London.

Endlich, R.N., J.D.Lee (1983): An improved diagnostic model for estimation wind energy. Rep. PNL4526, Pacific Northwest Lab., Richland, Washington.

Energiewerkstatt, editor (1993): Proceedings of the 2nd Austrian Wind Energy Symposium, St.Poelten.

Energiewerkstatt, editor (1995): Proceedings of the 3rd Austrian Wind Energy Symposium, St.Poelten.

Erdmann, N., F. Nanninga (2000): Erfahrungen bei der Planung und Projektierung eines offshore Windparks in der Nordsee. Proc. DEWEK 2000, 191-194.

Foken, T.(1984): Turbulenter Energieaustausch zwischen Atmosphäre und Unterlage. Bericht des Deutschen Wetterdienstes 180.

Frandsen, S., Chacon, L., Crespo, A., Enevoldsen, P., Gomez-Elvira, R., Hernandez, J., Holstrup, J., Manuel, F., Thomsen, K. and Sorensen, P.(1996): Measurements on and Modelling of Offshore Wind Farms. Riso-R-903 report.

Franquesa, M.(1989): Small Wind Weels (in German).

Garratt, J,R.(1992):The atmospheric boundary layer. Cambridge Atmospheric and Science Series.

Gasch, R., ed.(1991): Wind Power Plants (in German).

Gerdes, G., T.Pahlke, M.Strack (2000): Verification of energy yield forecast. In: Proc. DEWEK2000, 5th German Wind Energy Conference, Wilhelmshaven.

Goody, R.M. and Y.L. Yung (1989): Atmospheric Radiation. Theoretical Basis. Oxford Univ. Press.

Greenpeace International, GWEC (Global Wind Energy Council), 2005: Windforce 12, a blueprint to achieve 12 percent of the world's electricity from wind power by 2020, sixth version.

Grubb, M, N.I. Meyer (1993): Renewable Energy Sources for Fuels and Electricity, Chapt.4, Wind Energy: Resources, Systems and Regional Strategies; Island Press, Washington D.C.

Guo, X., J.P. Palutikof (1990): A Study of 2 Mass-Consistent Models: Problems and Possible Solutions. Boundary Layer Meteorol., 53, 303-322.

Hassan, G.(1995): Study of Offshore Wind Energy in the EC, Germanischer Lloyd and Windtest KWK.

Hassan, G. and Partners (1991): The Effect of Rotor Characteristics on the Loading Spectrum and Fatigue Life of a Wind Turbine within a Wind Farm. GH Report 197/R/2.

Hau, E.(1996): Wind Power Plants (in German).

Häckel, H.(1990): Meteorology. UTB 1338, Ulmer, Stuttgart (in German).

Hoff, A.M.(1987): Ein analytisches Verfahren zur Bestimmung der mittleren horizontalen Windgeschwindigkeiten über zweidimensionalen Hügeln. Rep. of the Inst of Meteorology and Climatology, University Hannover, Vol. 28.

Holton, J.(1992): An Introduction to Dynamic Meteorology, 3.Ed., Academic Press.

Holtslag, A.(1984): Estimates of diabatic wind speed profiles from near-surface weather observations. Boundary Layer Meteorol. 29, 225-250.

Hunt, J.C.R., P.S. Jackson (1975): Turbulent wind flow over a low hill. Quart.J.R.Met.Soc. 101, 929-955.

IEC (1998): IEC61400-10, 1998: Wind turbine generator systems - Part 12: Wind turbine power performance testing, 1. Ed.

Kalnay E.,M. Kanamitsu, R. Kistler, W. Collins, D. Deaven, L. Gandin, M. Iredell, S. Saha, G. White, J. Woollen, Y. Zhu, M. Chelliah, W. Ebisuzaki, W. Higgins, J. Janowiak, K.C. Mo, C. Ropelewski, J. Wang, A. Leetmaa, R. Reynolds, R. Jenne, D. Joseph (1996): The NCEP/NCAR 40-year reanalysis project. Bull. Amer. Meteor. Soc. 77, 437-471.

Kitada, T., k. Igarasci, M. Owada (1986): Numerical Analysis of Air Pollution in Combined Field of Land/Sea Breeze and Mountain/Valley Wind. J. of Climate and Appl. Meteorolog., 25, 767-784.

Kondo, J., H. Yamazawa (1986): Aerodynamic Roughness over an inhomogeneous ground surface. Boundary Layer Meteorol., 35, 331-348.

Lalas, P.D., C.F. Ratto, editors (1996): Modelling of atmospheric flow fields. World Scientific Publ.Comp., Singapure.

Lange, B. E. Aagaard, P.E. Andersen, A. Møller, S. Niklasson, A. Wickman (1999): Offshore wind farm Bockstigen – installation and operation experience. Proc.Europ.Wind Energy Conf.,1999, 300-303.

Langmuir, I.(1944): Supercooled water droplets in rising currents of cold saturated air. In: Collected work of I.Langmuir. Pergamon Press 1961; 135-393.

Langmuir, I., K.B. Blodgett (1945): A mathematical investigation of water droplet trajectories. In: Collected work of I.Langmuir. Pergamon Press 1961; 451-465.

Lettau, H.(1969): Note on Aerodynamic Roughness-Parameter Estimation on the Basis of Roughness-Element Description. J. Appl. Met. 8, 828-832.

List, R.(1977): Ice accretion on structures. J.of Glaciology, Vol.19, 451-465.

Lozwski, E.P., R.D. Amours (1980): A time-dependent numerical model for spherically symmetric hailstones growth thermodynamics under constant ambient conditions. Am.Met.Soc.Vol.37, 1808-1820.

Lumley, J.L., H.A. Panofsky (1964): The structure of atmospheric turbulence. Interscience, London.

Mahrt, L.(1986): On the shallow motion approximations. J.Atmos.Sci., 43, 1036-1044.

Markkonen L.(1981): Estimating intensity of atmospheric ice accretion on stationary structures. Am.Met.Soc., Vol.20, 595-600.

Markkonen L.(1983): Modelling of ice accretion on wires. Am.Met.Soc., Vol.23, 929-938.

Mason, P.J., R.I. Sykes (1979): Flow over an isolated hill of moderate slope. Quart.J.Roy.Merteor.Soc.105, 383-395.

Mason, P.J., J.K. King (1985): Measurements and predictions of flow and turbulence over an isolated hill of moderate slope. Quart.J.Roy.Merteor.Soc.111, 617-640.

Mengelkamp, H.-T.(1991): Boundary layer structure over an inhomogeneous surface: simulation with a non-hydrostatic mesoscale model. Boundary Layer Meteorol. 57, 323-341.

Molly, J.P.(1990): Wind Energy (in German).

Mortensen, N.G., L. Landsberg, I. Troen, E.L. Petersen (1993): Wind Atlas Analysis and Application Program (*WAsP*). Risø National Labs., Roskilde, Denmark.

Oke, T.R.(1987): Boundary Layer Climates. Halsted Press, NY.

Pennel, W.T.(1983): An evaluation of the role of numerical wind field models in wind turbine siting. Techn.Rep. Pacific Northwest Lab., Richland, Washington.

Penner, K.(1995): *WAsP*-Verification. DEWI-Magazin Nr.7 (in German).

Perera, M.D.(1981): Shelter behind two-dimensional solid and porous fences. J. of Wind Engineering and Industrial Aerodyn. 8, 93-104.

Petersen, E.L.(1990): Wind Resources in Complex Terrain, Measurement and Models. EC Wind Energy Conference.

Petersen, E.L., N.G. Mortensen, L. Landsberg, J. Højstrup, H.P. Frank (1998): Wind Power Meteorology. Part 1. Climate and Turbulence. Wind Energy 1 (pilot issue), 25-45.

Phillips, G.T. (1979): A preliminary user's guide for the NOABL Objective Analysis Code. DOE Contract No.AC06-77ETE20230, Science Appl. Inc. La Jolla, Calif.

Physick, W.L. (1988): Review: Mesoscale modelling in complex terrain. Earth-Science Reviews 25, 199-235

Press, Teukolsky, Vetterling, Flanney (1992): Numerical recipes in Fortran, 2nd edition, 660-664, Cambridge University Press.

Quarton, D.C., G. Hassan and partners (1998): The Evolution of Wind turbine Design Analysis – A Twenty year Progress Review. Wind Energy 1(pilot issue), 5-26.

Ratto, C.F., R. Festa, O. Nicora, R. Mosiollo, A. Ricci, P.D. Lalas, O.A. Frumento (1990): Wind field numerical simulation- a new user friendly code. In: W.Palz, (editor), Europ.Comm. Wind Energy Conference, H.S.Sthephens& Assoc., Madrid.

Raupach, M.R.(1992): Drag and drag partition on rough surfaces. Boundary Layer Meteorol., 60, 375-395.

Schlichting, H.; E. Truckenbrodt (1967): Aerodynamics of Aeroplanes (in German).

Sherman, C.A.(1978): A Mass-Consistent Model for Wind Fields over Complex Terrain. J.Appl.Meteorol.,17, 312-319.

Sörensen B.(2000): Renwable Energy. Its physics, engineering, use, environmental impact, economy and planning aspects. Academic Press.

Steinhauser, F.(1950): Wind amplification on mountain ridges. Report of Deutscher Wetterdienste in the US-Zone, No.12 (in German).

Strack, M., A.. Albers (1996): Analyse und Extrapolation des Windprofils am 130 Meteor Messmast des DEWI. DEWI Magazin Nr.8/2.

Stull, R.B.(1988): An Introduction to Boundary Layer Meteorology. Kluwer, Dordrecht.

Svabik, O.(1998): Documentation of Severe Weather : Thunderstorm and Hail Frequency in Europe. Advanced Weather Radar Systems, COST 75, European Commission, EUR 18567 EN.

Tammelin, B., K. Sänti, E. Peltola, R. Anderssen, eds (1996): BOREAS 3, Wind Energy Productions in Cold Climates. Proceedings, Finnish Met. Inst.

Tammelin, B., Sänti K., eds (1998): BOREAS 4, Wind Energy Productions in Cold Climates. Proceedings, Finnish Met. Inst.

Taylor, P.A., P.J. Mason, E.F. Bradley (1987): Boundary-layer flow over hills. Boundary Layer Meteorol. 36, 107-132.

Thomas, R.L.(1976): Large Experimental Wind Turbines - Where are we now. NASA Techn. Memorandum TMX-71890.

Tonbru, M., D.P.Lalas (1990):A telecoping procedure for local wind energy. In W. Palz, (editor), Europ. Comm. Wind Energy Conference, H.S. Sthephens & Assoc., Madrid.

Traci, R.M., G.T. Phillips, G.C. Patnaik, P.E. Freeman (1977): Development of a wind energy methodology. U.S. Dept. of Energy Rep. RLO/2440-11, 205 pp.

Troen, I., A. DeBaas (1986): A spectral diagnostic model for wind flow simulation in complex terrain. Proc. European Wind Energy Assoc. Rome, Italy.

Troen, I., L. Petersen (1989): European Wind Atlas. Riso Nat.Labs, Roskilde, Denmark.

Van der Hoven, I.(1956): Power spectrum of horizontal wind speed in the frequency range from 0.0007 to 900 cycles per hour. J.of Meteorol.,Vol.14, 160-164.

Walmsley, J.L., Salmon J. R. and Taylor P.A. (1982): On the Application of a Model of Boundary-Layer Flow over Low Hills to Real Terrain. Boundary-Layer Meteorology, 23, 17-46.

Walmsley, J.L., P.A. Taylor, T.Keith (1986): A simple model of neutrally stratified boundary layer flow over complex terrain with surface roughness modulations (MS3DJH/3R). Boundary LayerMeterol.,36, 157-186.

Walmsley, J.L., P.A. Taylor, J.R.Salmon (1989): Simple guidelines for estimating wind speed variations due to small scale topographic feature - an update. Climatol.Bull., 23 (1), 3-14.

Walmsley, J.L., P.A. Taylor (1996): Boundary-Layer flow over topography: Impacts of the Askervein study. Boundary Layer Meteorol. 78, 291-320.

Walmsley, J.L, I.Troen, D.P. Lalas, P.J. Mason (1990): Surface layer flow in complex terrain: Comparison of models and full-scale observations. Boundary Layer Meteorol., 52, 259-281.

Wieringa, J.(1973): Gust factors over open water and built-up country. Boundary Layer Meteorol. 3, 424-441.

Wieringa, J.(1976): An objective exposure correction method for average wind speeds measured at sheltered location. Quart.J.R.Met.Soc., 102, 241-253.

Wieringa, J.(1983): Description requirements for assessment of non-ideal wind stations - for example Aachen. J. Wind Engineering and Industrial Aerodynamics, 11, 121-131.

Wieringa, J.(1986): Roughness-Dependent Geographical Interpolation of Surface Wind Speed Averages. Quart.J.R.Met.Soc., 112, 867-889.

Wieringa, J.(1992): Updating the Davenport roughness classification. J.Wind Eng.Aerod.41, 357-368

Wieringa, J.(1993): Representative roughness parameters for homogenous terrain. Boundary Layer Meteorol., 63, 323-363.

Wieringa, J.(1994): Does representative wind information exist? East European Conference on Wind Engineering, Warzawa.

WMO, R.F.Jones (1962): Ice formation on Aircraft. Techn.Note No.39.

WMO, VanEimern, J., R. Karschon, L.A. Razumova, G.W. Robertson (1964): Windbreaks and Shelterbelts, Techn. Note No.59. WMO-No.147.TP.70, Geneva.

WMO (1981): Meteorological Aspects of the Utilization of Wind as an Energy Source; Techn. Note No.175, WMO-No.575, Geneva.

WMO, McKay, G.A.(1990): Information on Meteorological Extremes for the Design and Operation of Energy Systems. WCAP-13, WMO/TD-NO.385, Geneva.

WMO, Daniels, A., T. Schroeder: (1997): Meteorological Aspects and Recommendations for Assessing and Using the Wind as an Energy Source in the Tropics, WCASP-43, WMO/TD-No.826, Geneva.

Woods, J.C., S.J. Watson (1997): A new matrix method of predicting long-term wind roses with MCP. Journal of Wind Engineering and Industrial Aerodynamics, 66, 85-94.

Further reading (not cited in the text)

Wind Energy Basics

Manwell J.F., D.E.Cromack; (1985): Understanding Wind Energy (Understanding Technology).

Graham I. (1999): Wind Power (Energy Forever);; Library Binding.

Heier; S. (1998): Grid Integration of Wind Energy Conversion Systems.

Bailey D. (1991): Energy from Wind and Water (Facts About); Library Binding.

Gipe; P. (1993): Wind Power for Home & Business: Renewable Energy for the 1990s and Beyond.

Stoiaken L., D. Marier; (1984): Alternative Sources of Energy-Wind Power, No.66.

Kaplan H., editor (1984): (Boundary Layer Structure: Modelling and Application to Air Pollution and Wind Energy.

Aguilar J., C. Garcia-Legaz; (1986): El Viento: Fuente de Energia/The Wind: A Source of Energy.

Electricity Supply: Efforts to Develop Solar & Wind Energy; 1993.

Strojan C. (1985): Environmental and Aesthetic Assessment of Small Wind Energy Systems.

Foreign Applications and Export Potential for Wind Energy Systems; S. K. Griffith; 1985.

Non-Nuclear Energy-Joule II European Wind Turbine Standards Project; European Communities; 1996.

R. Guzzi R., C. G. Justus, editors (1988): Physical Climatology for Solar and Wind Energy.

The Potential for Wind Energy in Developing Countries: An Economic & Market Analysis for the Sale and Installation of Wind Energy Systems; Strategies Unlimited; 1988.

Selzer H. (1086): Potential of Wind Energy in the European Community.

Katzman M.T.(1984): Solar and Wind Energy: An Economic Evaluation of Current and Future Technologies.

Mitchell R. (1985): Technical and Economic Assessment on Tethered Wind Energy Systems.

Wind and Water Energy; 1990.

Wind and Water Energy; 1990.

Vas I., editor (1985): Wind Energy.

Swift-Hook D.T., editor (1989): Wind Energy and the Environment (Iee Energy Series V. 4).

Gipe P. (1995): Wind Energy Comes of Age (Wiley Series in Sustainable Design).

Wind Energy Utilization: A Bibliography With Abstracts; Technology Application Centre.

Griffith S.K..(1984): Wind Energy Systems: Export Market Potential.

Wind Energy Technology

Schmid J., W. Palz; (1986): European Wind Energy Technology: State of the Art of Wind Energy Converters in the European Community (Solar Energy R&D in the European Commnunity); Wind Energy Technology.

Walker F.J., N. Jenkins; (1997): (UNESCO Energy Engineering Series.

The Spec Guide 1985: Energy Products Specifications Conservation, Solar, Wind and Photovoltaics.

Wind Energy Technical Information Guide; 1987.

Wind Energy Technology and Implementation; Hulle; 1992.

Seiler F.S., editor (1984): Wind Energy Systems: North America Vol 1.

Seiler F.S., editor (1984): Wind Energy Systems: Europe, Asia, Africa, Latin America and Australia Vol 2.

Seiler F.S., editor (1984): Wind Energy Systems: Megawatt Wind Turbines Vol 4.

Wind Energy in Rural America; Rural Electric Wind Energy Workshop; 1983.

Wind farms

Anderson, M.B.,D.J. Milborrow, J.N. Ross (1982): Performance and Wake Measurements on a 3m Diameter Horizontal Axis Wind Turbine Rotor. Proc. 4th Intl. Symposium on Wind Energy Systems, Stockholm.

Beyer, H.G., T. Pahlke, W. Schmidt, H.-P. Waldl, U.de Witt (1989): Operational Behaviour of a Small Straight Line Wind Farm. EWTGS 89 Conference, Glasgow, 311-315.

Burch, S.F, F. Ravenscroft (1992): Computer Modelling of the UK Wind Resource. ETSU WN 7056, 1992.

ESDU 82026, Strong Winds in the Atmospheric Boundary Layer, Part 1 Mean Hourly Wind Speeds. Engineering Sciences Data Unit Ltd., 251 Regent St. London.

Harris, A. (1995): Wind Farm Test Data and the Assessment of Topographic and Wake Models of Wind Farm Output. ETSU Report W/32/00228/45/REP.

Hassan, U., A.G. Glendinning, C.A. Morgan (1990): A Wind Tunnel Investigation of the Wake Structure and Machine Loads within Small Wind Turbine Farms. 12th BWEA Conference, Norwich, 47-52.

Hojstrup, J., I. Katic, P. Norgard (1988): Supervising and Measuring at Taendpibe Windfarm. Proc. Euroforum New Energies Conference, Saarbruecken.

Larsen., A., P. Velk (1989): Wind Turbine Wake Interference - A Validation Study. EWTGS 89 Conference, Glasgow, 311-315.

Larsen, G.C. (1997): Cookery Book for Wind Farm Load Calculations. RISO.

Smith. D (1990): Multiple Wake Measurements and Analysis. 12th BWEA Conference, Norwich, 53-58.

Smith. D.,G.J. Taylor(1991): Further Analysis of Turbine Wake Development and Interaction Data. 13th BWEA Conference, Swansea.

ANNEX

List of Figures

List of Tables

Symbols

c_a	lift-coefficient
c_p	power-coefficient
c_w	drag-coefficient
C_s	drag coefficient of the (unobstructed) ground
C_R	drag coefficient of an isolated surface-mounted roughness element,
d	displacement height
F	rotor circle area
Fr	Froude-number
f_c	Coriolis parameter
g	gravity acceleration
G	gustfactor, gustiness
H	characteristic height of obstacle
H_o	height of the homogenous atmosphere
I	turbulence intensity
$\vec{k}$	unit vector in the vertical
k	wave number
K_m	eddy viscosity (eddy diffusivity, turbulent-transfer coefficient)
l	mixing-length
L^*	Monin-Obuchov length
L_H	term that accounts for latent heat release during phase transitions.
m	mass
N_f	Brunt-Väisälä frequency
p'	exponent in the power law
p	pressure
Q_H	turbulent heat flux
r_{sat}	water-vapour saturation mixing ratio
r_L	liquid-water mixing ratio
R	gas constant
RB	term associated with radiation divergence
t	time
T	absolute temperature (K)
u_*	friction velocity.
V	wind speed, v(u,v,w)
x,y,z	coordinates
z_0	roughness length
α	angle of attack
δi	height of the internal boundary layer
ε	lift-drag ratio (c_a/ c_w)
$\Phi(z/L^*)$	non-dimensional function
κ	von Karman constant
κ'	isentropic exponent (for air $\kappa' = 1{,}4$)
λ	tip-speed-ratio (u/v_w)
λ_a	atmospheric wavelength
ρ	air density
ν	kinematic viscosity.
ν_θ	thermal diffusivity,
θ	potential temperature
τ	shear stress
ω	angular velocity of earth = 7.3×10^{-5} rad/s.

Österreichische Beiträge zu Meteorologie und Geophysik

bisher erschienen:

Heft	Publ.Nr.	Fachgebiet	Autor	Titel und Umfang	Preis in Euro
1	329	Meteorologie		*Tagungsbericht EURASAP, Wien, 14.-16. Nov. 1988, Evaluation of Atmospheric Dispersion Models Applied to the Release from Chernobyl.* Wien 1989, 20 Beiträge, 198 S., 100 Abb., 17 Tab.	14,53
2	332	Geophysik		*Tagungsbericht über das 5. Internationale Alpengravimetrie Kolloquium - Graz 1989.* Herausgeber: H. LICHTENEGGER, P. STEINHAUSER und H. SÜNKEL, Wien 1989, 256 S., 100 Abb., 17 Tab.	vergriffen
3	336	Geophysik		*Schwerpunktprojekt S47-GEO: Präalpidische Kruste in Österreich, Erster Bericht.* Herausgeber: V. HÖCK und P. STEINHAUSER, Wien 1990, 15 Beiträge, 257 S., 104 Abb., 17 Tab., 23 Fotos	20,35
4	338	Meteorologie	LANZINGER, A. et al:	*Alpex-Atlas.* FWF-Projekt P6302 GEO, Wien 1991, 234 S., 23 Abb., 2 Tab., 200 Karten	18,17
5	341	Meteorologie	BÖHM, R.:	*Lufttemperaturschwankungen in Österreich seit 1775.* Wien 1992, 95 S., 34 Abb., 24 Tab.	vergriffen
6	343	Geophysik	MEURERS, B.:	*Untersuchungen zur Bestimmung und Analyse des Schwerefeldes im Hochgebirge am Beispiel der Ostalpen.* Wien 1992, 146 S., 72 Abb., 9 Tab.	11,63
7	351	Meteorologie	AUER, I.:	*Niederschlagsschwankungen in Österreich seit Beginn der instrumentellen Beobachtungen durch die Zentralanstalt für Meteorologie und Geodynamik.* Wien 1993, 73 S., 18 Abb., 5 Tab., 6 Farbkarten	23,98
8	353	Meteorologie	STOHL, A., H. KROMP-KOLB:	*Analyse der Ozonsituation im Großraum Wien.* Wien 1994, 135 Seiten, 73 Abb., 8 Tabellen	23,98
9	356	Geophysik		*Tagungsbericht über das 6. Internationale Alpengravimetrie-Kolloquium, Leoben 1993.* Herausgeber: P. STEINHAUSER und G. WALACH, Wien 1993, 251 Seiten, 146 Abb.	23,98
10	357	Meteorologie	ZWATZ-MEISE, V.:	*Contributions to Satellite and Radar Meteorology in Central Europe.* Wien 1994, 169 Seiten, 25 Farbabb., 42 SW-Abb., 13 Tab.	23,98
11	359	Geophysik	LENHARDT W. A.:	*Induzierte Seismizität unter besonderer Berücksichtigung des tiefen Bergbaus.* Wien 1995, 91 S., 53 Abb.	23,98
12	361	Meteorologie	AUER, I., R. BÖHM, N. HAMMER †, W. SCHÖNER., WIESINGER W., WINIWARTER W.:	*Glaziologische Untersuchungen im Sonnblickgebiet: Forschungs-programm Wurtenkees.* Wien 1995, 143 S., 59 SW-Abb., 13 Farbabb., 9 SW-Fotos, 47 Tab.	23,98
13	372	Meteorologie	PIRINGER, M.:	*Results of the Sodar Intercomparison Experiment at Dürnrohr, Austria.* Wien 1996	23,98
14	373	Geophysik	MEURERS, B.:	*Proceedings of the 7th International Meeting on Alpine Gravimetry, Vienna 1996.* Wien 1996	23,98
15	374	Meteorologie	RUBEL, F.:	*PIDCAP - Quick Look Precipitation Atlas.* Wien 1996	23,98

Heft	Publ.Nr.	Fachgebiet	Autor	Titel und Umfang	Preis in Euro
16	378	Meteorologie	DOBESCH, H., KURY G.:	*Wind Atlas for the Central European Countries Austria, Croatia, Czech Republic, Hungary, Slovak Republic and Slovenia,* Wien 1997	23,98
17	382	Meteorologie		*Proceedings of the 9th International Symposium on Acoustic Remote Sensing and Associated Techniques of the Atmosphere and Oceans, Vienna 1998*, 329 Seiten, Wien 1998	23,98
18	383	Meteorologie	RUBEL, F.:	*PIDCAP - Ground Truth Precipitation Atlas.* 84 Seiten, 99 Farbkarten, Wien 1998	36,34
19	384	Meteorologie		*Proceedings of the 2nd European Conference on Applied Climatologie, 19 to 23 Oct. 1998, Vienna.* CD-ROM, Wien 1998	23,98
20	387	Meteorologie		*Proceedings of the 2nd International Conference on Experiences with Automatic Weather Stations, 27 to 29 Sept. 1999, Vienna.* CD-ROM, Wien 1999	23,98
21	388	Meteorologie		*Bericht über den Workshop Umweltforschung im Hochgebirge - Ergebnisse von GAW-Dach und verwandten Projekten, 05. bis 06. Okt. 1999, Wien.* 147 Seiten, Wien 1999	23,98
22	389	Meteorologie	DOBESCH, H., H. V. TRAN:	*The Diagnostic Wind Field Model ZAWIMOD2.* 47 Seiten, 8 Farbabb., Wien 1999	23,98
23	392	Meteorologie		*Proceedings of the 26th International Conference on Alpine Meteorology; 11 to 15 Sept. 2000, Innsbruck.* CD-ROM, Wien 2000	23,98
24	395	Meteorologie	SABO, P.:	*Hochnebelprognose mittels eines objektiven Inversionsindexes für die synoptische Praxis,* 80 Seiten, Wien 2000	23,98
25	397	Meteorologie	AUER, I., R. BÖHM, W. SCHÖNER:	*Austrian long-term climate 1767-2000 - Multiple instrumental climate time series from central Europe,* 160 Seiten, 31 Farbseiten, CD-ROM, Wien 2001	25,00
26	398	Geophysik	MEURERS, B.:	*Proceedings of the 8th International Meeting on Alpine Gravimetry, Leoben 2000,* 240 Seiten, 4 Farbseiten, Wien 2001	25,00
27	399	Meteorologie		*Proceedings of the Deutsch-Österreichisch-Schweizerische Meteorologentagung; 18 to 21 Sept. 2001, Vienna.* CD-ROM, Wien 2001	25,00
28	408	Meteorologie	AUER, I., R. BÖHM, M. LEYMÜLLER, W. SCHÖNER:	*Das Klima des Sonnblicks – Klimaatlas und Klimatographie der GAW Station Sonnblick einschliesslich der umgebenden Gebirgsregion,* 305 Seiten, 130 Farbabbildungen, CD-ROM, Wien 2002	50,00
29	409	Meteorologie		*Scientific Contributions of Austria to the Mesoscale Alpine Programme (MAP),* 74 Seiten, 38 Farbseiten, Wien 2003	25,00
30	411	Meteorologie	HUBER-POCK, F.:	*Die atmosphärischen Gleichungen in den meteorologischen Koordinatensystemen,* 160 Seiten, 1 Farbseite, Wien 2003	25,00

Heft	Publ.Nr.	Fachgebiet	Autor	Titel und Umfang	Preis in Euro
31	412	Geophysik	MEURERS, B., R. PAIL:	*Proceedings of the 1st Workshop on International Gravity Field Research, Graz 2003,* 204 Seiten, 3 Farbseiten, Wien 2004	25,00
32	413	Meteorologie	BAUMANN-STANZER, K.:	*Qualitätsprüfung, Verifikation und Anwendung von Windprofilerdaten in Österreich,* 133 Seiten, 29 Farbseiten, Wien 2004	25,00
33	414	Meteorologie	SPAN, N., A. FISCHER, M. KUHN, M. MASSIMO, M. BUTSCHEK:	*Radarmessungen der Eisdicke östereichischer Gletscher, Band I: Messungen 1995 bis 1998,* 154 Seiten, Wien 2005	25,00
34	415	Meteorologie	DOBESCH, H., D. NIKOLOV, L. MAKKONEN:	*Physical Processes, Modelling and Measuring of Icing Effects in Europe,* 75 Seiten, 18 Farbseiten, Wien 2005	25,00
35	416	Meteorologie	KAISER, A., E. PETZ, I. CUHALEV:	*Ermittlung der Gesamtbelastung durch Luftschadstoffe im Kurzzeitmittel anhand von Zeitreihen der Vor- und Zusatzbelastung; Vergleich mit statistischen Methoden Das zur Berechnung von Zeitreihen der Zusatzbelastung adaptierte ÖNORM M 9440 Modell ONGAUSSplus;* 61 Seiten, 6 Farbseiten, Wien 2005	25,00
36	417	Meteorologie	SVABIK, O., A. HOLZER:	*Kleinräumige, konvektiv verursachte Stürme und Wirbelstürme (Tornados) in Österreich,* 97 Seiten, 14 Farbseiten, Wien 2005	25,00
37	418	Meteorologie	WANG Y., T. HAIDEN, A. KANN:	*The operational Limited Area Modelling system at ZAMG: ALADIN-AUSTRIA,* 39 Seiten, 9 Farbseiten, Wien 2006	25,00
38	419	Meteorologie	DOBESCH H., G. KURY:	*Basic meteorological concepts and recommendations for the exploitation of wind energy in the atmospheric boundary layer,* 128 Seiten, Wien 2006	25,00